THE PRESSURE FIELD GENERATED BY A FLUID FILM ENTRAINED BETWEEN TWO NON-CONFORMING ELASTIC BODIES

A THESIS

Presented to

The Faculty of the Division of Graduate Studies

By

Richard Kerr Kunz

In Partial Fulfillment

of the Requirements for the Degree

Doctor of Philosophy in the

School of Engineering Science and Mechanics

Georgia Institute of Technology

September, 1978

THE PRESSURE FIELD GENERATED BY A FLUID FILM ENTRAINED

BETWEEN TWO NON-CONFORMING ELASTIC BODIES

Approved:

G. M. Rentzepis, Chairman

W. O. Winer

T.-S. Wang

M. P. Stallybrass

R. W. Shreeves

Date approved by Chairman July 18, 1978

ACKNOWLEDGMENTS

The author would like to thank his thesis advisory committee for their time, interest, and helpful suggestions. In particular, the advice and assistance of my advisor, Dr. George M. Rentzepis, is greatly appreciated. His guidance, assistance, insight, and encouragement helped make this thesis continually interesting and challenging.

The author is grateful to the National Science Foundation for three years of fellowship support. The research reported herein was supported in part by NASA Grant NGR-11-002-133.

I wish also to thank my family for their quiet confidence in me, and for their encouragement of my work. I owe a special debt of gratitude to my wife, Stephanie, to whom this thesis is dedicated, for her unbounded patience and forebearance over the last few years.

TABLE OF CONTENTS

LIST OF ILLUSTRATIONS

LIST OF ILLUSTRATIONS (Continuation)

SUMMARY

In this thesis, methods are developed for analytically determining the pressure field in an elastohydrodynamic (EHD) system, assuming that experimentally obtained film thickness data are available. The EHD system consists of two elastic bodies with non-conforming surfaces, separated by a thin fluid film which is entrained between them due to their relative motion. In addition, there is a normal force transmitted between the bodies through the fluid. The hydrodynamic pressures generated in the fluid are sufficiently high to elastically deform the solid surfaces. Hence, the liquid is subjected to the dynamic application of high pressures and, in some cases, high shear rates.

By using experimentally obtained film thicknesses in the analysis, the pressure is computed through consideration only of the elasticity of the solid components; no assumption need be made about the rheological behavior of the fluid. Due to the small film thicknesses involved, the pressure is assumed constant through the film thickness. Therefore, the same pressure distribution acts on both surfaces. The problem of obtaining the relation between pressure field and surface deformation is formulated in terms of a stress boundary value problem, with the pressure being manifested as a normal surface traction acting over a portion of the surface of each body.

Two cases are investigated - the two-dimensional case, in which the solid bodies consist of two parallel cylinders or a cylinder

and a half-plane; and the three-dimensional case, consisting of two spheres or a sphere and a half-space. Solutions to the elasticity problems for the cylinder and the half-plane are obtained through use of the complex representation of plane elasticity. Solutions for the sphere and half-space are expressed in terms of Boussinesq-Papkovich potentials. An error analysis is presented to demonstrate the feasibility of the methods, and to ascertain the effects of experimental errors in film thickness on the calculated pressure distributions. Also given are listings of computer programs developed to accept as input the film thickness values throughout the EHD zone, and compute the pressure field for both two- and three-dimensional cases.

Since the pressure fields obtained by the methods developed herein are independent of the state of the liquid, a subsequent investigation may use the results of this work to study the behavior of liquids subjected to non-equilibrium thermodynamic conditions, such as those developed in an EHD process.

NOMENCLATURE

The following symbols are employed in the text. Where necessary for clarity, the equation or figure in which a symbol is first defined is given in parentheses.

a	Half-width of EHD region
a_n	Expansion coefficients
a_{ij}	Matrix of coefficients for linear algebraic system
b_j	Vector of unknowns for linear algebraic system
c	$\sin \theta_o$ (Figure 15)
C	Region over which pressure acts
$C(k,\theta)$	Cosine integral (equation (34))
c_i	Vector of unknown right-hand sides for linear algebraic system
F_x, F_y	Surface tractions in x,y directions, respectively
$h(\bar{x})$	Film thickness
$h_o(\bar{x})$	Surface separation in unloaded configuration
$\hat{k}$	Unit vector in z-direction
M	Number of terms used in pressure expansion
N	Number of data points used
p	Concentrated force
$p(\bar{x})$	Pressure
$p_n(\bar{x})$	Expansion functions
p_n, q_n	Unknown pressure coefficients
P	Total normal load

P_n	Legendre polynomial
$\bar{r}$	Position vector
r_o	Radius of cylinder or sphere
r_i	Residuals
r_1, r_2	Geometric quantities for the cylinder (Figure 5)
(r,θ)	Polar coordinates
R_1, α_1	Transformed variables of integration (Equation (74))
$(R,\hat{\alpha})$	Location of concentrated load on half-space (Figure 14)
s	$\sin\theta_o$ (Figure 15)
$S(k,\theta)$	Sine integral (Equation (34))
$\bar{u}(\bar{r})$	Displacement vector
$u(\bar{x})$	Surface deformation
$u(\bar{x};\bar{\xi})$	Surface deformation for concentrated load problem
u,v	Displacement components in x,y directions, respectively
$u_1(\bar{x}), u_2(\bar{x})$	Surface deformation of bodies 1 and 2, respectively
$\bar{x}$	Location of a point on the surface of solid body, or of a point in the film plane
$\hat{x}$	Distance measured from point of contact of surfaces in undeformed configuration
(x,y,z)	Cartesian coordinates - fixed reference system
(X,Y,Z)	Cartesian coordinates - reference system oriented with concentrated load
z	Complex variable, $= x + iy$ or $re^{i\theta}$
z_1, z_2	Location of concentrated loads on surface of cylinder
(α,β)	Geometric quantities for the cylinder (Figure 5)

(α,β)	Spherical polar coordinates - sphere (Figure 16)
α_o	Half-angular extent of EHD region for the cylinder
(α_o,β_o)	Coordinates describing location of concentrated load for the sphere
γ	Rigid-body translation of solid bodies
$\eta(\bar{r})$	General function obtained as part of total solution to elasticity problem (e.g., stress, strain, displacement component)
θ_1,θ_2	Geometric quantities for the cylinder (Figure 5)
$\theta_o,\theta_1,\theta_2$	Geometric quantities for the sphere (Figure 15)
λ,μ	Lame elastic constants
ν	Poisson's ratio
$\bar{\xi}$	Location of concentrated load applied to boundary
ρ	Distance of point on surface of half-space, measured from concentrated load (Figure 14)
ρ_0,ρ_1,ρ_2	Geometric quantities for the sphere (Figure 15)
τ_{ij}	Stress components
$\phi,\psi,\bar{\psi}$	Potential functions
ϕ_1,ψ_1	Potential functions for singular solution of the sphere
ϕ_2,ψ_2	Potential functions for residual solution of the sphere

CHAPTER I

INTRODUCTION

The physical properties of a liquid depend to a large extent on the conditions to which the liquid is subjected. An experimental investigation into the behavior of a liquid must, out of practical considerations, be performed over a limited range of conditions. The investigation may yield enough information to arrive at constitutive equations for the liquid, which essentially yield the characteristic coefficients of the material medium. Such constitutive relations describe the behavior of the liquid over the range of conditions of the investigation. However, the same constitutive equations may prove inadequate in describing liquid behavior over a different range of conditions. For instance, the physical behavior of a liquid under moderate temperatures and pressures and quasistatic conditions may differ significantly in character from that at more extreme conditions of high pressure, low temperature, or high shear rate. The character of the physical response of a liquid may thus depend on its state, as described by specification of the thermodynamic variables, and the manner in which this state is changing.

Most experimental investigations into the physical properties of liquids under extreme pressures and temperatures are performed under static conditions. Investigations of viscoelastic or glass-transition behavior have been made using dilatometry [1,2]*,

*Numbers in brackets denote references cited in the Bibliography.

differential scanning calorimetry [2,3], dielectric techniques [4], and light-scattering analysis [5], all with the system at, or slightly perturbed about, a thermodynamic equilibrium state. Even under these conditions, the manner in which the experiment is performed (i.e. the thermodynamic history of the substance) may affect the properties of the material being considered [1,3]. It appears reasonable, therefore, that when the liquid is subjected to the dynamic application of high pressure, for instance, the liquid's response may differ significantly from its behavior under the same high pressure but under equilibrium conditions. The rate of application of the pressure, as well as its magnitude, may affect the description of the physical properties of the liquid. It is, therefore, of interest to study the physical behavior of liquids under dynamic, or non-equilibrium thermodynamic conditions.

In such a study, it is important to know the thermodynamic state of the liquid, in order to obtain an accurate description of the conditions to which the liquid is subjected. Since the physical properties are expected to depend on the independent thermodynamic variables of pressure and temperature, as well as on the rate at which they change, an accurate description of the pressure and temperature fields as a function of position and time is essential to an understanding of the liquid's behavior.

In order to examine the behavior of the liquid in such a dynamic state, the following system is introduced. Consider two elastic bodies whose surfaces are non-conforming, separated by a

fluid which is entrained between them due to their relative motion (Figure 1). This motion is such that the rate of change of the normal approach between the two solid bodies is zero. Furthermore, let there be a normal force transmitted between the bodies through the fluid. Since the surfaces of the solid bodies are non-conforming, the hydrodynamic pressure generated in the liquid film in order to support the normal load is sufficiently high to elastically deform the solid components of the system. Hence, the liquid is subjected to high pressures and, in some cases, high shear rates as it is forced to pass between the surfaces. Such a system will be referred to in this work as an elastohydrodynamic (EHD) system. Such systems arise in practice in the lubrication of non-conforming machine elements such as gears, cams, and rolling element bearings. The behavior of the liquid under EHD conditions is not well understood, in part because the severity of the operating conditions inhibits knowledge of precisely what these conditions are . In spite of the experimental difficulties, a great deal of research, both analytical and experimental, has been devoted to the study of elastohydrodynamic lubrication, and significant progress has been made in understanding the EHD process.

It is therefore of interest to study the behavior of liquids when subjected to an EHD process, both for the purpose of understanding in more detail the lubrication mechanism, and for gaining a more fundamental understanding of the behavior of liquids under non-equilibrium conditions. The EHD process is a convenient device for such an investigation in part because use may be made of the results

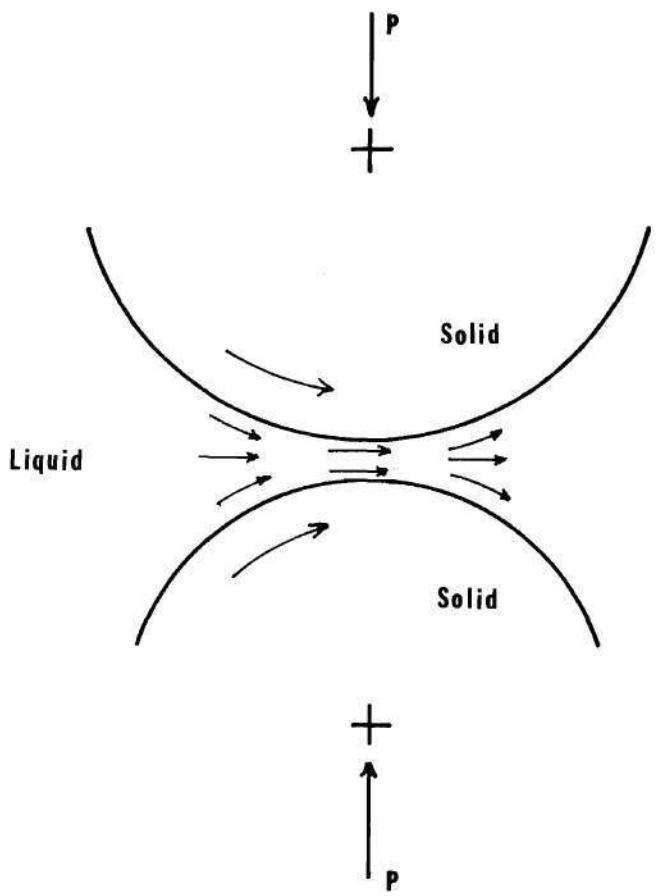

Figure 1. The EHD System

of extensive research efforts of the last several years in the area of elastohydrodynamic lubrication. In addition, the EHD system provides a convenient means for subjecting a liquid to thermodynamic states not easily attained otherwise.

The successful use of the EHD process for this purpose depends on the ability to determine with reasonable accuracy the thermodynamic variables - pressure and temperature - and the velocity of the liquid. Detailed mappings of the fluid temperature, averaged through the thickness of the film, may be obtained experimentally by detecting the infrared radiation emitted from the EHD zone [6,7]. A reasonable approximation for the velocity field may be estimated from the kinematics of the solid components. In order to complete the description of the thermodynamic state of the fluid, it is therefore necessary to determine the pressure to which the fluid is subjected during its passage through the EHD zone. With this information - the pressure field, the experimentally obtained temperature field, and the estimated velocity field - one has a complete description of the thermodynamic state of the liquid and how that state changes with time as the liquid passes through the EHD zone. This description of the conditions to which the liquid is subjected may then be used to study the behavior of the liquid itself.

The primary scope of this thesis, then is to provide the missing piece of information so that such a study may be undertaken; that is, to analytically determine the pressure distribution in the EHD zone. As will be shown subsequently, this will primarily involve the

determination of the response of the solid components of the system to an arbitrary loading distributed normal to their surfaces.

In the discussions and analyses of the EHD region which follow, two types of configuration will be under consideration. In the two-dimensional case, the solid components of the system consist either of two elastic cylinders with parallel generators, or an elastic cylinder and an elastic plate. The three-dimensional case will here refer to two elastic spheres, or an elastic sphere and an elastic plate.

Previous research efforts in the area of elastohydrodynamic lubrication have also sought to determine the pressure distribution in the EHD zone both analytically and experimentally. Among the earliest two-dimensional efforts was that of Grubin (see [8]), who obtained an approximate solution by assuming the deformation of the solid surfaces to be identical to that obtained by Hertz for the dry contact problem (see [9]). The pressure distribution was then assumed by Grubin to be Hertzian except near the fluid inlet region, where a higher pressure was assumed to be generated hydrodynamically to effect a separation of the surfaces. These assumptions were based primarily on physical insight into the problem, and in fact violate the equations of elasticity and hydrodynamics. Nevertheless, the analysis was used quite successfully by Grubin to predict film thickness, and has since been extended to predicting frictional forces [10], incorporating thermal effects [11], and analyzing the three-dimensional problem [12]. The Grubin-type analysis, while yielding many useful and practical results, assumes a Newtonian fluid, which further

restricts its generality. Additional efforts to incorporate a non-Newtonian fluid in simplified analyses of the EHD problem have merely assumed a Hertzian pressure distribution throughout the zone [13,14].

More rigorous analytical and numerical solutions, in which no initial assumption is made concerning the shape of the pressure or film thickness profile, have appeared in the literature. Such analyses require simultaneous solution of those equations which govern the EHD system. These include the Reynolds equation, which incorporates the momentum and continuity equations from fluid mechanics for the special geometry of a thin fluid film; an equation based on elasticity relating the pressure distribution to the surface deformation of the solid components; and, for non-isothermal analyses, the energy equation. The resulting set of nonlinear partial differential equations may then be solved numerically for the film thickness profile, the pressure distribution, and the temperature field. Pressure and film thickness profiles have been thus obtained for the two-dimensional isothermal problem [15,16], the two-dimensional problem with temperature effects included [17], and the three-dimensional isothermal case [18,19]. In each of these studies, however, a Newtonian fluid was assumed. Similar analytical solutions have been obtained for a viscoelastic fluid [20], and for a Newtonian fluid which solidifies above a certain pressure [21,22]. As far as this thesis is concerned, the methods just described for obtaining the pressure contain a major drawback - they must assume a rheological model for

the fluid. Implicit in the derivation of the Reynolds equation is a specific constitutive equation for the liquid. Since the present work is ultimately concerned with the behavior of the fluid itself, it is of the utmost importance to determine the pressure independent of any particular rheological model. In addition, the elasticity analyses in all the studies cited above regarded all solid components as semi-infinite bodies.

There have, in addition, been several attempts to measure the pressure directly in the EHD zone. Such efforts have been hampered by the high pressures generated, and by the small extent and film thickness of the EHD zone. The difficulty lies in obtaining an accurate measurement of the pressure without significantly disturbing the EHD process. Some success has been achieved in the two-dimensional case using a photoelastic technique [23], and by employing a pressure transducer evaporated onto one of the solid surfaces [24,25,26]. Only limited agreement has been obtained with the analytical solutions mentioned previously, and some questions remain as to the accuracy of the experimental results.

A great deal of experimental effort in the area of elasto-hydrodynamic lubrication has been devoted to the measurement of film thickness profiles, due to the close correlation between bearing life and surface separation. Among the most successful techniques is an optical interference method, by which the film thickness as a function of position may be measured quite accurately in the EHD region [27,28]. In addition, the total force transmitted across the film and the initial

geometry and physical properties of the solid components of the EHD system are readily known. The film thickness profile is obviously quite closely related to the surface deformation of the solid bodies in the EHD zone. Furthermore, the EHD-generated pressure on the fluid is manifested as surface tractions on the solid bodies. Therefore, once the film thickness profile is known from experiment, the problem of determining the pressure distribution becomes that of finding the surface traction which results in appropriate surface deformation to yield the measured film thickness profile. This formulation has the advantage that the pressure calculation is independent of the state of the fluid, and so lends itself to subsequent study of the fluid itself. If it is assumed that the thermoelastic effects on deformation are negligible, the method of analysis is independent of the temperature distribution, so that the method is applicable to non-isothermal as well as isothermal cases. Furthermore, the results of this analysis for finding the pressure distribution may be extended in a straightforward manner to yield further information, such as subsurface stresses, which could be of use in studying the fatigue of the solid components.

CHAPTER II

PROBLEM FORMULATION AND GENERAL CONSIDERATIONS

As indicated in the preceding chapter, the primary purpose of this thesis is to develop a method by which the pressure distribution in the EHD zone may be analytically determined, through the use of existing film thickness measurements. Both the two- and three-dimensional cases will be considered in this work. Prior to dealing with these two cases individually, the present chapter will be concerned with the basic underlying assumptions, formulation of the problem, and certain considerations common to both cases.

As natural consequences of the physical situation under consideration, several assumptions and their physical justifications are given below.

i) The solid surfaces are assumed to be perfectly smooth initially. Film thicknesses under consideration here fall generally in the range of 0.1 - 1.5 μm. Since asperities on the surfaces of the solid bodies may be made to average about 0.01 μm, their effect on the EHD process is neglected. In some physical situations, the film thickness may be so small that asperity interactions become significant. Such situations will not be considered here; this work deals only with those cases in which the film thickness is large enough that asperity interactions are negligible.

ii) The pressure is assumed constant across the thickness of the film. The extent of the EHD zone in directions perpendicular to

the film thickness is approximately 0.25 mm, and radii of curvature of the solid bodies are on the order of 10 mm. Since the film thickness is several orders of magnitude less than either of these dimensions, the pressure variation through the film thickness is neglected.

iii) Surface traction on the solid surfaces is presumed to arise solely from the hydrodynamic fluid pressure. Tangential surface forces arising from shearing of the fluid due to relative motion of the solid surfaces are recognized to exist in addition to the normal surface tractions exerted by the pressure. However, the contribution of the tangential forces to the normal displacement of the surfaces (which is the quantity of interest due to its relation to the film profile) will be of secondary importance to that of the normal forces. Furthermore, experimental results indicate that the total shearing force is generally less than 10% of the normal load carried by the film [29]. For these reasons, the normal pressure forces acting on the surfaces are assumed to be the only surface forces contributing to the normal displacement, which results in the measured film thickness profile.

iv) The elastic plates in both the two- and three-dimensional cases are analyzed as semi-infinite bodies. The extent of the EHD zone is several orders of magnitude less than the thickness of the plates.

v) Thermoelastic and dynamic effects are neglected in the analysis of the elastic solid bodies. The contributions to the surface deformations due to motion of the bodies (and consequent dynamic loading) and to temperature variations are much smaller than

expected errors in the film thickness measurements. As a result, the elasticity analysis of the solid bodies may be performed assuming quasistatic and isothermal conditions, without seriously restricting the generality of the results.

A schematic diagram of the EHD region, both before and after application of the load and formation of the hydrodynamic film, is shown in Figure 2. A position in a plane parallel to the film is denoted by $\bar{x}$ in the Figure, and is measured from the point of contact in the undeformed configuration. Note that, in the two-dimensional case, $\bar{x}$ is expressed by a single coordinate x; in the three-dimensional problem, two coordinates, say x and y, are required to specify the position $\bar{x}$ in the film plane. The film thickness at any location in the film plane is given by

$$h(\bar{x}) = h_o(\bar{x}) + \gamma - u_1(\bar{x}) + u_2(\bar{x}) \quad , \tag{1}$$

where $h_o(\bar{x})$ is the separation of the surfaces in the unloaded configuration, γ is the rigid-body translation of the solid bodies, and $u_1(\bar{x})$ and $u_2(\bar{x})$ are the surface deformations of bodies 1 and 2 respectively. The deformation of the solid bodies results from the surface tractions to which they are subjected. By assumption (iii) above, the surface tractions are due solely to the hydrodynamic fluid pressure, $p(\bar{x})$. Furthermore, by assumption (ii), the pressure does not vary through the film thickness, so that bodies 1 and 2 are subjected to the same surface traction.

In equation (1), $h(\bar{x})$ may be found from the experimental film

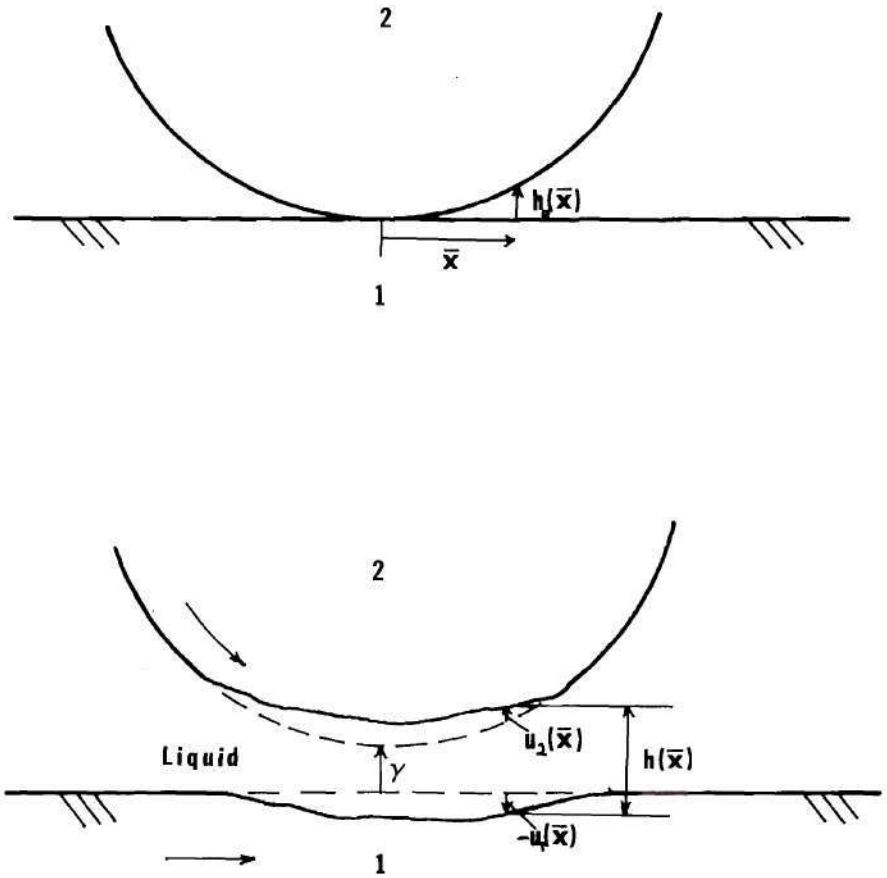

Figure 2. The EHD Zone

thickness data, and $h_0(\bar{x})$ is known from the geometry of the undeformed surfaces. In addition, the total applied normal load P is known from experimental information, and is related to the pressure field by

$$P = \iint_C p(\bar{x})\, dA \quad , \tag{2}$$

where C denotes the region over which the pressure is acting. Condition (2) arises from equilibrium of the system in the direction normal to the film plane. What remains to be determined, then, are the functional relationships between the pressure $p(\bar{x})$ and the surface displacements; i.e.

$$u_1(\bar{x}) = F_1[p(\bar{x})]; \qquad u_2(\bar{x}) = F_2[p(\bar{x})] \ . \tag{3}$$

When equation (3) is substituted into equation (1),

$$h(\bar{x}) = h_0(\bar{x}) + \gamma - F_1[p(\bar{x})] + F_2[p(\bar{x})] \tag{4}$$

Equations (2) and (4) represent two equations for the two unknowns - the pressure distribution $p(\bar{x})$ and the constant γ. Hence, once the functional relations F_1 and F_2 are determined, equations (2) and (4) may be used to solve for $p(\bar{x})$.

In order to consider both the two- and three-dimensional configurations, the relationship between surface deformation and pressure distribution must be established for four separate cases - the cylinder and the half-plane in the two-dimensional case, and the sphere and the half-space in the three-dimensional problem.

The method used for determining these relations is conceptually the same for each of the four cases; therefore, general considerations will be discussed before the individual problems are dealt with.

It should first be noted that the extent of the EHD zone, or the region over which the pressure is acting, is not precisely known a priori. Let the actual pressure region be denoted by $\bar{C}$; outside of this region, the pressure is zero. In the subsequent development, a region C will be assumed as the EHD region, and the integration in equation (2), for example, will be performed over this region C. As long as the true pressure region $\bar{C}$ lies wholly within C, the correct solution for the pressure distribution will be obtained; in that part of C which lies outside of $\bar{C}$, the solution process will yield a value of zero for the pressure, as it should. However, should a portion of $\bar{C}$ lie outside of C, an erroneous solution will be obtained. It is therefore vital that the region C be chosen large enough that $\bar{C}$ lies entirely within it.

Figure 3 shows a body of finite extent, representing the cylinder in the two-dimensional case or the sphere in the three-dimensional case. Surface tractions are acting normal to the surface over the region C, and are equilibrated by the surface tractions on C'. C may be thought of as the region over which the hydrodynamic pressure is acting, and C' is the region over which the reaction, which maintains body in equilibrium, is acting. The remainder of the boundary is denoted by the region D, and is free of stress. The exact nature and location of the reaction force distribution are not known;

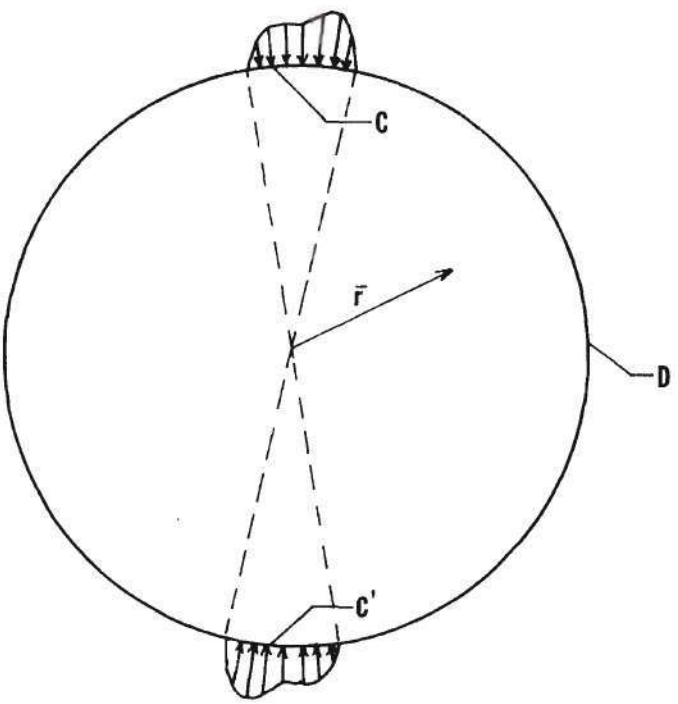

Figure 3. Finite Body with Surface Loading

however, since we are primarily concerned with results near the EHD zone (i.e. in the vicinity of C), the details of precisely how the reaction is manifested are not important (see Appendix A). Consequently, the surface tractions at C' are taken to be equal and opposite to those at C, and acting over the region diametrically opposite to C. It should also be noted that, for the semi-infinite bodies under consideration (the half-plane and the half-space), it is not necessary to consider the region C'. The discussion which follows, which deals with a finite body, may easily be extended to the semi-infinite bodies.

The problem posed in Figure 3, then, is that of an elastic body subjected to an arbitrary normal surface traction, equal to the pressure distribution $p(\bar{x})$, acting over the regions C and C', and to zero surface stresses acting over the remainder of the boundary, D. The problem is hence formulated as a boundary value problem of the first kind, in which surface tractions are specified over the entire surface of the body. Complete solution of this elasticity problem will yield all associated functions of position - such as stresses and displacements in the interior or on the surface, potential functions, and so forth - in terms of the arbitrary loading distribution $p(\bar{x})$. A desired function of position from the solution of the elasticity problem is denoted by $\eta(\bar{r})$, where $\bar{r}$ is any interior or boundary point. Specifically, for the purposes of obtaining expressions of the form of equation (3), it is desired to solve for the normal displacement

at the surface of the body in terms of $p(\bar{x})$. This will be the functional relationship necessary for use in equation (1). Hence, solution of the elasticity problem suggested by Figure 3 will result in the required expressions in the film thickness equation (4).

The solution to the boundary value problem posed above may be obtained by first solving the problem of a unit concentrated load applied normal to the surface at an arbitrary boundary point $\bar{\xi}$. As before, this load is equilibrated by an equal and opposite load applied at the other end of the diameter. The solution of this concentrated load problem will yield the desired function of position as $\eta(\bar{r};\bar{\xi})$; that is, η will be a function of position $\bar{r}$, and of the point of application of the concentrated load $\bar{\xi}$. Because of the linearity of the equations, this solution to the concentrated load problem may then be used as the Green's function associated with this problem, to determine the solution to the problem with arbitrary loading. Hence, once $\eta(\bar{r};\bar{\xi})$ is found, then $\eta(\bar{r})$ for the arbitrary loading $p(\bar{x})$ may be expressed as

$$\eta(\bar{r}) = \iint_C \eta(\bar{r};\bar{\xi})p(\bar{\xi})dA \tag{5}$$

Specifically, if the normal surface displacement for the concentrated load problem, $u(\bar{x};\bar{\xi})$, has been found, the corresponding quantity for the arbitrary loading is given by

$$u(\bar{x}) = \iint_C u(\bar{x};\bar{\xi})p(\bar{\xi})dA \tag{6}$$

Equation (6) is the desired functional relationship of the form of equations (3), which relates the surface displacement to the pressure distribution.

In order to facilitate the solution of the resulting equations, the pressure distribution acting over the region C is expanded in terms of an infinite series of the form

$$p(\bar{x}) = \sum_{n=1}^{\infty} a_n \, p_n(\bar{x}) \tag{7}$$

where the $p_n(\bar{x})$ form a complete set of known functions of position, and the a_n are constant coefficients to be determined. Equation (6) may then be expressed as

$$u(\bar{x}) = \sum_{n=1}^{\infty} a_n \iint_C u(\bar{x};\bar{\xi}) p_n(\bar{\xi}) dA \ . \tag{8}$$

If the solution to the concentrated load problem $u(\bar{x};\bar{\xi})$ is known, the integral in equation (8) may be evaluated, and the result is a linear algebraic expression relating $u(\bar{x})$ to the unknown pressure coefficients a_n. As a practical consideration, the series (7) will be truncated past a finite number of terms, M. Hence, when equations (7) and (8) are used in equations (4) and (2), the result may be written as

$$h(\bar{x}_i) - h_o(\bar{x}_i) = \sum_{n=1}^{M} a_n \left[- \iint_C u_1(\bar{x}_i;\bar{\xi}) p_n(\bar{\xi}) dA \right.$$

$$\left. + \iint_C u_2(\bar{x}_i;\bar{\xi}) p_n(\bar{\xi}) dA \right] + \gamma \ , \qquad (9)$$

$$i = 1, 2, \ldots, N$$

$$P = \sum_{n=1}^{N} a_n \iint_C p_n(\bar{\xi}) \, dA \qquad (10)$$

where $\bar{x}_i$ are locations at which film thickness measurements are available, and $u_1(\bar{x};\bar{\xi})$ and $u_2(\bar{x};\bar{\xi})$ are the solutions to the concentrated load problems for bodies 1 and 2 respectively. Equations (9) and (10) represent N + 1 linear algebraic equations in the M + 1 unknowns (a_n, n = 1,M; and γ). For N = M, the equations may be solved for the expansion coefficients a_n, and the pressure distribution then expressed through equations (7).

Once the expansion coefficients a_n are obtained, the elasticity problem is completely determined. The associated stress and strain tensor fields as well as the displacement vector field are then obtainable. Thus, the expression

$$\eta(\bar{r}) = \sum_{n=1}^{M} a_n \iint_C \eta(\bar{r};\bar{\xi})\, p(\bar{\xi})\, dA \qquad (11)$$

may be evaluated if the a_n are known. Hence, the values of, for example, critical stresses for the purpose of studying the fatigue of the solid components, may be obtained from equation (11) as a straightforward extension of the results of this work.

Equations (9) and (10) complete the general formulation of the problem of determining the pressure distribution in the EHD zone. The succeeding chapters will deal with the two- and three-dimensional cases individually. This will primarily involve solution of the concentrated load problems in each case, and the use of these solutions in equations (9) and (10) for the purpose of solving for the expansion coefficients of the pressure distribution.

CHAPTER III

THE TWO-DIMENSIONAL CASE

In the present chapter, the elasticity solutions will be obtained for the half-plane and the cylinder acted on by an arbitrary pressure distribution, and appropriate expressions for the surface deformations will be generated. These expressions will then be used to determine the relationship between the measured film thickness profile and the pressure distribution in the two-dimensional case. In addition, some numerical considerations will be discussed, and numerical results for several test cases will be presented.

Solutions from Two-Dimensional Elasticity

The complex representation of the theory of plane elasticity, presented in detail in Muskhelishvili [30], may be used for expressing the solutions to the problems for the half-plane and the cylinder. In the two-dimensional problem, all quantities are assumed to be independent of the axial direction, and the elasticity problems may be formulated as problems in plane strain. In this representation, the stress and displacement fields may be represented in terms of two complex holomorphic functions $\phi(z)$ and $\psi(z)$ by [30],

$$\tau_{xx} + \tau_{yy} = 2[\phi'(z) + \overline{\phi'(z)}]$$

$$\tau_{yy} - \tau_{xx} + 2i\,\tau_{xy} = 2[\bar{z}\,\phi''(z) + \psi'(z)] \qquad (12)$$

$$2\mu(u + iv) = \frac{\lambda + 3\mu}{\lambda + \mu} \phi(z) - z\overline{\phi'(z)} + \overline{\psi(z)}$$

where τ_{xx}, τ_{yy}, τ_{xy} denote stresses; u, v denote displacements in the x and y directions respectively; z is the complex variable x + iy or $re^{i\theta}$; ' represents differentiation with respect to the argument; $\overline{\quad}$ denotes the complex conjugate; and λ and μ are the Lamé elastic constants. If the body is subjected to surface tractions represented by $(F_x + iF_y)$, then ϕ and ψ must also satisfy the boundary condition

$$\phi(\sigma) + \sigma\,\overline{\phi'(\sigma)} + \overline{\psi(\sigma)} = f \tag{13}$$

with f defined as

$$f = i\int_0^{\sigma} (F_x + i\,F_y)ds$$

where σ represents a boundary point, and s is the arc coordinate on the boundary.

The Half-Plane

Let the body occupy the lower half-plane $y < 0$, and be subjected to surface tractions

$$\tau_{yy} = N(x)$$
$$\tau_{xy} = T(x) \qquad -\infty < x < \infty \quad .$$

The boundary conditions (13) then simplify to

$$N(x) - iT(x) = \phi'(x) - \overline{\phi'(x)} + x\,\overline{\phi''(x)} + \overline{\psi'(x)} \quad .$$

Solving the stated boundary-value problem for this set of boundary conditions yields the following stress functions $\phi(z)$ and $\psi(z)$, as shown by Muskhelishvili [30]

$$\phi(z) = \frac{1}{2\pi} \int_{-\infty}^{\infty} (T + iN)\, \ell n(t - z)dt$$

$$\psi(z) = \frac{z}{2\pi} \int_{-\infty}^{\infty} (T + iN)\, \frac{dt}{t-z} - \frac{1}{2\pi} \int_{-\infty}^{\infty} (T - iN)\, \ell n(t - z)dt \quad .$$

For the particular case under consideration, the surface tractions are generated by normal stresses only, acting over a portion of the boundary surface, Figure (4). That is,

$$N(x) = 0 \qquad -\infty < x < -a$$

$$N(x) = -p(x) \qquad -a < x < a$$

$$N(x) = 0 \qquad a < x < \infty$$

$$T(x) = 0 \qquad -\infty < x < \infty$$

The solution for this loading becomes

$$\phi(z) = -\frac{i}{2\pi} \int_{-a}^{a} p(t)\, \ell n(t - z)dt \qquad (15)$$

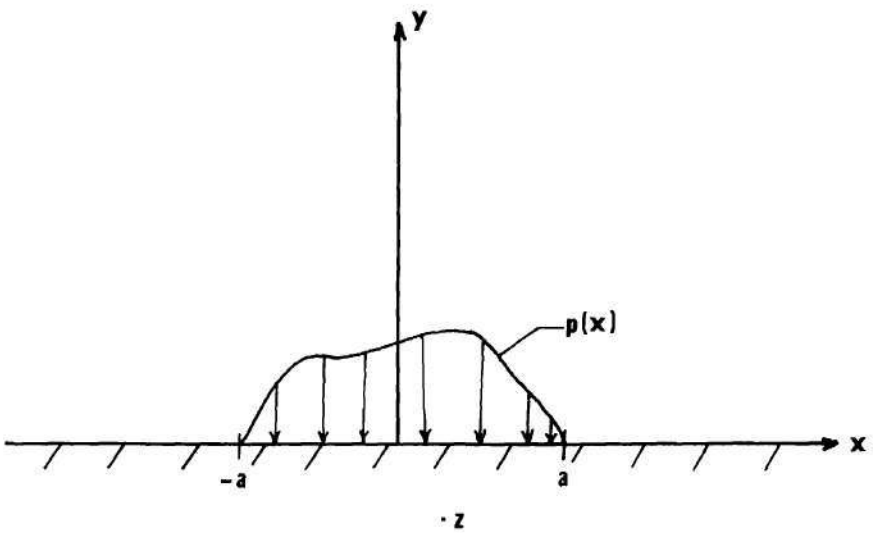

Figure 4. The Half-Plane

$$\psi(z) = -\frac{iz}{2\pi}\int_{-a}^{a} p(t)\,\frac{dt}{t-z} - \frac{i}{2\pi}\int_{-a}^{a} p(t)\,\ell n(t-z)dt \qquad (16)$$

It should be noted that this solution is already in the desired integral form, so there is no need to solve the concentrated load problem explicitly. The solution to the singular problem may be obtained directly from the integrand of equation (15).

The displacements, as obtained from equation (12), are

$$4\pi\mu(u + iv) = -i\int_{-a}^{a} p(t)\left[\frac{\lambda + 3\mu}{\lambda + \mu}\,\ell n(t-z) + \ell n(t-\bar{z})\right]dt$$

$$+ i(z-\bar{z})\int_{-a}^{a} p(t)\,\frac{dt}{t-z} \qquad (17)$$

Since the purpose of this analysis is to relate the pressure distribution to the film thickness, the quantity of primary importance is the normal displacement at the surface, $v(x)$. Separating real and imaginary parts in (17), and evaluating at the surface, one obtains

$$v(x) = -\frac{\lambda + 2\mu}{2\pi\mu(\lambda + \mu)}\int_{-a}^{a} p(t)\,\ell n(t-x)dt \qquad (18)$$

If the half-plane is labelled as Body 1 in Figure 2, then equation (18) gives the expression for $u_1(x)$. Equation (18) expresses the desired

functional relationship, in the form of equation (6), between the normal surface displacement and the pressure distribution on the surface, p(x).

The Cylinder

The solution to the problem of a cylinder acted on by distributed surface tractions $F_x(\sigma) + iF_y(\sigma)$ may be shown to be [30]

$$\sigma(z) = \frac{1}{2\pi i} \int_L \frac{f d\sigma}{\sigma - z} - \bar{a}z - \frac{1}{2\pi i} \int_L \frac{f d\sigma}{\sigma} \tag{19}$$

$$\psi(z) = \frac{1}{2\pi i} \int_L \frac{\bar{f} d\sigma}{\sigma - z} - r_o^2 \frac{\phi'(z)}{z} + r_o^2 \frac{a}{z} \tag{20}$$

where f is given by equation (14), r_o is the radius of the cylinder, $\int_L$ represents the line integral over the boundary, and $a = \bar{a} = \phi'(0)$. Let n concentrated forces (F_{1x},F_{1y}), (F_{2x},F_{2y}), ..., (F_{nx},F_{ny}) be applied at boundary points $z_1 = r_o e^{i\alpha_1}$, $z_2 = r_o e^{i\alpha_2}$, ..., $z_n = r_o e^{i\alpha_n}$ respectively. These forces are such that the cylinder as a whole is in equilibrium. For this loading case, equations (19) and (20) become

$$\phi(z) = -\frac{1}{2\pi} \sum_{k=1}^{n} (F_{kx} + i\, F_{ky}) \ln(z_k - z)$$

$$- \frac{z}{4\pi r_o^2} \sum_{k=1}^{n} (F_{kx} + i\, F_{ky}) \bar{z}_k \tag{21}$$

$$\psi(z) = \frac{1}{2\pi} \sum_{k=1}^{n} (F_{kx} - i F_{ky}) \ln(z_k - z)$$

$$- \frac{1}{2\pi} \sum_{k=1}^{n} \frac{F_{kx} + i F_{ky}}{z_k - z} \bar{z}_k \qquad (22)$$

Specifically, consider the case when two equal and opposite forces (0,-p) and (0,p), parallel to the y-axis, act on the surface of the cylinder at $z_1 = r_o e^{i(\pi/2-\alpha)}$ and $z_2 = -r_o e^{i(\pi/2+\alpha)}$, as in Figure 5. Equations (21) and (22) then become

$$\phi(z) = \frac{ip}{2\pi} \left\{ \ln \frac{z_1 - z}{z_2 - z} + \frac{z}{2r_o^2} (\bar{z}_1 - \bar{z}_2) \right\} \qquad (23)$$

$$\psi(z) = \frac{ip}{2\pi} \left\{ \ln \frac{z_1 - z}{z_2 - z} + \frac{\bar{z}_1}{z_1 - z} - \frac{\bar{z}_2}{z_2 - z} \right\} \qquad (24)$$

Then, using equations (23) and (24) in equation (12) gives for the displacements

$$2\mu(u + iv) = \frac{ip}{2\pi} \left\{ \frac{\lambda+3\mu}{\lambda+\mu} \ln \frac{z_1 - z}{z_2 - z} + \ln \frac{\bar{z}_1 - \bar{z}}{\bar{z}_2 - \bar{z}} - \frac{2\mu}{\lambda+\mu} \frac{iz}{r_o} \cos\alpha \right.$$

$$\left. + \frac{z_1 - z}{\bar{z}_1 - \bar{z}} - \frac{z_2 - z}{\bar{z}_2 - \bar{z}} \right\} \qquad (25)$$

Separating real and imaginary parts, and using, from Figure 5, that

$$z_1 - z = - r_1 e^{-i\theta_1}$$

$$z_2 - z = - r_2 e^{i\theta_2}$$

yields

$$u = \frac{p}{4\mu\pi}\left\{\frac{2\mu}{\lambda+\mu}(\theta_1 + \theta_2) + \frac{2\mu}{\lambda+\mu}\frac{x}{r_o}\cos\alpha + \sin 2\theta_1 + \sin 2\theta_2\right\} \qquad (26)$$

$$v = \frac{p}{4\mu\pi}\left\{\frac{2(\lambda + 2\mu)}{\lambda + \mu}\ell n\frac{r_1}{r_2} + \frac{2\mu}{\lambda+\mu}\frac{y}{r_o}\cos\alpha + \cos 2\theta_1 - \cos 2\theta_2\right\} \qquad (27)$$

In these relations, one may note from Figure 5 that (r_1,θ_1) and (r_2,θ_2) denote the location of an arbitrary interior point $z = x + iy$ relative to the points of application of the concentrated loads p. As was the case in consideration of the half-plane just presented, the quantity of interest in this analysis is the displacement in the direction normal to the film plane at the surface of the cylinder; i.e., the displacement v evaluated at an arbitrary surface location $z = r_o e^{i\beta}$. The appropriate surface displacement is, from evaluating equation (27) at the surface,

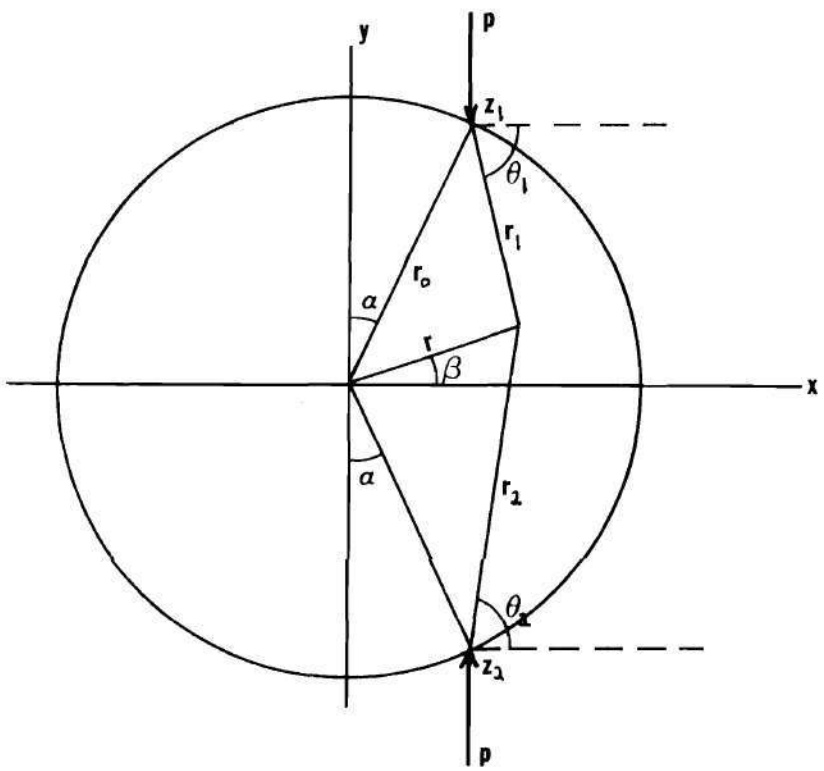

Figure 5. Cylinder Subjected to Concentrated Loads

$$v(\beta;\alpha) = \frac{(\lambda+2\mu)p}{2\mu\pi(\lambda+\mu)}\left\{\frac{1}{2}\ell n\left[\frac{1-\sin(\beta+\alpha)}{1+\sin(\beta-\alpha)}\right] + \sin\beta\cos\alpha\right\} \qquad (28)$$

Hence, equation (28) expresses the y-component of the surface displacement for a cylinder loaded by a pair of parallel concentrated forces of intensity p, as shown in Figure 5. As discussed previously, this solution may be used as the Green's function for this problem to determine the surface displacement due to an arbitrary loading distribution $p(\theta)$ acting over a portion of the surface, where $\theta = \beta + \frac{\pi}{2}$ is the angle measured counterclockwise from the negative y-axis (See Figure 6). The resulting component of the surface displacement, as obtained by integrating equation (28), is

$$v(\theta) = \int_{-\alpha_o}^{\alpha_o} v(\theta;\alpha)p(\alpha)r_o d\alpha$$

$$= \frac{(\lambda+2\mu)r_o}{2\mu\pi(\lambda+\mu)}\int_{-\alpha_o}^{\alpha_o} p(\alpha)\left[\ell n\frac{\cos\frac{1}{2}(\theta+\alpha)}{\sin\frac{1}{2}(\theta-\alpha)} - \cos\theta\cos\alpha\right] d\alpha \qquad (29)$$

If the cylinder is denoted as Body 2 in Figure 2, then equation (29) gives the required expression for $u_2(\theta)$. Hence, equation (29) fills the same role for the cylinder as equation (18) does for the half-plane; that is, it gives the functional relationship between the surface displacement and the pressure distribution, in the same form as equation

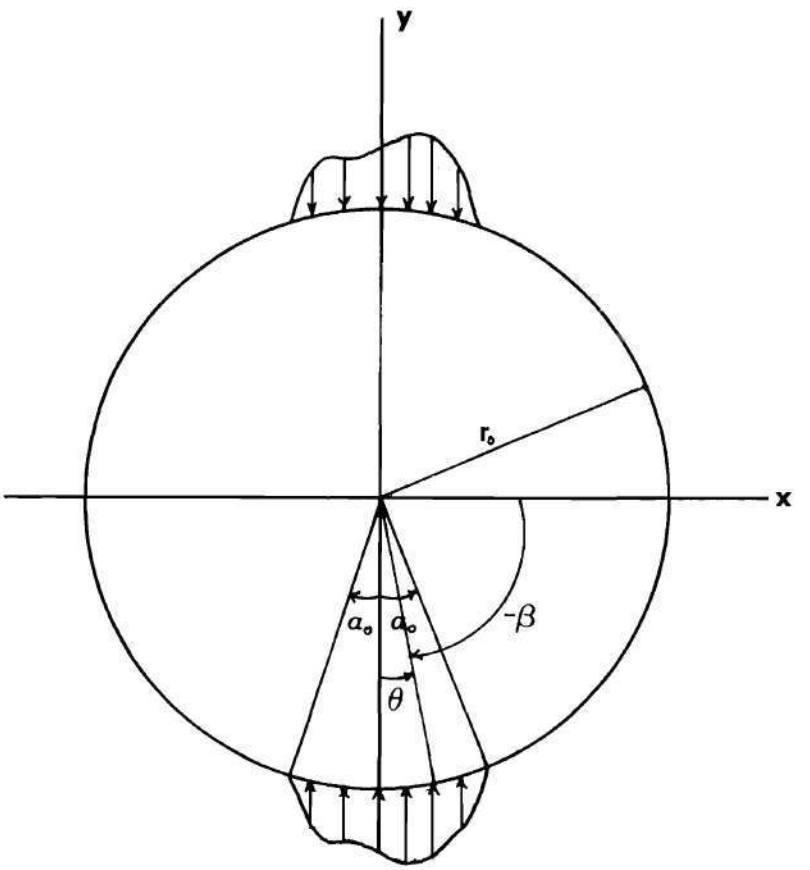

Figure 6. Cylinder Subjected to Distributed Surface Load

(6) of Chapter II.

It should be pointed out that the solution obtained above is for the cylinder acted on by surface tractions directed parallel to the y-axis, Figure 6. In fact, the surface tractions due to the fluid pressure would be acting in the radial direction, or normal to the surface of the cylinder. However, since the angular extent of the pressure region in the EHD process, $2\alpha_o$, is very small, negligible error is incurred by this solution. In fact, experimental film thickness measurements indicate that the film profile is nearly parallel over a large portion of the EHD zone, indicating that, in the deformed configuration, the normal surface tractions are very nearly parallel to the y-axis. If the assumption of linear elasticity is valid, then, there must be negligible error in assuming the surface tractions parallel to the y-axis in the undeformed state.

Surface Displacement for an Arbitrary Pressure Distribution

Figure 7 shows schematically the conjunction of the cylinder, subjected to surface traction $p_2(\theta)$, and the half-plane, subjected to surface traction $p_1(x)$. By assumption (ii) of Chapter II, the pressure is constant across the film thickness. Since, from the figure, $x = r_o \sin\theta$, and $-\alpha_o \leq \theta \leq \alpha_o$, where α_o is very small (on the order of .03 radians), then one may conclude that

$$p_1(r_o\theta) = p_2(\theta) \quad .$$

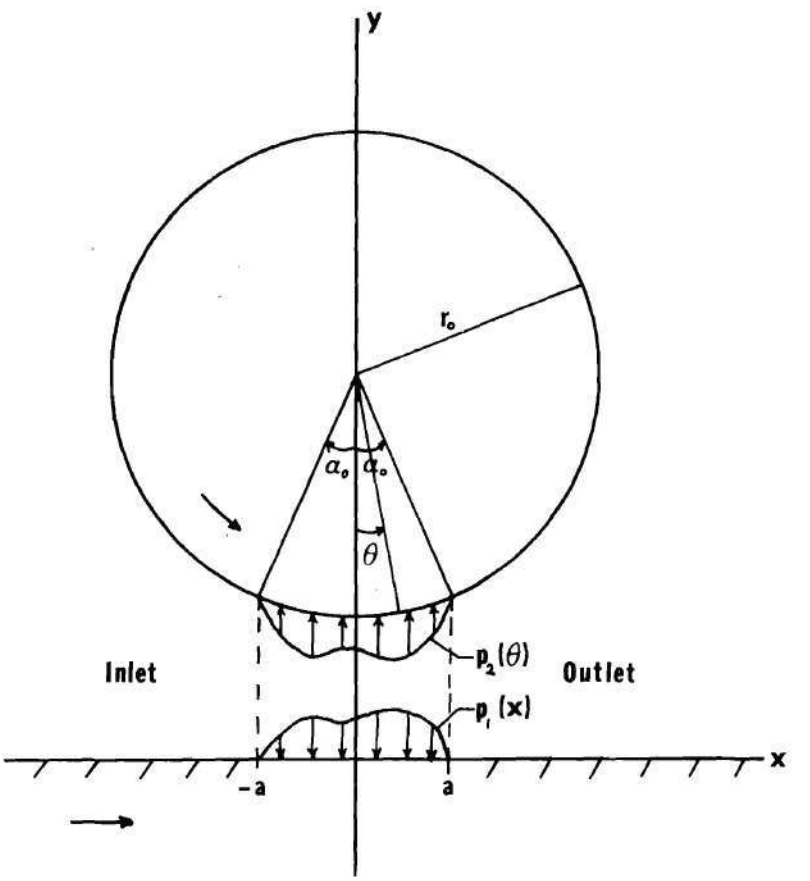

Figure 7. The Conjunction of the Cylinder and the Half-Plane in the EHD Zone

Hence, the pressure may be expressed by the single function $p(x)$ acting on the half-plane, and $p(r_o\theta)$ acting on the cylinder.

The pressure distribution may be expressed, in the form of equation (7), by the series

$$p(x) = \sum_{n=o}^{\infty} p_n \cos\left(\frac{2n+1}{2}\,\pi\,\frac{x}{a}\right) + \sum_{n=1}^{\infty} q_n \sin\frac{n\pi x}{a} \tag{30}$$

where p_n and q_n are unknown coefficients to be determined. In this series, it will be noted that the first summation is a complete set of functions symmetric about $x = 0$, and the second is a complete set of antisymmetric functions, both subject to the restriction that $p(\pm a) = 0$. The pressure distribution may thus be thought of as being broken up into a symmetric and an antisymmetric component, and the corresponding symmetric and antisymmetric displacements for the half-plane and cylinder may be obtained from equations (18) and (29).

The symmetric displacement solution for the half-plane may be determined from

$$u_{1s}(x) = -\frac{\lambda+2\mu}{2\pi\mu(\lambda+\mu)} \sum_{n=0}^{\infty} p_n \int_{-a}^{a} \left[\cos\frac{2n+1}{2a}\,\pi t\right] \ell n(t-x)\,dt \ .$$

Upon performing the indicated integration, the resulting symmetric displacement may be expressed as

$$u_{1s}(x) = \sum_{n=0}^{\infty} p_n\, U_{1s}(x) \tag{31}$$

where

$$U_{1s}(x) = -\frac{a}{m\pi}\frac{(\lambda+2\mu)}{2\pi\mu(\lambda+\mu)}\left\{(-1)^n \ell n\left(1-\frac{x^2}{a^2}\right) + \sin\frac{m\pi x}{a}\left[\ell n\frac{a+x}{a-x} - C\left(\frac{m\pi}{a}, a+x\right) + C\left(\frac{m\pi}{a}, a-x\right)\right] - \cos\frac{m\pi x}{a}\left[S\left(\frac{m\pi}{a}, a+x\right) + S\left(\frac{m\pi}{a}, a-x\right)\right]\right\} \tag{32}$$

with the notation that

$$m = \frac{2n+1}{2} \tag{33}$$

and

$$S(k,\theta) = \int_0^\theta \frac{\sin kx}{x}\,dx \;; \qquad C(x,\theta) = \int_0^\theta \frac{1-\cos kx}{x}\,dx \tag{34}$$

Equation (34) is a form of the so-called sine and cosine integrals, respectively. These are tabulated in many mathematical handbooks ([31], for example). In addition, computer subroutines for rapid calculation of these specific integrals are widely available (e.g., subroutine SICI in [32]).

Similarly, the antisymmetric half-plane displacement is obtained, through the use of equations (18) and (30), as

$$u_{1a}(x) = - \frac{\lambda+2\mu}{2\pi\mu(\lambda+\mu)} \sum_{n=1}^{\infty} q_n \int_{-a}^{a} \left[\sin \frac{n\pi t}{a}\right] \ell n(t-x)dt \ .$$

The results of the integration may be written as

$$u_{1a}(x) = \sum_{n=1}^{\infty} q_n \, U_{1a}(x) \tag{35}$$

where

$$U_{1a}(x) = - \frac{\lambda+2\mu}{2\pi\mu(\lambda+\mu)} \cdot \frac{a}{n\pi} \left\{ \left[(-1)^n - \cos \frac{n\pi x}{a}\right] \ell n \frac{a+x}{a-x} \right.$$

$$+ \cos \frac{n\pi x}{a} \left[C\left(\frac{n\pi}{a}, a + x\right) - C\left(\frac{n\pi}{a}, a - x\right) \right]$$

$$\left. - \sin \frac{n\pi x}{a} \left[S\left(\frac{n\pi}{a}, a - x\right) + S\left(\frac{n\pi}{a}, a + x\right) \right] \right\} \tag{36}$$

The displacement of the half-plane corresponding to an arbitrary pressure distribution over the region $-a \leq x \leq a$ may be obtained from equations (31) and (35) as the sum of the symmetric and antisymmetric components; i.e.

$$u_1(x) = \sum_{n=0}^{\infty} p_n \, U_{1s}(x) + \sum_{n=1}^{\infty} q_n \, U_{1a}(x) \quad . \tag{37}$$

The displacement for the cylinder in terms of the unknown pressure coefficients p_n and q_n may be obtained similarly. The symmetric displacement for the cylinder is found by substituting the first summation of equation (30) into equation (29) to yield

$$u_{2s}(\theta) = \frac{(\lambda+2\mu)r_o}{2\mu\pi(\lambda+\mu)} \sum_{n=0}^{\infty} p_n \int_{-\alpha_o}^{\alpha_o} \cos \frac{2n+1}{2\alpha_o}\pi\alpha \left[\ell n \frac{\cos \frac{1}{2}(\theta+\alpha)}{\sin \frac{1}{2}(\theta-\alpha)} - \cos\theta \cos\alpha \right] d\alpha \quad .$$

The result of performing the integration is

$$u_{2s}(\theta) = \sum_{n=0}^{\infty} p_n U_{2s}(\theta) \tag{38}$$

where

$$U_{2s}(\theta) = \frac{(\lambda+2\mu)r_o\alpha_o}{2\mu\pi(\lambda+\mu)} \left\{ \frac{m\pi}{m^2\pi^2+\alpha_o^2} (-1)^n \cos\alpha_o \cos\theta + \frac{1}{m\pi} \left[(-1)^n \ell n \frac{\alpha_o^2-\theta^2}{4} + \sin \frac{m\pi\theta}{\alpha_o} \left[\ell n \frac{\alpha_o+\theta}{\alpha_o-\theta} + C\left(\frac{m\pi}{\alpha_o}, \alpha_o-\theta\right) - C\left(\frac{m\pi}{\alpha_o}, \alpha_o+\theta\right) \right] - \cos \frac{m\pi\theta}{\alpha_o} \left[S\left(\frac{m\pi}{\alpha_o}, \alpha_o-\theta\right) + S\left(\frac{m\pi}{\alpha_o}, \alpha_o+\theta\right) \right] \right] \right\} \tag{39}$$

The quantities m, $S(k,\theta)$ and $C(k,\theta)$ are defined as before by equations (33) and (34).

The antisymmetric cylinder displacement is expressed by the integral, from equation (29) and (30)

$$u_{2a}(\theta) = \frac{(\lambda+2\mu)r_o}{2\mu\pi(\lambda+\mu)} \sum_{n=1}^{\infty} q_n \int_{-\alpha_o}^{\alpha_o} \sin \frac{n\pi\alpha}{\alpha_o} \left[\ell n \frac{\cos \frac{1}{2}(\theta+\alpha)}{\sin \frac{1}{2}(\theta-\alpha)} - \cos\theta \cos\alpha \right] d\alpha \ .$$

After integration, the resulting expression for the displacement is

$$u_{2a}(\theta) = \sum_{n=1}^{\infty} q_n \, U_{2a}(\theta) \tag{40}$$

with $U_{2a}(\theta)$ given by

$$U_{2a}(\theta) = \frac{\lambda+2\mu}{2\mu\pi(\lambda+\mu)} \frac{r_o\alpha_o}{n\pi} \left\{ \left[(-1)^n - \cos \frac{n\pi\theta}{\alpha_o} \right] \ell n \left(\frac{\alpha_o+\theta}{\alpha_o-\theta} \right) \right.$$

$$+ \cos \frac{n\pi\theta}{\alpha_o} \left[C\left(\frac{n\pi}{\alpha_o} , \alpha_o + \theta \right) \right.$$

$$\left. - C\left(\frac{n\pi}{\alpha_o} , \alpha_o - \theta \right) \right] - \sin \frac{n\pi\theta}{\alpha_o} \left[S\left(\frac{n\pi}{\alpha_o} , \alpha_o + \theta \right) \right.$$

$$\left. \left. + S\left(\frac{n\pi}{\alpha_o} , \alpha_o - \theta \right) \right] \right\} \ . \tag{41}$$

The displacement of the cylinder resulting from an arbitrary pressure distribution over the region $-\alpha_o \leq \theta \leq \alpha_o$ may be obtained from equations (38) and (40) as a combination of its symmetric and anti-symmetric components,

$$u_2(\theta) = \sum_{n=0}^{\infty} p_n \, U_{2s}(\theta) + \sum_{n=1}^{\infty} q_n \, U_{2a}(\theta) \quad . \tag{42}$$

Determination of the Pressure Distribution in the EHD Zone

Equation (37) for the half-plane and equation (42) for the cylinder yield the surface displacements of these bodies in terms of the unknown pressure coefficients, in the form of equation (8) of Chapter II. These quantities are related to the measured film thickness through the use of equation (4). For the particular geometry under consideration, a cylinder and a flat plate, the surface separation in the undeformed configuration, $h_o(x)$, is, from Figure 7,

$$h_o(x) = r_o(1 - \cos\theta)$$

or, for small θ,

$$h_o(x) = \frac{r_o\theta^2}{2} = \frac{x^2}{2r_o} \tag{43}$$

recalling that $x = r_o\theta$ for small θ. If the film thickness is known at N locations x_i, then the film thickness equation (4) becomes, after

truncating the series in equations (37) and (42) for the purpose of computation,

$$h(x_i) - \frac{x_i^2}{2r_o} = \sum_{n=0}^{K-1} p_n \left[U_{2s}\left(\frac{x_i}{r_o}\right) - U_{1s}(x_i) \right]$$

$$+ \sum_{n=1}^{L} q_n \left[U_{2a}\left(\frac{x_i}{r_o}\right) - U_{1a}(x_i) \right] + \gamma \, , \qquad (44)$$

$$i = 1, 2, \ldots, N \; ; \; K + L = M \quad .$$

Furthermore, the relationship that the total pressure force must equal the applied normal load must also be satisfied. Using the pressure expansion, equation (30), in the total load condition, equation (2), and evaluating the integral, yields the relation

$$p = \frac{4a}{\pi} \sum_{n=0}^{\infty} p_n \frac{(-1)^n}{2n+1} \quad . \qquad (45)$$

Equations (44) and (45) are of the form of equations (9) and (10). They form a set of N+1 linear algebraic equations in the M+1 unknowns p_n, q_n and γ'. Therefore, the determination of the pressure distribution in the EHD zone from measured film thickness data may be accomplished by solving this set of equations for the pressure coefficients. Once these coefficients have been determined, the pressure as

a function of position is obtained from the expansion (30).

Numerical Considerations

As a practical consideration for the purposes of computation, a finite number of terms, M, must be selected from the series representation of the pressure, equation (30). M must be large enough so that the truncated series may accurately represent the true pressure distribution. If N locations are selected at which the film thickness is known, equations (44) and (45) yield sufficient information to solve for the pressure coefficients, provided N = M. However, due to unavoidable inaccuracies in the measurements of the film thickness, solving the N + 1 equations in M+1 unknowns, where N = M, is not suitable for determining the pressure, for the following reason.

Since the measurements made at each point in the EHD zone are in error, the total effect of the experimental error increases as the number of points used, N, increases. At the same time, a sufficient number of points must be used to adequately characterize the shape of the film thickness profile. In addition, there clearly must be at least as many data points as selected terms in the pressure expansion. To alleviate the problem of the build-up of experimental error as the number of data points increases, N and M are chosen with N greater than M; i.e. more equations than unknowns. Equations (44) and (45) are of the form

$$a_{ij}\, b_j = c_i \quad ; \quad \begin{matrix} i = 1, 2, \ldots, N + 1 \\ j = 1, 2, \ldots, M + 1 \end{matrix} \quad , \qquad (46)$$

with $N > M$; where b_j are the unknown coefficients. Equation (46) represents an overdetermined system for which, in general, there is no exact solution. However, since there are experimental errors contained in the right-hand side, c_i, it makes no difference that an exact solution does not exist; rather, since the measured film thickness is at least close to the true film thickness, it is sufficient to find a solution to (46) which is close, in some way, to an exact solution. Accordingly, the residuals, r_i, are defined as

$$a_{ij}\, b_j - c_i = r_i \quad . \tag{47}$$

The unknowns b_j are then determined so as to minimize the sum of the squares of the residuals. Hence, if $r_i r_i = 0$, the solution is exact; since no such solution exists, one seeks to make $r_i r_i$ as small as possible. The requirement that $r_i r_i$ be a minimum results in the following system of linear equations [33,34]

$$a_{ip}\, a_{ik}\, b_k = a_{ip} c_i \; ; \quad p = 1, 2, \ldots, M + 1 \quad . \tag{48}$$

That the solution of this system does in fact minimize $r_i r_i$ is shown in Appendix B. The solution of equation (48) has the effect of smoothing out errors in the data while coming as close as possible to solving equations (46), in recognition of the fact that the data is the best available estimate to the true film thickness. The amount of smoothing depends on the degree to which N is greater than M.

In consideration of the above, the following ad hoc procedure

was adopted for selecting N and M. The number of data points, N, is chosen sufficiently large so as to adequately represent the shape of the film thickness profile. If the series (30) for the pressure is to converge toward the true pressure, the coefficients must eventually go to zero as M, the number of terms, is increased. Hence, once N is selected, the amount of smoothing required is determined by increasing M until the pressure coefficients begin to grow, indicating that the experimental errors are predominating. As a check on the acceptability of the results, the magnitudes of the residuals may be compared to the expected error in the film thickness measurements. In fact, from equation (47), the residuals may be seen to be the difference between the experimentally measured film thickness, and the film thickness obtained from the calculated pressure distribution.

In addition to N and M, a value for a, the half-width of the pressure distribution, and the location of the point $x = 0$ must be selected (note that the film thickness equation may be formulated such that the position $x = 0$ need not coincide with the point of contact between the bodies in the undeformed state). As discussed in Chapter II, the precise extent of the pressure region is not known a priori, and it is essential that the region $-a \leq x \leq a$ encompass the entire pressure region. Considerations involved in the selection of these two quantities will be discussed subsequently.

Based on the calculation procedure for the pressure distribution, several qualitative observations may be made concerning the accuracy of the results. It should be noted that the calculations for

the pressure are based on the displacement of the surfaces of the solid bodies from their undeformed states, rather than on the film thickness itself. From equation (4), since $h_o(x)$ is known from geometry, and γ is a constant, the magnitude of the absolute error in total displacement u_2-u_1 is approximately the same as the error in the film thickness. Consequently, near the center of the EHD zone, where the film thickness is small but the surface deformation is large, a small relative error in film thickness results in a yet smaller relative error in the displacement. Hence, the pressure calculated in that portion of the EHD zone where deformations are large is expected to be quite accurate. Conversely, in the inlet region of the EHD zone, where the pressure is building up gradually from zero, the film thickness is large due to the undeformed geometry, while the displacements are small because of the lower pressure. Therefore, a small relative error in film thickness in the inlet region may result in a large relative error in displacement, so that the pressure calculated in this region is somewhat less reliable. Because of this, it is sometimes beneficial to introduce additional information in this region by requiring that the pressure gradient at $x = -a$ vanish. This is a consequence of the fact that the pressure is generated by the hydrodynamic action of the fluid, and has the effect of introducing an additional equation into the set to be solved; i.e. from equation (30), $\left.\frac{dp}{dx}\right|_{x=-a} = 0$ implies that

$$\sum_{n=0}^{K-1} (-1)^n \frac{2n+1}{2} p_n + \sum_{n=1}^{L} (-1)^n n q_n = 0 \quad . \tag{49}$$

This procedure tends to offset somewhat the effect of errors in the inlet region, and to aid in the convergence of the series.

Because of the method by which pressures are calculated, an error in film thickness which is constant in magnitude throughout the EHD zone has no effect on the calculated pressures. Such an error has the character of a rigid body translation of one of the solid surfaces, and is therefore absorbed in the normal separation constant, γ, of equation (4), leaving the displacement field, and hence the pressure, unaffected. Consequently, the range of film thickness errors encountered, rather than their magnitudes, determines the accuracy of the calculated pressure distribution.

Test Cases and Evaluation

In order to test the procedures described above, and to evaluate the effects of certain types of errors in the input data, a number of test cases were run. The computer program used to calculated the pressure distribution by solution of equations (44), (45) and (49) is listed in Appendix C.

In the first test case, the following step pressure distribution was employed:

$$p(x) = \begin{cases} 0 , & -\infty < \hat{x} < -x_o \\ p_o , & -x_o < \hat{x} < x_o \\ 0 , & x_o < \hat{x} < \infty \end{cases} \qquad (50)$$

where $\hat{x} = 0$ is the contact point of the undeformed surfaces.

Closed-form solutions for the displacements of the half-plane and cylinder for this pressure distribution were obtained from equations (18) and (29). These displacements were then used to generate film thickness data to obtain a series expression for the pressure of the form of equation (30), which could then be evaluated by comparison with the given pressure distribution, equation (50). The calculated pressure curve which resulted is shown in Figure 8, which represents equation (30) with ten terms included, and $a = 1.3\ x_o$ with $x = \hat{x}$. The major disagreement between this result and equation (50) occurs near $x = \pm\ x_o$, where there is a discontinuity in the pressure field; this is to be expected due to the nature of the series, and is not considered a serious drawback since such discontinuities are not expected in a fluid film. Note that the selection of $a = 1.3\ x_o$ results in small negative pressures near the inlet and outlet.

As a second test case, the film thickness was taken as zero over the region $-x_o < \hat{x} < x_o$; as before, $\hat{x}$ is the position measured from the contact point in the undeformed configuration. This is the case of two solid bodies in contact over the region, for which the pressure distribution should approximate the Hertzian semi-elliptic distribution [9]. This case served as a test of not only the computational method, but of the equations forming the basis of the method as well. The results are shown in Figure 9 for nine terms in the series of equation (30), with a and $x = 0$ chosen such that the pressure is forced to zero at $\hat{x} = -\ 1.33\ x_o$ and $\hat{x} = 1.1\ x_o$. The agreement is good except near $\hat{x} = \pm\ x_o$ where there is a discontinuity

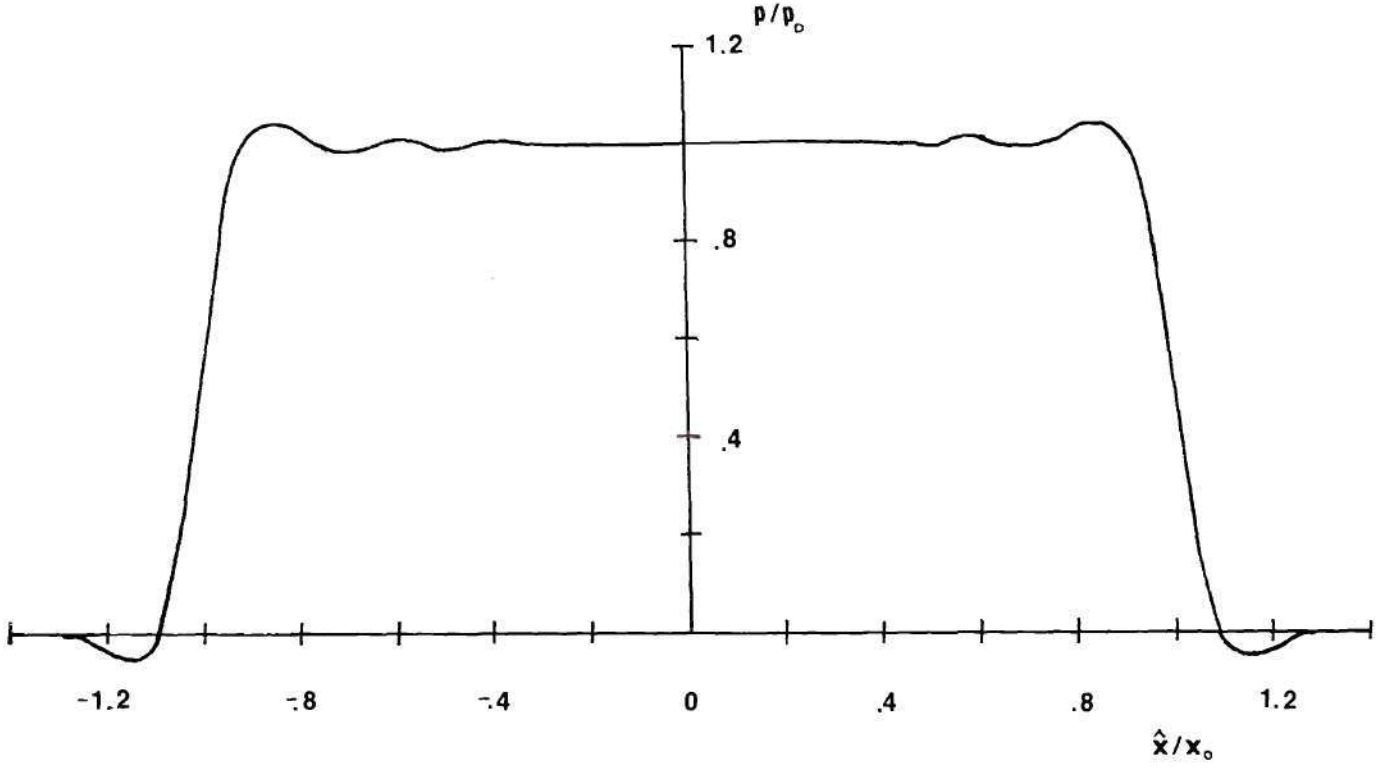

Figure 8. Test Case 1 - Uniform Pressure Distribution

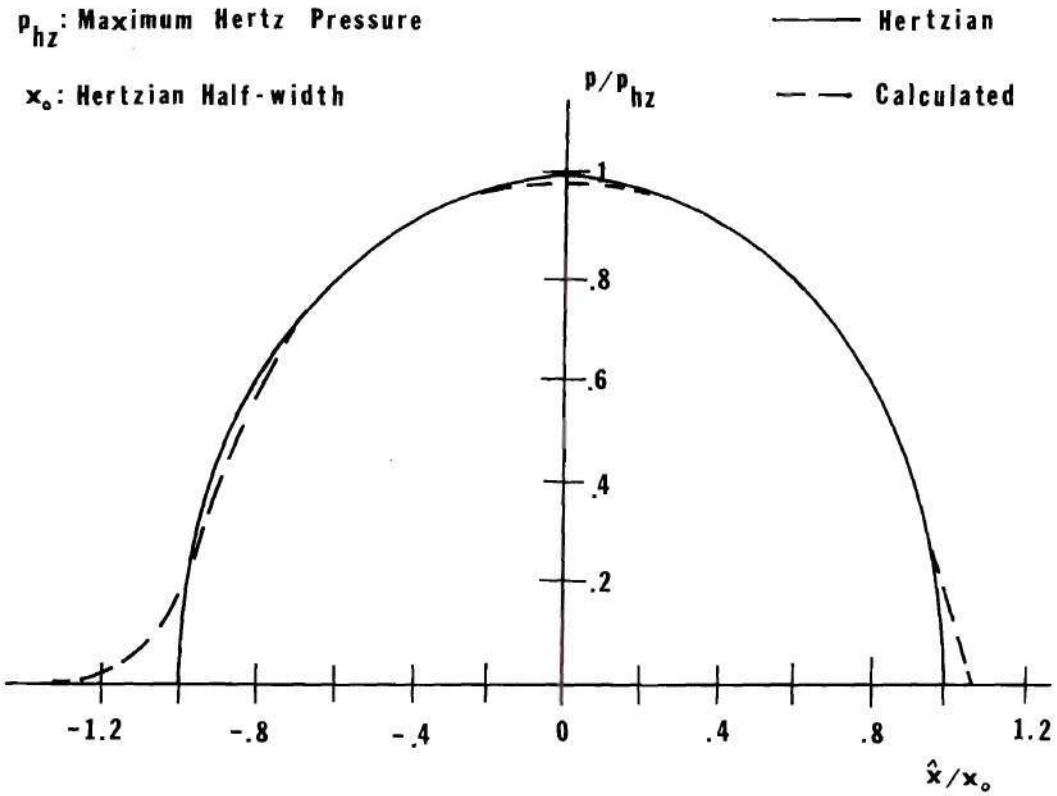

Figure 9. Test Case 2 - Hertzian Contact

in the pressure gradient. In the presence of such a discontinuity, inaccuracy in the series expansion is to be expected, since equation (30) implies continuous derivatives.

A third test case was examined using a pressure distribution expressed by a third-degree polynomial, shown in Figure 10. As in the first case, a closed-form expression for the displacement field on the surfaces was obtainable, and the resulting film thickness profile is shown in Figure 10 also. The values of total load, elastic constants of the solids, cylinder radius, and minimum film thickness were selected so as to approximate those of an actual two-dimensional EHD zone [35]. As in the first test case, the calculated film thickness was used to obtain a series solution for the pressure. When the inlet and outlet points ($x = \pm a$) were specified correctly, the series expression for the pressure showed negligible deviation from the polynomial expression throughout the pressure region. Because the pressure distribution of Figure 10 in some ways resembles that expected in an EHD region, this test case was examined further in order to study the effects of certain types of errors. It is estimated that, using the optical interference method of measuring film thickness, the maximum error in film thickness at a given location is approximately .025 μm [36]. Accordingly, three sets of randomly-generated errors in the range (-.025, .025) μm were introduced into the film thickness input. This was considered to be a fairly severe test, because in actuality the errors would most likely be distributed in a Gaussian fashion over the range (-.025, .025) μm; the introduced errors were uniformly

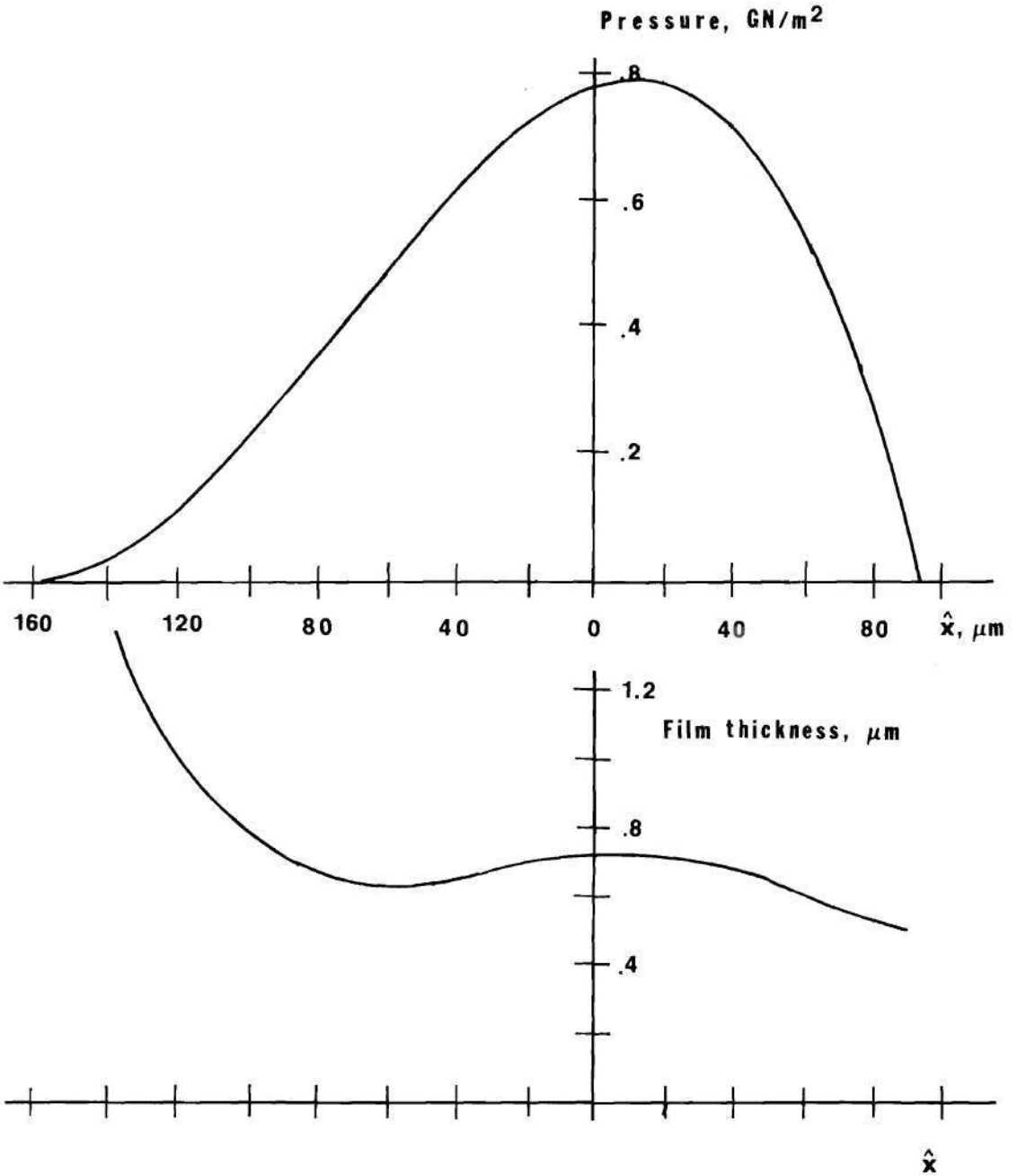

Figure 10. Test Case 3 - Polynomial Pressure Distribution

distributed over this range. The pressure distributions calculated from film thickness data with these three sets of errors introduced are shown in Figure 11. Sets 1 and 3 show the largest errors on the side corresponding to the inlet of the EHD region, as might be expected from the previous discussion. The general shape of the pressure distribution is preserved in all three cases shown in the figure.

The effects of errors in location of the beginning and end of the pressure were also examined. The results of varying the point of zero pressure at the inlet of the EHD zone are shown in Figure 12. When the inlet point is located too far in, a hump in the calculated pressure appears, and convergence of the series becomes somewhat slower. The presence of these conditions indicates that the inlet point should be moved further out. When the inlet point is located too far out, the calculated pressure comes in at zero up to the true inlet, and blends into the exact distribution. When the change in pressure near the inlet is more abrupt, however, as in Figure 8, negative pressures may result if the inlet point is set too far out. Since the locations of zero pressure are not known ahead of time, these conclusions may be helpful in locating the inlet point when calculating the pressure distribution. Similar conclusions may be drawn concerning the location of the outlet point. However, the determination of this point in an actual EHD region is generally less of a problem; near the outlet of the EHD zone, the film constricts, and the pressure distribution must go to zero in the vicinity of this exit constriction.

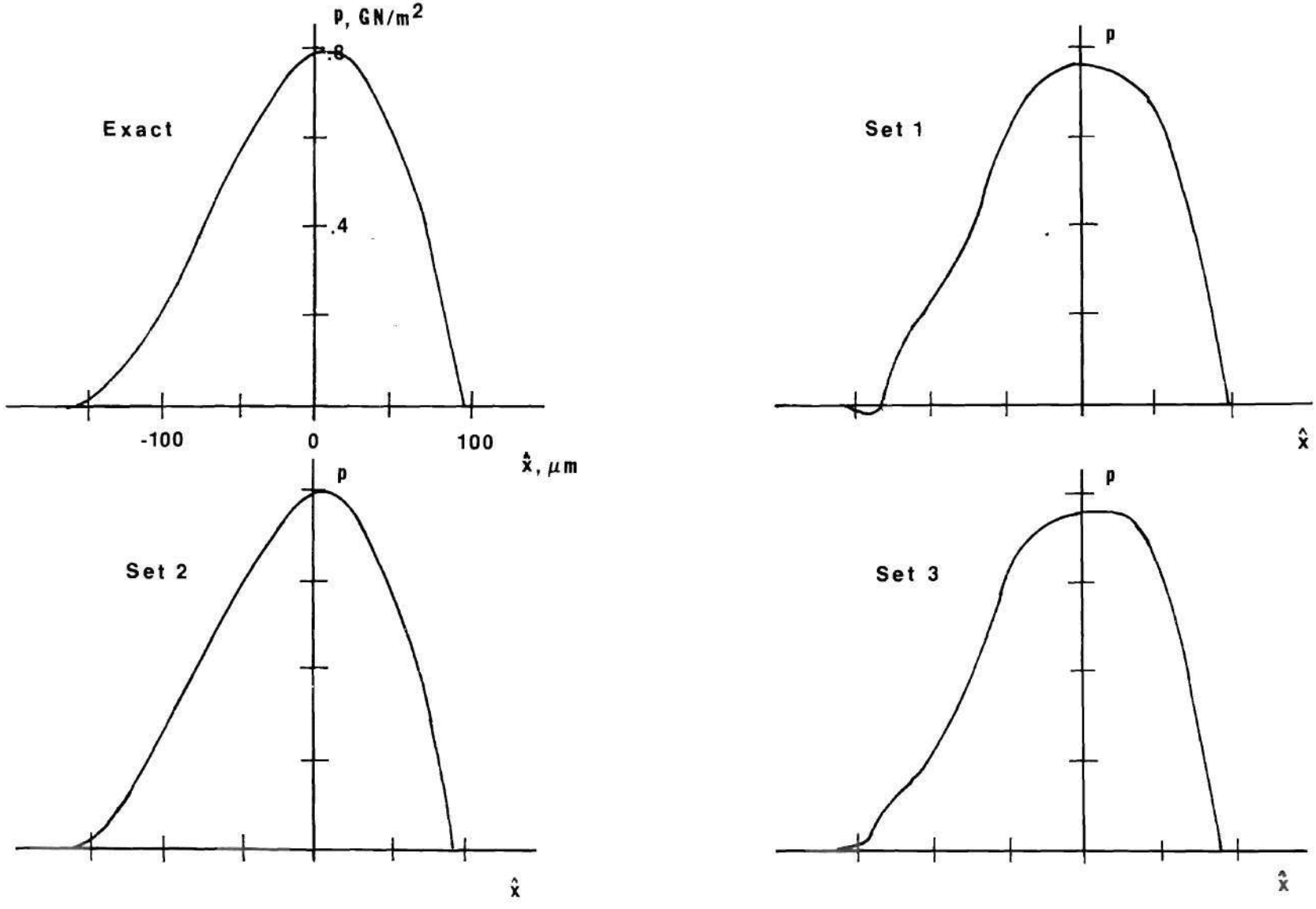

Figure 11. Test Case 3 - Random Errors Introduced in to Film Thickness Values

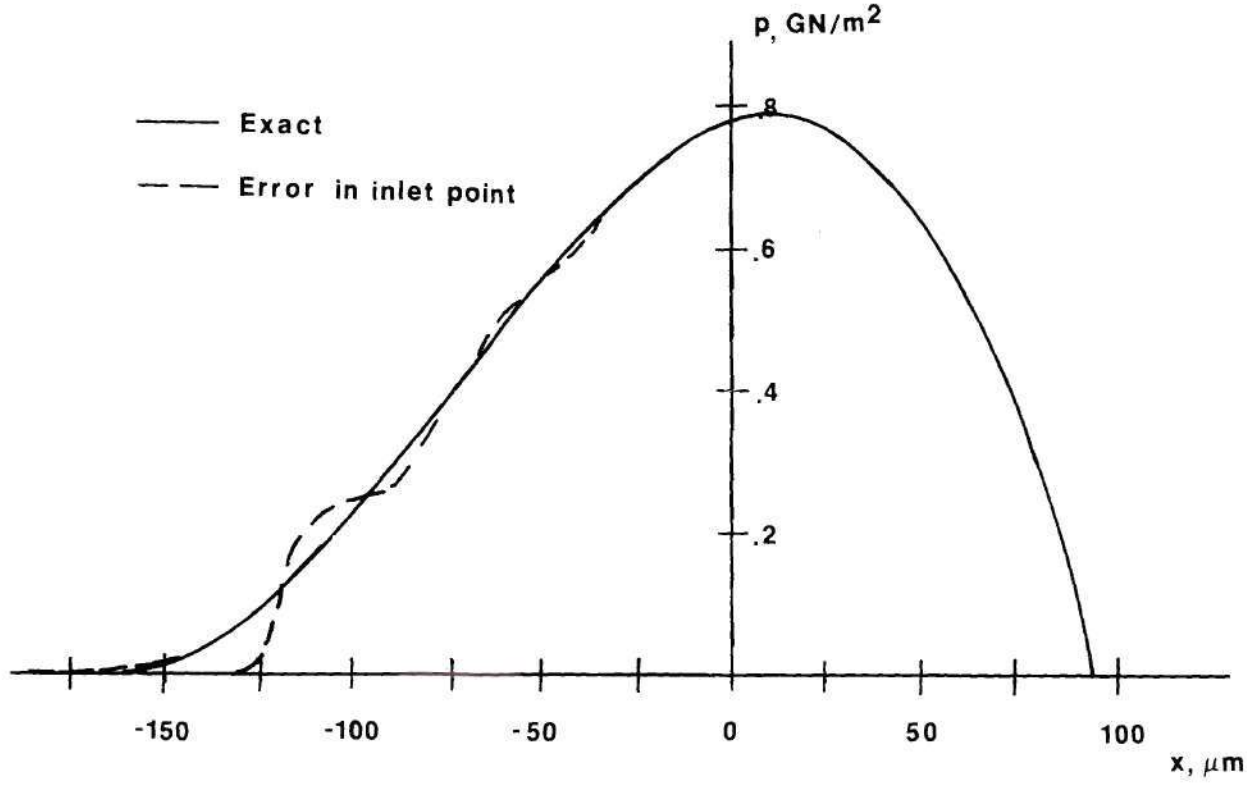

Figure 12. Test Case 3 - Errors Introduced into Location of Inlet Point

In addition, small (three percent) errors were introduced in the elastic constants, the total load, and the radius of the cylinder. The calculated pressure distribution was found to be relatively insensitive (approximately one percent error) to such errors in the elastic constants and the load, and somewhat more sensitive to errors in the radius. This is not considered a serious drawback, since the radius may be measured to a relatively high degree of precision.

At present, accurate data for the film thickness in an actual EHD zone are not available to this author. However, the tests just described were designed to examine the feasibility of the method and to provide an indication of the effects which expected errors might have on the accuracy of the computed pressure distribution.

Wymer and Cameron [35] show measured two-dimensional film thickness profiles, but from their published figures, it is possible to determine the film thickness only to within .05-.07 μm at a given location in the EHD zone. Nevertheless, a pressure distribution was calculated based on these published measurements, and the results shown in Figure 13 where it is compared with a Hertzian pressure distribution. The film thickness profile obtained from [35] is also shown in the figure. It was noted that the residuals which resulted were quite large (as much as .05 μm) near the exit region. In this region, the magnitude of the slope of the film thickness profile is quite large, which increases the difficulty in reading the points from the figures in [35]. Because of the large residuals near the exit, and the inaccuracy of the input data used, the pressure distribution of

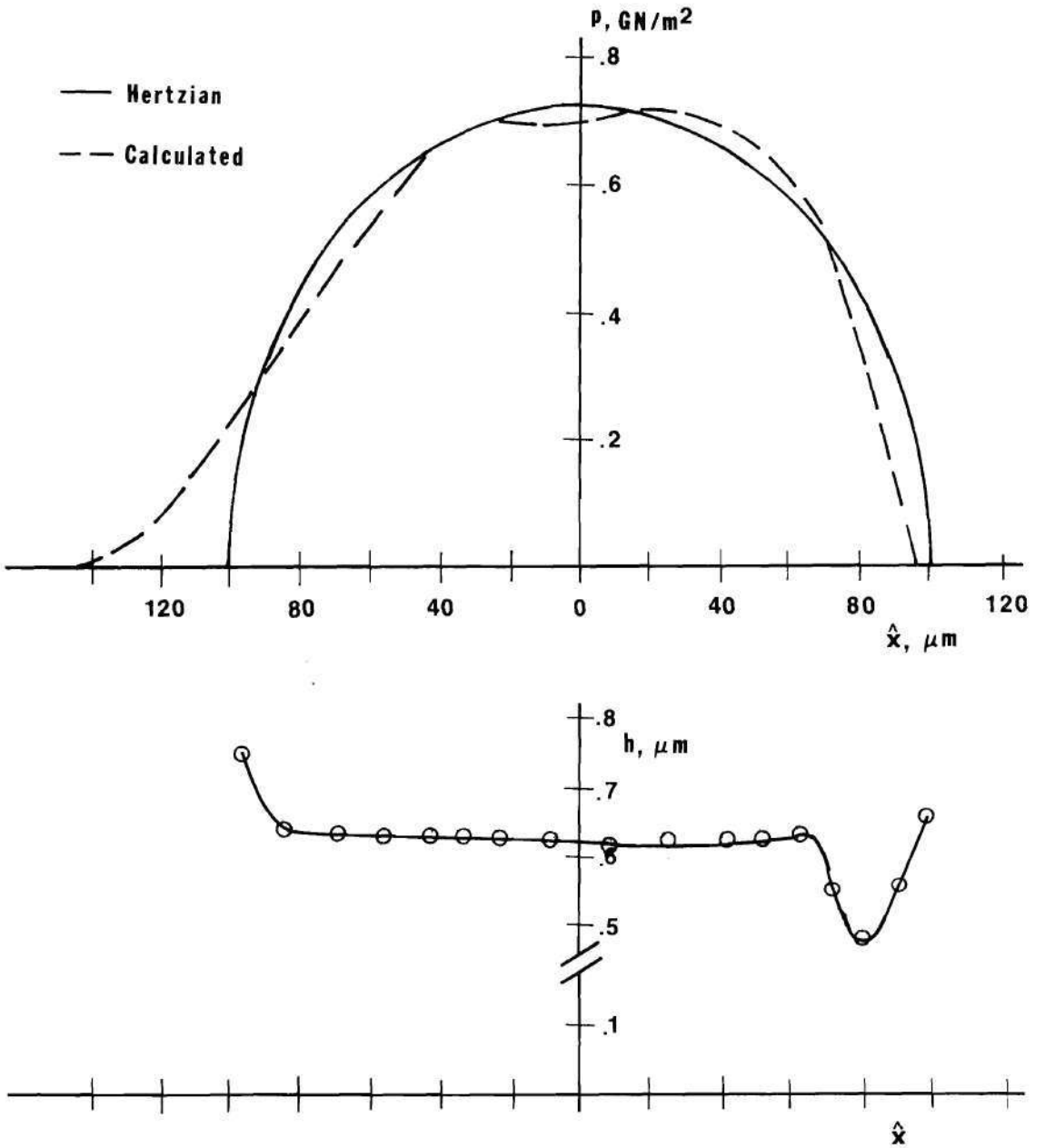

Figure 13. Calculations Based on Experimental Film Thickness Measurements [35]

Figure 13 should be viewed as a rather rough approximation of the true pressure.

The results of this section indicate that the method for determining the pressure distribution in a two-dimensional EHD process as developed in this chapter is a feasible one. The information required to perform the calculation includes the elastic constants and dimensions of the solid bodies, the total normal load applied to the system, and the film thickness as a function of position, measured to a sufficient degree of precision. The computer program listed in Appendix C may be used to calculate the pressure distribution from the required information.

CHAPTER IV

THE THREE-DIMENSIONAL CASE

The present chapter deals with the pressure distribution generated in the EHD region formed by the conjunction of a sphere and a half-space. As in the previous chapter, the solutions from linear elasticity for a sphere and a half-space acted on by an arbitrary pressure distribution will be obtained, and the appropriate surface deformations will be determined. As before, these expressions will then be used to generate the relationship between the measured film thickness profile and the EHD pressure field.

Solutions from Three-Dimensional Elasticity

The problems of the elastic sphere and the elastic half-space subjected to an arbitrary normal surface traction may be formulated in terms of the Boussinesq-Papkovich potentials [37,38]. The equilibrium equation, in terms of displacements, for an isotropic, homogeneous, linearly elastic medium in the absence of body forces, is

$$\nabla^2\bar{u} + \frac{1}{1-2\nu}\nabla\nabla\cdot\bar{u} = 0 \tag{51}$$

where ν is Poisson's ratio for the material. It can be shown (see Appendix D) that a general solution to equation (51) may be obtained in terms of displacement potentials ϕ and $\bar{\psi}$ by expressing the

displacement vector as

$$2G\bar{u} = \nabla(\phi + \bar{r} \cdot \bar{\psi}) - 4(1 - \nu)\bar{\psi} \quad , \tag{52}$$

where G is the shear modulus, and provided that ϕ and $\bar{\psi}$ are harmonic; i.e.,

$$\nabla^2\phi = 0 \quad ; \quad \nabla^2\bar{\psi} = 0 \quad . \tag{52}$$

Hence, the three-dimensional elasticity problem becomes that of determining the harmonic functions ϕ and $\bar{\psi}$ such that given boundary conditions on stress and/or displacement are satisfied. For the general three-dimensional problem, four harmonic functions must be obtained - the scalar function ϕ and three cartesian components of the vector function $\bar{\psi}$. Eubanks and Sternberg [39] prove that, under certain circumstances, any one of these four functions may be taken as zero without affecting the completeness of the solution. Furthermore, for a problem possessing torsionless axisymmetry, it has been shown [39] that the components of $\bar{\psi}$ in the plane perpendicular to the axis of symmetry may be set equal to zero without loss of completeness. In this instance, the problem reduces to finding two harmonic scalar functions - ϕ and the component of $\bar{\psi}$ in the direction of the axis of symmetry.

The Half-Space

The problem of a concentrated load acting normal to the surface of an elastic half-space is treated in most elasticity texts [9,38], and was first solved by Boussinesq. The potential functions ϕ and $\bar{\psi}$ obtained in the case of a concentrated load of unit magnitude acting at the origin O', normal to the surface of the half-space $Z < 0$

(Figure 14) is given by [38]

$$\phi = -\frac{1-2\nu}{2\pi} \ell n\,[(\rho^2 + Z^2)^{1/2} - Z]$$

$$\bar{\psi} = \frac{1}{2\pi(\rho^2 + Z^2)^{1/2}}\,\hat{k}$$

where ρ is the cylindrical coordinate measured from O' (Figure 14), and $\hat{k}$ is the unit vector in the Z-direction. As observed above, the only non-zero component of the vector potential $\bar{\psi}$ is that in the Z-direction, due to axisymmetry of the body and loading.

For the case of a concentrated normal load applied at an arbitrary point on the surface, the potentials ϕ and $\bar{\psi}$ may be expressed in terms of the system with origin at the fixed point O by a simple coordinate translation. The resulting expression is

$$\phi = -\frac{1-2\nu}{2\pi} \ell n[(\rho^2 + z^2)^{1/2} - z]$$

$$\bar{\psi} = \frac{1}{2\pi(\rho^2 + z^2)^{1/2}}\,\hat{k} \qquad (54)$$

where, in terms of the fixed coordinate system of Figure 14,

$$\rho = [r^2 + R^2 - 2r\,R\,\cos(\hat{\alpha} - \theta)]^{1/2} \quad . \qquad (55)$$

As in the two-dimensional case, the quantity of interest for the purpose of relating displacement to film thickness is the normal

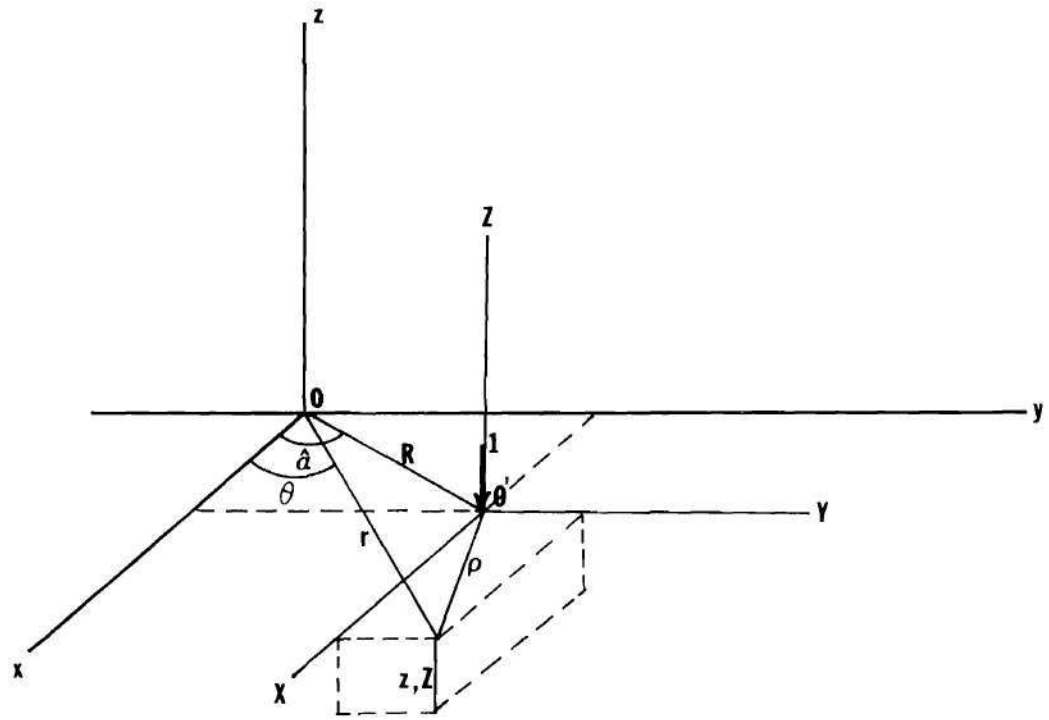

Figure 14. Half-Space Under Concentrated Load

component of displacement evaluated at the surface, $u_z(z = 0)$. This quantity may be determined by using ϕ and $\bar{\psi}$, given by equation (54), in equation (52), and evaluating the z-component of the result at the surface. The resulting expression for the vertical surface displacement is

$$u_z(r,\theta;\ R,\hat{\alpha}) = u_z\Big|_{z=0} = -\frac{1-\nu}{2G\pi}\left[r^2 + R^2 - 2r\,R\cos(\hat{\alpha} - \theta)\right]^{-1/2} \qquad (56)$$

Equation (56) is the desired solution for the surface displacement at (r,θ) due to a concentrated load of unit magnitude at the point $(R,\hat{\alpha})$.

As in the previous cases, the solution to the concentrated load problem may be used as the Green's function for this case to obtain solution for the body subjected to an arbitrary distributed load. For the half-space subjected to normal load $p(r,\theta)$ distributed over a circle of radius a centered at the origin, the surface displacement is obtained from

$$u_z(r,\theta) = \int_0^{2\pi}\int_0^a p(R,\hat{\alpha})u_z(r,\theta;\ R,\hat{\alpha})RdRd\hat{\alpha}\ ;$$

that is,

$$u_1(r,\theta) \equiv u_z(r,\theta) = -\frac{1-\nu}{2G\pi}\int_0^{2\pi}\int_0^a \frac{Rp(R,\hat{\alpha})}{\left[r^2 + R^2 - 2rR\cos(\hat{\alpha}-\theta)\right]^{1/2}}\,dRd\hat{\alpha} \qquad (57)$$

Hence, equation (57) yields the required functional relationship, in the form of equation (6), between the normal surface displacement and the pressure distribution acting on the surface. If the half-space is designated as Body 1 in Figure 2, then equation (57) gives the expression for $u_1(r,\theta)$.

The Sphere

The problem of an elastic sphere subjected to radial concentrated forces acting at its poles was solved by Sternberg and Rosenthal [40]. The displacement potentials ϕ and $\bar{\psi}$ obtaioned as the solution to the problme are expressed in [40] as the sum of two parts - a closed-form portion, ϕ_1 and ψ_1, representing terms with the appropriate singularities at the poles; and an infinite series part, ϕ_2 and ψ_2, which represent the solution to the residual problem of removing the surface stresses induced by ϕ_1 and ψ_1. The singular solution is given by

$$\phi_1 = -\frac{r_o}{2\pi}\left(\frac{1}{\rho_1}+\frac{1}{\rho_2}\right) + \frac{3(3-4\nu)}{8\pi r_o}\left[\rho_1(c_1\omega_1-1) - \rho_2(c_2\omega_2+1)\right]$$

$$- \frac{(1+12\nu-16\nu^2)(1-\nu)}{16\pi r_o^2}\left\{\rho_1^2[(1-3c_1^2)\omega_1 + c_1^2 + 3c_1 - 1]\right.$$

$$\left. + \rho_2^2\,[(1-3c_2^2)\omega_2 + c_2^2 - 3c_2 - 1]\right\} \qquad (58)$$

$$\psi_1 = -\frac{1}{2\pi}\left(\frac{1}{\rho_1} - \frac{1}{\rho_2}\right) + \frac{(1-2\nu)}{2\pi r_o}(\omega_1-\omega_2)$$

$$+ \frac{(1+12\nu-16\nu^2)}{8\pi r_o^2}[\rho_1(c_1\omega_1-1) + \rho_2(c_2\omega_2+1)]$$

where ρ_1, ρ_2, r_o, θ_1 and θ_2 are as shown in Figure 15, and

$$c_1 = \cos\theta_1 \quad ; \qquad c_2 = \cos\theta_2 \quad ;$$

$$\omega_1 = \ell n \frac{\rho_1(1+c_1)}{r_o} \quad ; \qquad \omega_2 = \ell n \frac{\rho_2(1-c_2)}{r_o}$$

The solution to the residual problem is

$$\phi_2 = \sum_{n=1}^{\infty} a_n \rho_o^{2n} P_{2n}(c) + \sum_{n=0}^{\infty} b_n(2n-2-4\nu)\rho_o^{2n+2} P_{2n+2}(c)$$

$$\psi_2 = -\sum_{n=0}^{\infty} b_n(4n+3)\rho_o^{2n+1} P_{2n+1}(c) \qquad (59)$$

where

$$c = \cos\theta_o$$

$$a_n = \frac{(4n^2 + 4n - 1 + 2\nu)\xi_{2n} + (2n+1)(4n^2 - 2n - 2 - 2\nu)\eta_{2n}}{2(2n-1)[4n^2 + 2(1+2\nu) + 1 + \nu]r_o^{2n-2}}$$

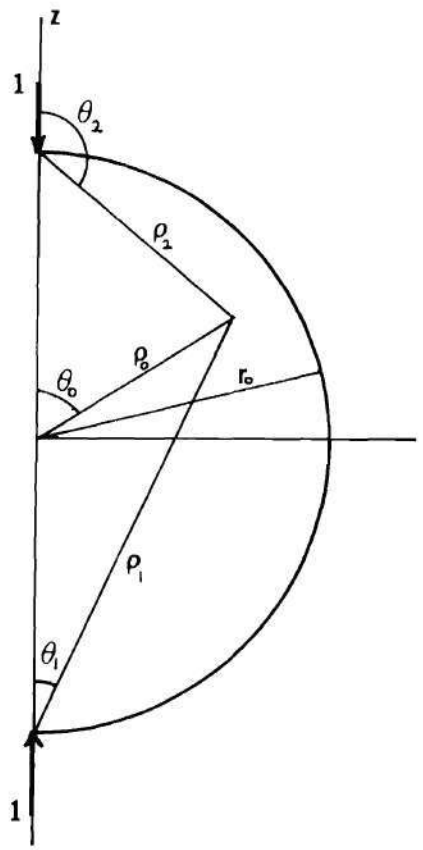

Figure 15. Definition of Some Geometrical Quantities for the Sphere

$$b_n = \frac{\xi_{2n} + 2n\,\eta_{2n}}{2[4n^2 + 2(1+2\nu)n + 1 + \nu]r_o^{2n}}$$

$$\xi_{2n} = \frac{1}{4\pi r_o^2} \frac{24(1+2\nu-4\nu^2)n^2 + 8(-2+7\nu+8\nu^2-16\nu^3)n-(1+\nu)(1+12\nu-16\nu^2)}{n(n-1)(4n-1)(4n+3)}$$

$$\eta_{2n} = \frac{1}{8\pi r_o^2} \frac{-16(1+\nu)(1+12\nu-16\nu^2)n^2-36(1+2\nu-4\nu^2)n + (31+2\nu-124\nu^2+80\nu^3)}{n(n-1)(4n-1)(4n+3)(2n+1)} \tag{60}$$

and $P_n(c)$ is the Legendre polynomial of degree n. The solution to the problem of a sphere acted on by unit normal forces at its poles is given by the sum of the singular and residual solutions,

$$\phi = \phi_1 + \phi_2$$

$$\bar{\psi} = (\psi_1 + \psi_2)\,\hat{k} \tag{61}$$

For the problem of the concentrated normal load acting at an arbitrary surface point, a coordinate transformation must be made, as was the case in the problem of the half-space. Hence, equation (61) gives the solution referred to the XYZ coordinate system of Figure 16, and the two angles α_o and β_o defined the location of the concentrated load with respect to the fixed xyz axes. In order to express ϕ and $\bar{\psi}$ in terms of the fixed xyz system, a coordinate rotation would be necessary. The operation is a straightforward one, but has the effect that the displacement potential $\bar{\psi}$ has three non-zero components when

expressed in the fixed coordinate system. Components of the displacement vector $\bar{u}$ could then be obtained from equation (52). However, because the above operation is a lengthy one due to the complexity of the expressions for ϕ and $\bar{\psi}$, and because only the radial component of surface displacement is required, an alternate procedure was adopted. The radial surface displacement was obtained for the concentrated loads applied at the poles, Figure 15, by using equations (61) in equation (52). The radial surface displacement for the concentrated load applied at an arbitrary boundary point was then obtained by a coordinate rotation as in Figure 16. Hence, rather than transforming the displacement potentials directly, and thus generating three components of $\bar{\psi}$, the desired displacement was obtained first and then expressed in terms of the fixed xyz system.

In order to accomplish this, the singular and residual solutions were treated separately. The singular portion of the radial surface displacement was obtained using bipolar coordinates, with the poles of the coordinate system coinciding with the points of load application. At the surface of the sphere, the radial direction coincides with one of the bipolar coordinate directions, $\hat{e}_2$. Some details of the coordinate system used are given in Appendix E. Consequently, the $\hat{e}_2$-component of the displacement vector was determined using equations (58) in equation (52), and evaluated at the sphere's surface. The resulting expression for the radial surface displacement, after a considerable amount of algebra, is

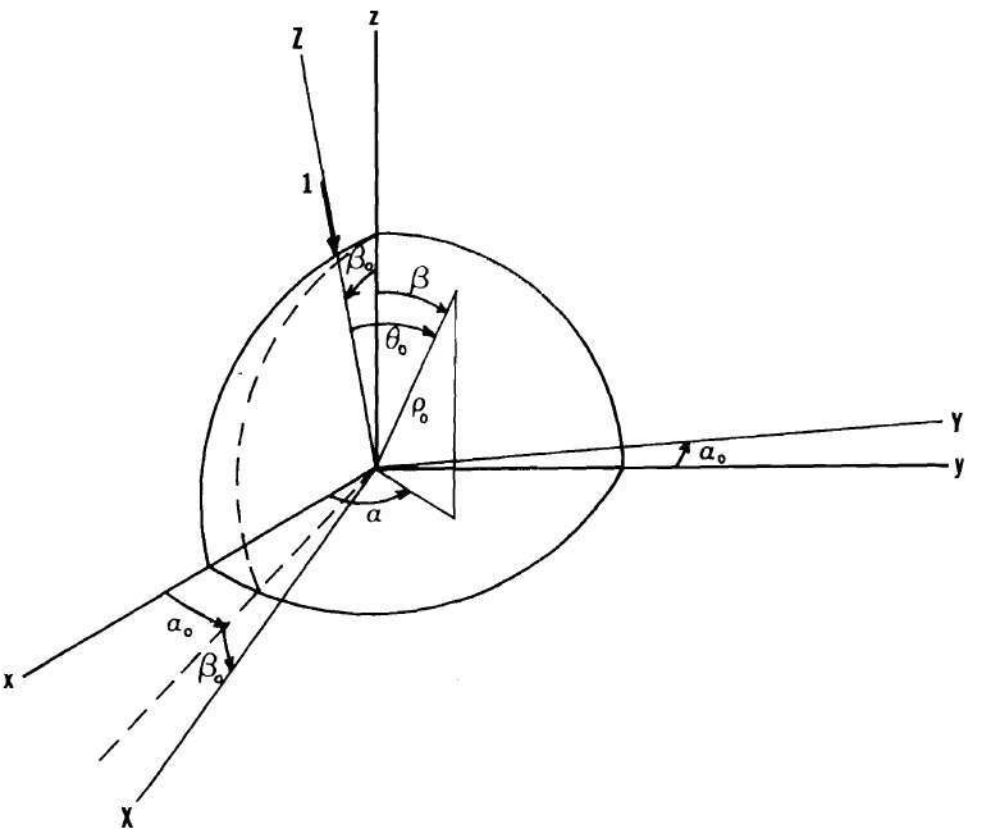

Figure 16. Sphere Under Concentrated Load

$$u_{r_1} = -\frac{1}{16G\pi r_o}\Big\{(1 + 12\nu - 16\nu^2)[(1+\nu)(s^2\,\bar{\omega}_o - 2s\sqrt{1+s}) - 2\nu\,\bar{\omega}_o$$

$$- 2\nu\,cs\,\bar{\omega}_1 + (3-\nu)s^2] + 4(1-2\nu)^2\,c\bar{\omega}_1 - 4(6 + 11\nu - 36\nu^2 + 16\nu^3)$$

$$+ 4\sqrt{1+s}\;\;[2(1-\nu)/s\;\; + (3 + 8\nu - 16\nu^2)]\Big\} \qquad (62)$$

where

$$\bar{\omega}_o = \ell n\,\frac{s}{4}\,(2 + s + 2\sqrt{1+s})$$

$$\bar{\omega}_1 = \ell n\,\left[\frac{2-s-\alpha\sqrt{1-s}}{s}\right]$$

$$s = \sin\theta_o \qquad c = \cos\theta_o$$

and θ_o is defined as in Figure 15.

The residual portion of the radial surface displacement was obtained using spherical polar coordinates (See Appendix E). The radial component of the displacement vector was obtained using equations (61) in equation (52) and evaluated at the surface of the sphere ($\rho_o = r_o$). The results of this computation are

$$u_{r_2} = \frac{1}{2G}\Big\{\sum_{n=1}^{\infty} a_n\,2n\,r_o^{2n-1}\,P_{2n}(c)$$

$$+ \sum_{n=0}^{\infty} 2b_n(2n+1)(-n+1-2\nu)r_o^{2n+1}\,P_{2n}(c)\Big\} \qquad (63)$$

where a_n and b_n are given by equations (60).

Hence, the radial component of the displacement at the surface of the sphere is the sum of the singular and residual contributions,

$$u_r = u_{r_1} + u_{r_2} \tag{64}$$

Note that the result, as expected due to the axisymmetry of the problem, depends only on θ_o, the angle measured from the line connecting the point of application and the center of the sphere.

In order to express the radial displacement in terms of the fixed xyz reference system, with the load applied at an arbitrary point defined by angles α_o and β_o (Figure 16), a transformation equation for this coordinate rotation must be obtained. It should be pointed out that, since the transformation involves only a rotation about the center of the sphere, a line directed toward the origin coincides with the radial direction in both coordinate systems shown. Hence, to express the radial surface displacements referred to the fixed reference system, it is necessary only to express θ_o in equation (64) in terms of α, β, α_o, and β_o. It may be shown that the required transformations are

$$c = \sin\beta \sin\beta_o \cos(\alpha - \alpha_o) + \cos\beta \cos\beta_o$$

$$s = [\sin^2\beta \cos^2\beta_o \cos^2(\alpha-\alpha_o) - 2 \sin\beta \cos\beta \sin\beta_o \cos\beta_o \cos(\alpha-\alpha_o) + \cos^2\beta \sin^2\beta_o + \sin^2\beta \sin^2(\alpha-\alpha_o)]^{1/2} \quad . \tag{65}$$

These relations, used in equation (64), yield the radial component of displacement at a point on the sphere due to a unit normal load applied at an arbitrary surface location; i.e., the result is $u_r(\alpha, \beta; \alpha_o, \beta_o)$, where (α,β) determine the point under consideration, and (α_o,β_o) locate the point of application of the load.

As before, this result may be used as the Green's function to determine the radial surface displacement due to a distributed normal load $p(\alpha,\beta)$ acting over the region $0 < \alpha < 2\pi$, $0 < \beta < \beta_1$. This may be expressed in integral form as

$$u_2(\alpha,\beta) \equiv - u_r(\alpha,\beta) = - r_o^2 \int_0^{2\pi} \int_0^{\beta_1} p(\alpha_o,\beta_o) u_r(\alpha,\beta; \alpha_o,\beta_o) \sin\beta_o d\beta_o d\alpha_o \tag{66}$$

where $r_o^2 \sin\beta_o d\beta_o d\alpha_o$ is the differential element of surface area. Since the sphere is labelled as Body 2 in Figure 2, then the normal surface displacement given by equation (66) is appropriately designated as $u_2(\alpha,\beta)$.

Equation (66) provides the required functional relationship, in the form of equation (6), between the surface displacement and the pressure distribution for the sphere. Hence, equations (57) for the half-space and (66) for the sphere yield the relations necessary for relating the pressure distribution to the film thickness for the three-dimensional EHD problem.

Surface Displacement for an Arbitrary Pressure Distribution

Figure 17 shows schematically the conjunction of the sphere and

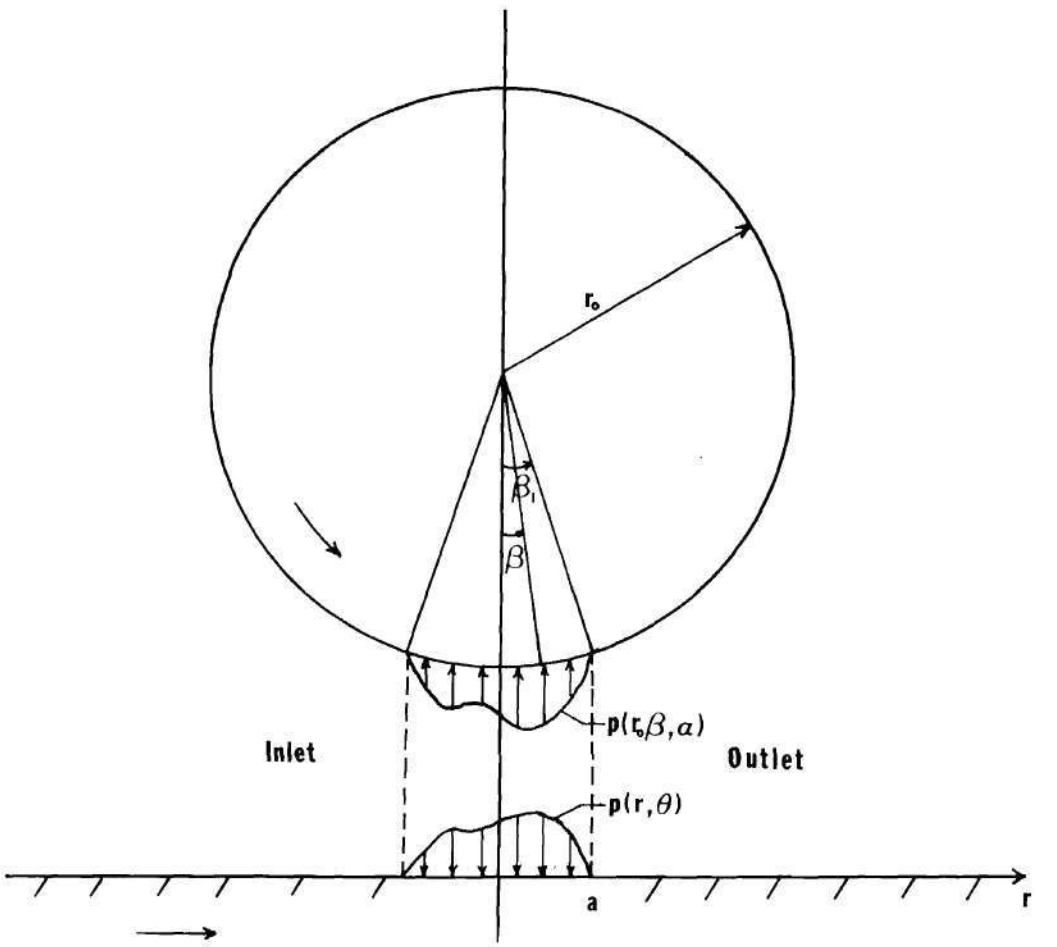

Figure 17. The Conjunction of the Sphere and the Half-Space in the EHD Zone

the half-space in the EHD zone, in which the film plane is perpendicular to the plane of the figure. As in the two-dimensional case, the pressure is assumed constant through the film thickness. Because the distance a, representing the extent of the EHD region, is much smaller than r_o, the radius of the sphere, the point (r,θ) on the surface of the half-space corresponds to the point (β,α) on the sphere's surface; i.e.,

$$r = r_o\beta \quad ; \qquad \theta = \alpha \; ; \qquad a = r_o\,\beta_1 \tag{67}$$

are the relations between corresponding surface points on the two bodies. The quantities a and β_1 define the extent of the circular EHD pressure region. Figure 18 shows the EHD region on the sphere and half-space, where the film plane is parallel to the plane of the figure.

As in the previous two-dimensional case, it is desirable to express the pressure distribution $p(r,\theta)$ acting on both bodies in series form. The desired series should be zero on the boundary of the EHD zone, and consist of a complete set of functions of position in the EHD region. The following series in the form suggested in [41], satisfies these requirements,

$$p(x,y) = \left(1 - \frac{x^2}{a^2} - \frac{y^2}{a^2}\right)[a_o + a_1x + a_2y + a_3x^2 + a_4xy + a_5y^2 + \ldots]$$

This series may be expressed in terms of coordinates (r,θ) for the half-space (which are related to coordinates (β,α) for the sphere by equation (67)). Because of the symmetry of the flow geometry about the line $\theta = 0$, all anti-symmetric terms may be dropped, and the resulting

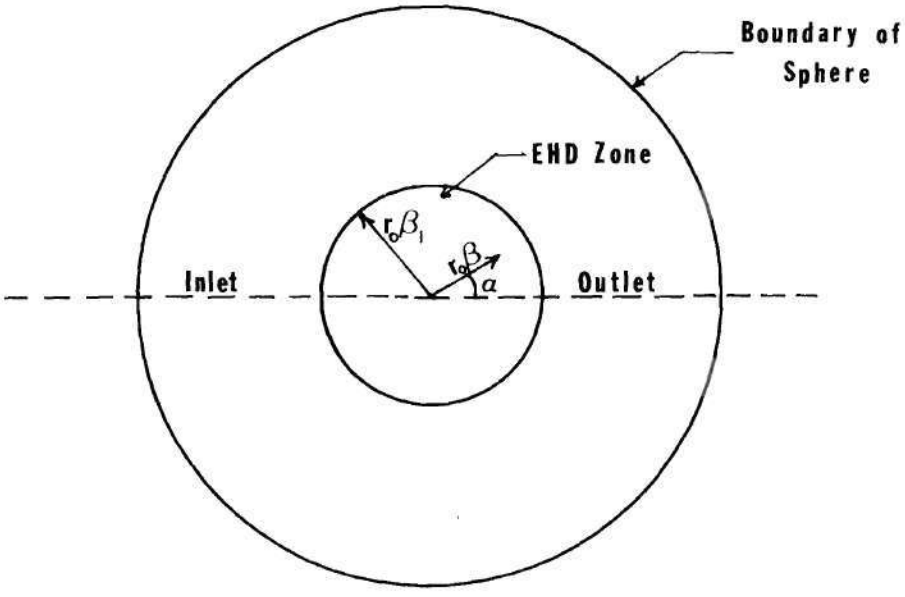

a) The EHD Zone on the Surface of the Sphere

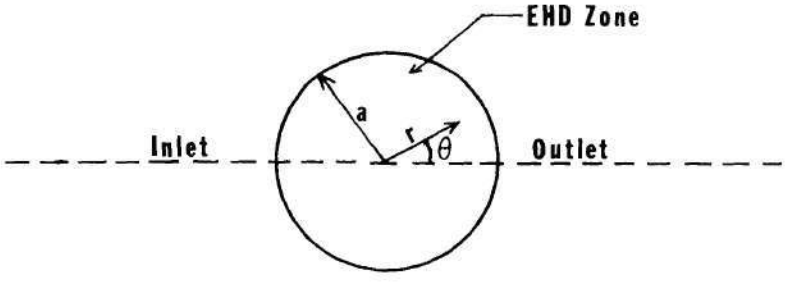

b) The EHD Zone on the Surface of the Half-Space

Figure 18. The EHD Region for the Sphere and Half-Space

series expressed in the form

$$p(r,\theta) = \left(1 - \frac{r^2}{a^2}\right)\left[p_0 + p_1 \frac{r}{a}\cos\theta + p_2 \frac{r^2}{a^2} + p_3 \frac{r^2}{a^2}\cos^2\theta + p_4 \frac{r^3}{a^3}\cos\theta \right.$$

$$+ p_5 \frac{r^3}{a^3}\cos^3\theta + p_6 \frac{r^4}{a^4} + p_7 \frac{r^4}{a^4}\cos^2\theta$$

$$\left. + p_8 \frac{r^4}{a^4}\cos^4\theta + \ldots\right] \quad . \tag{68}$$

The factor $\left(1 - \frac{r^2}{a^2}\right)$ forces the condition that the pressure be zero on the boundary to the EHD zone, while allowing the normal derivative to be finite there. The series in brackets is symmetric about the line $\theta = 0$. This series expression for the pressure may be used in equations (57) and (66) to obtain, once the indicated integrations are performed, the relations between the surface displacement and the unknown pressure coefficients p_i, in the form of equation (8). The required integrations themselves are quite involved, and no closed-form expression was obtained for them, contrary to the two-dimensional case of Chapter III. The integrals were evaluated numerically, and certain consideration involved in their evaluation follow.

Clearly, the integral indicated in equation (66) promises to be a difficult one to evaluate, due to the complexity of the expression for u_r given by equations (62) - (64), and of the transformation equations (65). Some simplification is possible for the specific case under consideration, however. The extent of the EHD

region itself is extremely small compared to the radius of the sphere. Hence, β_1 is a small quantity (on the order of .01 radians), as is β_o in the integrand. Since the main concern here is in the surface displacement in the neighborhood of the EHD region, the coordinate β is of the same order of magnitude as β_1 and β_o in the region of interest. Consequently, subject to these restrictions on the magnitudes of β, β_o, and β_1 for use in the EHD problem, the transformation equations (65) may be approximated by

$$c = 1 - \frac{1}{2}(\beta^2 + \beta_o^2) + \beta\beta_o\cos(\alpha-\alpha_o)$$

$$s = [\beta^2 + \beta_o^2 + 2\beta\beta_o\cos(\alpha-\alpha_o)]^{1/2} \qquad (69)$$

Based on the above order of magnitude argument, the expressions (62)-(64) may also be simplified, since s in equation (69) is of the same order as β. Equation (62), the singular part of the displacement, may be written, assuming s to be small and hence expanding certain terms such as $\sqrt{1-s}$ into their power series, as

$$\begin{aligned} u_{r_1} = -\frac{1}{16\pi r_o G}\Bigg\{ & (1+12\nu-16\nu^2)[(1+\nu)s^2 - 2\nu]\ln\frac{s}{4}(4+s) \\ & + \left[-2\nu(1+12\nu-16\nu^2)\left(s - \frac{1}{2}s^3\right)\right. \\ & \left. + 4(1-2\nu)^2\left(1 - \frac{1}{2}s^2\right)\right]\ln\frac{s}{4}\left(1+\frac{s}{4}\right) + \left[1 + \frac{37}{2}\nu - 48\nu^2 + 32\nu^3\right]s^2 \\ & + \frac{1}{4}[4 + 21\nu - 20\nu^2 - 16\nu^3]s^3 + 8(1-\nu)\frac{1}{s} - 8[1 + 2\nu - 10\nu^2 + 8\nu^3] \\ & + [3 - 9\nu - 24\nu^2 + 32\nu^3]s\Bigg\} \end{aligned} \qquad (70)$$

The various terms of equation (70) were then numerically integrated separately in integrals of the form of equation (66), with $p(\alpha_o,\beta_o) = 1$, in order to get an estimate of the relative magnitudes of their contribution to the total displacement. Based on this calculation, several terms were found to be negligible. In addition, the constant term may be deleted since it contributes only a rigid-body displacement.

A similar calculation was performed on the individual terms of the residual solution (63). Each term of the residual solution involves only a Legendre polynomial $P_n(c)$, and c is very close to 1 throughout the region of interest (equation (69)). Since $P_n(1) = 1$, it was found that the contributions of the terms of the residual solution to the total displacement differ from a constant displacement throughout the EHD zone by an negligible amount. Hence, the residual solution contributes only a rigid-body displacement (to the degree of approximation employed above) and may therefore be disregarded.

As a result of the above comparison of the contributions of the various terms to the total displacement, the resulting expression for the surface displacement of the sphere, after dropping the appropriate terms, is

$$u_r(\alpha,\beta;\alpha_o,\beta_o) = -\frac{1}{8\pi r_o G}\left[(2-9\nu-4\nu^2+16\nu^3)\ell n\ s + 4(1-\nu)\frac{1}{s}\right] \quad (71)$$

where, as before,

$$s = [\beta^2 + \beta_o^2 - 2\beta\beta_o \cos(\alpha-\alpha_o)]^{1/2} \quad .$$

Equation (71) is the approximation of equation (64) for small s, and is to be used in the integral expression of equation (66). Hence, substituting equation (71) into (66) (with the surface displacement for body 2 denoted as u_2), and using equations (67) to express the displacement in terms of r and θ, yields

$$u_2(r,\theta) = + \frac{1}{8\pi G r_o}\int_0^{2\pi}\int_0^{a} p(R,\hat{\alpha})\left\{(2-9\nu-4\nu^2+16\nu^3)\,\ell n\,\frac{[r^2+R^2-2rR\cos(\theta-\hat{\alpha})]^{1/2}}{r_o}\right.$$

$$\left. + \frac{4(1-\nu)r_o}{[r^2+R^2-2rR\cos(\theta-\hat{\alpha})]^{1/2}}\right\} RdRd\hat{\alpha} \qquad (72)$$

Consequently, equations (57) and (72), with $p(r,\theta)$ given by expansion (68) must be integrated in order to find the relation between the surface displacement and the pressure coefficients p_i. These integrals must be evaluated numerically. However, due to the integrable singularities in the integrands (when the quantity $(r^2+R^2-2rR\cos(\theta-\hat{\alpha})) = 0$), the two equations in their present form are not well-suited for numerical integration. In order to eliminate the singularities, the integrals were transformed as follows. Both equations (57) and (72) are in the form

$$I(r,\theta) = \int_0^{2\pi}\int_0^{a} f(r,\theta;R,\hat{\alpha})RdRd\hat{\alpha} \qquad (73)$$

The variables of integration $(R,\hat{\alpha})$ were transformed to variables (R_1,α_1) through the relations

$$R_1 = [R^2 + r^2 - 2Rr\cos(\theta-\hat{\alpha})]^{1/2}$$

$$\alpha_1 = \tan^{-1}\left[\frac{R\sin(\hat{\alpha}-\theta)}{r-R\cos(\hat{\alpha}-\theta)}\right] \tag{74}$$

The inverse transformation is given by

$$R = [R_1^2 + r^2 - 2R_1 r\cos\alpha_1]^{1/2}$$

$$\hat{\alpha} = \theta + \tan^{-1}\left[\frac{R_1\sin\alpha_1}{r-R_1\cos\alpha_1}\right] \tag{75}$$

Under the indicated transformation, the integrand of equation (73) becomes

$$f(r,\theta;\ R,\hat{\alpha}) \rightarrow g(r,\theta;\ R_1,\alpha_1)$$

and the integral assumes the form

$$I(r,\theta) = \int_{-\pi}^{\pi}\int_{0}^{s_0(\alpha_1)} g(r,\theta;\ R_1,\alpha_1)R_1\,dR_1\,d\alpha_1$$

where

$$s_0(\alpha_1) = r\cos\alpha_1 + a\sqrt{1 - \frac{r^2}{a^2}\sin^2\alpha_1} \tag{76}$$

This transformation has the effect of eliminating the singularity in the integrands of equations (57) and (72). Under this transformation, equation (57) becomes

$$u_1(r,\theta) = -\frac{1-\nu}{2\pi G}\int_{-\pi}^{\pi}\int_{0}^{s_0(\alpha_1)} \bar{p}(R_1,\alpha_1)\,dR_1\,d\alpha_1 \tag{77}$$

and equation (72) becomes

$$u_2(r,\theta) = \frac{1}{8\pi G r_0}\int_{-\pi}^{\pi}\int_{0}^{s_0(\alpha)}\left\{\bar{p}(R_1,\alpha)\,(2-9\nu-4\nu^2+16\nu^3)R_1 \ell n\,\frac{R_1}{r_0} + 4(1-\nu)r_0\right\} dR_1\,d\alpha_1 \tag{78}$$

where $\bar{p}(R_1,\alpha_1)$ is the transformed pressure expansion; i.e.

$$\bar{p}(R_1,\alpha_1) = p\left(\left[R_1^2 + r^2 - 2R_1 r\cos\alpha_1\right]^{1/2}, \left[\theta + \tan^{-1}\left(\frac{R_1\sin\alpha_1}{r-R_1\cos\alpha_1}\right)\right]\right) \tag{79}$$

With the integrals expressed in this form, the singularity in the integrand has been eliminated, and hence equations (77) and (78) lend themselves more readily to numerical integration. The pressure distribution $\bar{p}(R_1,\alpha_1)$ is expressed in terms of the expansion (68). Once the numerical integration has been performed, equations (77) and (78) yield the surface displacements for the half-space and the sphere, respectively, in terms of the unknown coefficients in the pressure expansion.

Determination of the Pressure Distribution in the EHD Zone

Equations (77) and (78) are related to the film thickness in the EHD zone through the use of equation (4). For the particular geometry under consideration - a sphere and a flat plate - the surface separation in the undeformed configuration, $h_o(r,\theta)$, is, from Figure 17

$$h_o(r,\theta) = r_o(1 - \cos\beta)$$

where, as before, $\beta = r/r_o$. For small values of β,

$$h_o(r,\theta) = \frac{r^2}{2r_o} \tag{80}$$

Hence if the film thickness is known at N locations (r_i,θ_i), then the film thickness equation (4) becomes

$$h(r_i,\theta_i) - \frac{r_i^2}{2r_o} = u_2(r_i,\theta_i) - u_1(r_i,\theta_i) + \gamma \ , \quad i = 1, 2, \ldots, N \tag{81}$$

where u_1 and u_2 are given by equations (77) and (78), and contain the unknown pressure coefficients p_j, $j = 0, 1, 2, \ldots, M-1$ if the series in equation (68) is truncated after M terms.

In addition, the relationship that the total pressure force must equal the applied normal load, equation (2), must be satisfied. Using the pressure expansion (68) in the total load condition and evaluating the integral yields the relation

$$P = \frac{\pi}{a^2}\left[\frac{1}{2}p_o + \frac{1}{6}p_2 + \frac{1}{12}p_3 + \frac{1}{12}p_6 + \frac{1}{24}p_7 + \frac{1}{32}p_8 + \ldots\right] \tag{82}$$

Equations (81) and (82) form a set of N+1 linear algebraic equations in the M+1 unknowns p_j and γ.

The numerical problem in the three-dimensional case is thus precisely analogous to the formulation in the two-dimensional EHD problem presented in Chapter III. Equations (81) and (82) correspond to equations (45) and (46) in the two-dimensional case. Due to the similarity of the two problems, the numerical considerations for solution of the system of equations are identical to those in Chapter III. Because of the presence of errors in the film thickness data to be used, the linear algebraic equations are once again set up as an overdetermined system, and a least-squares solution obtained through a set of equations of the form of equation (48). Furthermore, similar conclusions may be drawn concerning the expected relative magnitudes of error in the computed pressure distribution in the various regions of the EHD zone. That is, it is expected as before that errors in the inlet region where deformations are small will be greater than errors in the high-pressure region of the EHD zone where deformations tend to be larger. Once again, in an attempt to offset the higher error in the inlet region, the physical requirement that the pressure gradient be zero at the inlet point $(r,\theta) = (a,\pi)$ is introduced into the mathematical formulation of the problem. This results in the additional equation

$$p_0 - p_1 + p_2 + p_3 - p_4 - p_5 + p_6 + p_7 + p_8 - \ldots = 0 . \qquad (83)$$

A computer program was written to accept as input the film thickness at various locations in the EHD zone, and to use this information

to solve equations (81), (82) and (83) for the unknown pressure coefficients using the methods discussed above. The numerical integrations required to evaluate the coefficients of p_j were performed using Subroutine GMI, available in the CDC Math-Science Library [42]. A listing of the computer program is provided in Appendix F.

In order to test the results obtainable from this program, the film thickness was taken as zero over the circular region $x_o^2 + y_o^2 < c^2$, where $x_o = 0$, $y_o = 0$ is the point of contact in the undeformed state. This corresponds to the Hertzian case of dry contact between two non-conforming bodies, and should result in a semi-ellipsoidal pressure distribution [9]. The pressure distribution was calculated under the assumption that the pressure was exerted over the region $r < a$, with $a > c$, and the point $r = 0$ located at $x_o = -(a-c)$. Hence, the true region over which the pressure acts is a subregion of the assumed pressure region. The resulting calculated pressure distribution is shown in Figure 19 compared with the Hertzian solution. In Figure 19, the pressure as a function of x_o is shown for four different values of y_o. In this instance, 20 terms were used in the expansion (68), and 56 data points were used. As in the two-dimensional test case, the primary difference between the calculated pressure and the Hertzian solution arises as a result of the discontinuity in the pressure gradient on the boundary of the Hertzian region. Because of the nature of the series expansion used to approximate the pressure, such a discrepancy is to be expected. When the

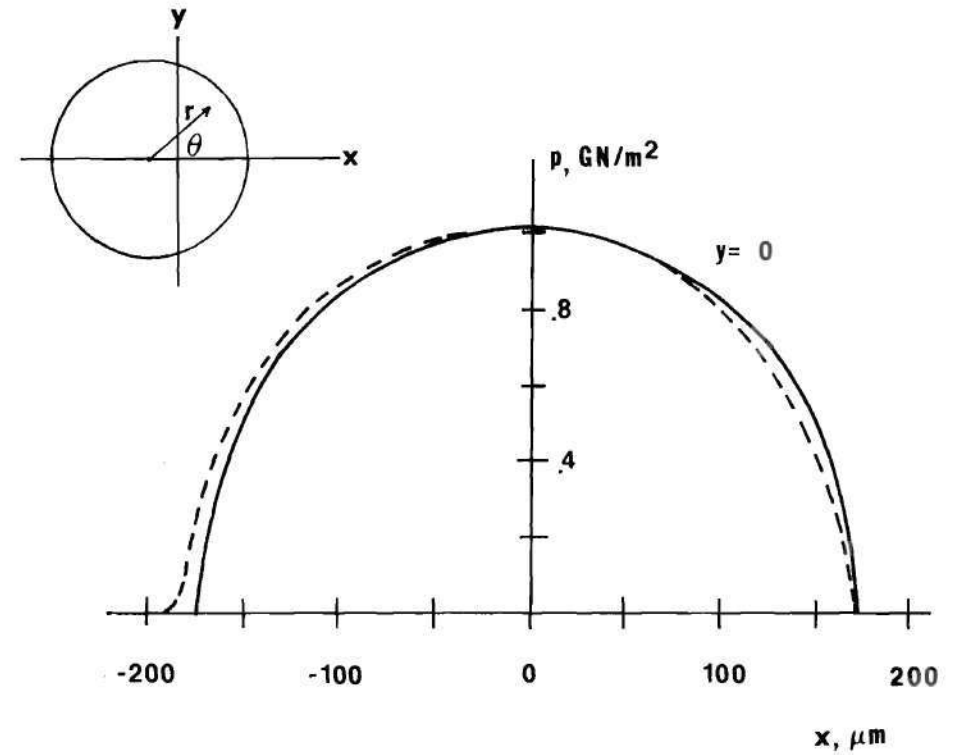

—— Hertz

— — Calculated

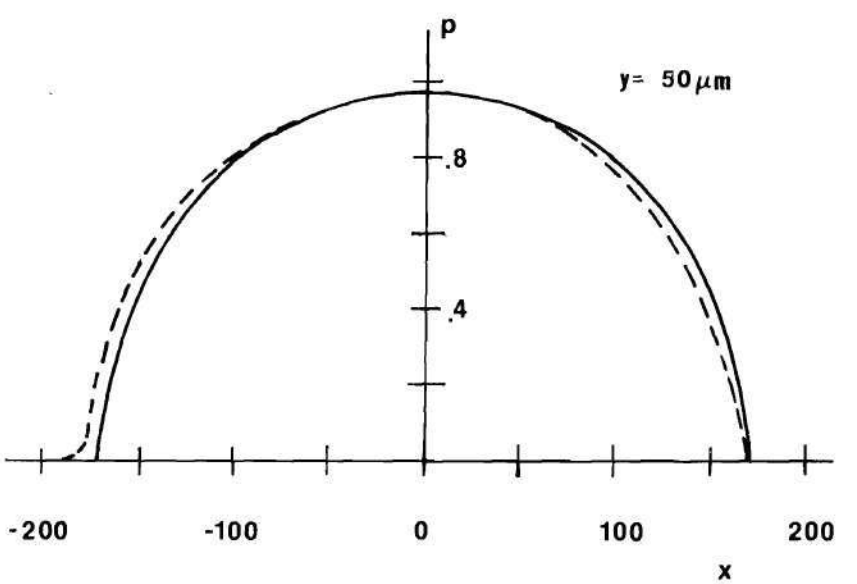

Figure 19. Test Case - Hertz Input

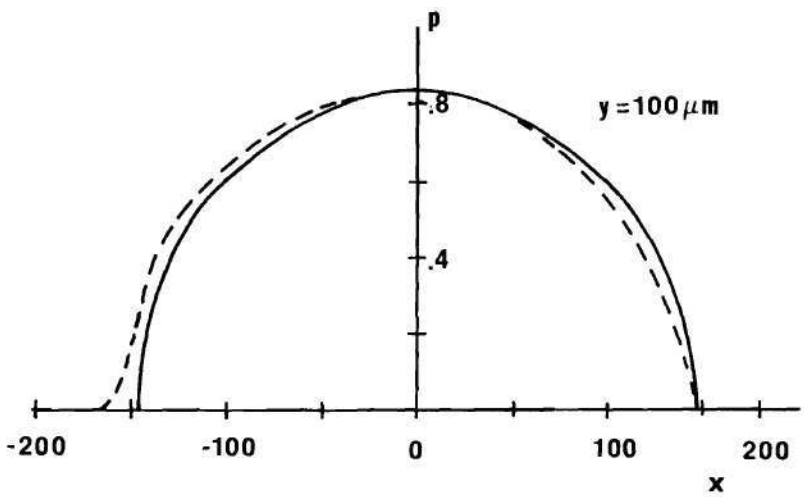

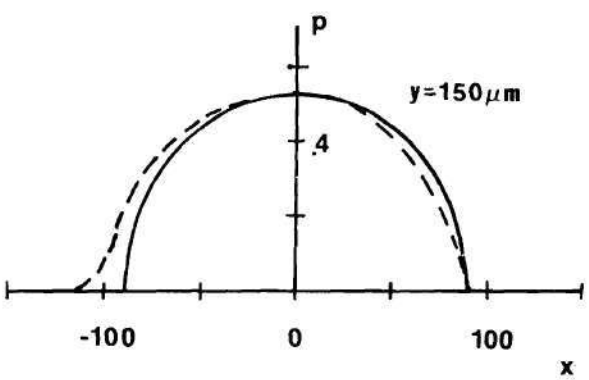

Figure 19. (Continued)

pressure was calculated with a = c, the discrepancy from the Hertz pressure was negligible throughout the region.

The pressure distribution in an actual EHD zone was calculated using the method described above. The film thickness data used for the calculation was obtained by H. S. Nagaraj [36] using the EHD simulator in the School of Mechanical Engineering at Georgia Institute of Technology. The experimental rig consisted of a steel ball lubricated on a plate made of synthetic sapphire. Film thicknesses were measured using the optical interference technique described in [36]. Some of the pertinent details of the experimental apparatus are presented in Appendix G.

The pressure distribution was calculated from film thickness data obtained with a normal load of 67 N and a sliding speed of 1.4 m/s. The lubricant used was a naphthenic hydrocarbon designated as Fluid N1 in [36]. The calculated pressure distribution for these conditions is plotted in Figure 20. In this computation, 20 terms were retained in the expansion (68) for the pressure distribution, and 56 data points were used.

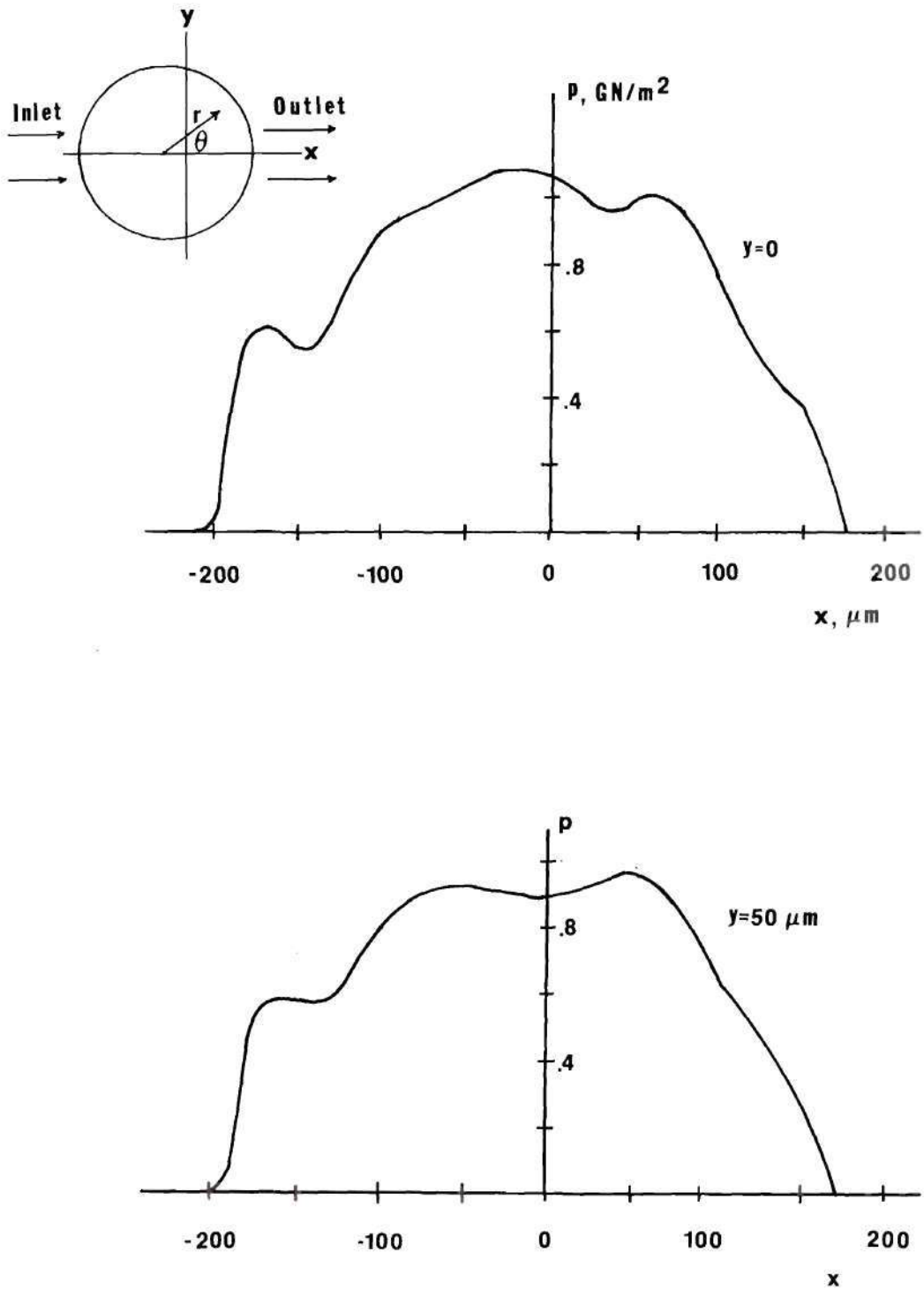

Figure 20. Calculations Based on Experimental Film Thickness Data [36]

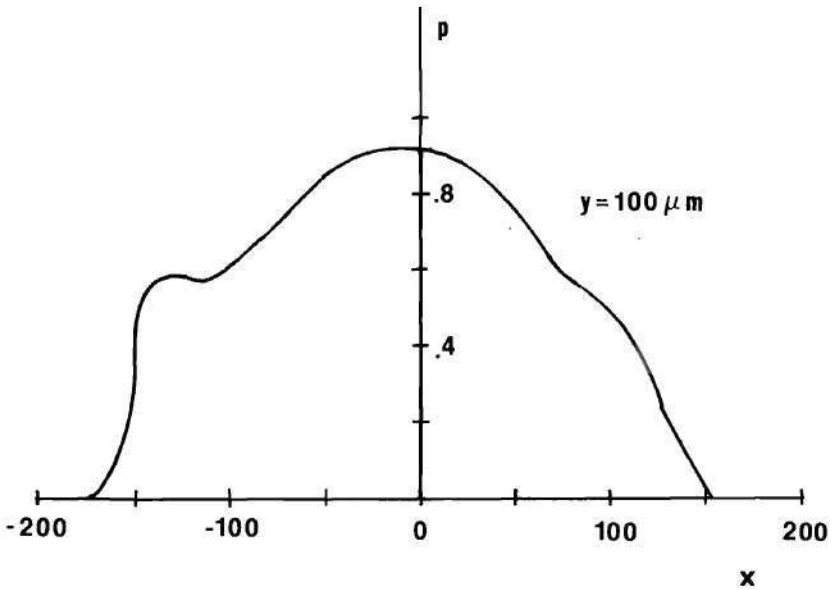

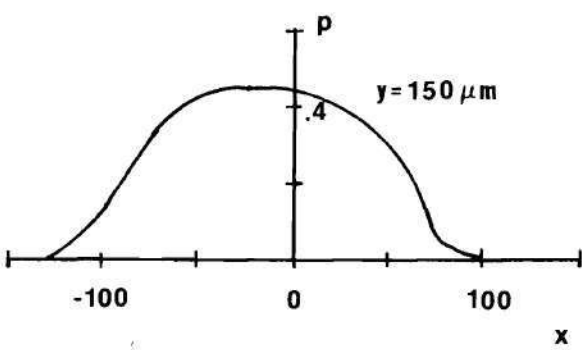

Figure 20. (Continued)

CHAPTER V

CONCLUSIONS AND RECOMMENDATIONS

In the foregoing work, procedures have been developed for analytically determining the pressure distribution in both two-dimensional and three-dimensional elastohydrodynamic zones. The development of the methods primarily involved consideration of the elasticity of the solid components of the EHD system. Expressions for the surface deformation resulting from the application of an arbitrary pressure loading distributed over a portion of the surface were obtained for each of the four solid bodies under consideration - the cylinder and the half-plane in the two-dimensional case, and the sphere and the half-space in the three-dimensional problem. These expressions were then cast in a form by which the pressure distributions could be determined from experimentally obtained film thickness profiles. The required calculations involve the solution of a set of linear algebraic equations in which the unknowns are the coefficients in a series expansion of the pressure as a function of position.

By using these methods, the pressure distribution in the EHD zone may be calculated from the following information - the film thickness as a function of position, the elastic constants and undeformed geometry of the solid components, and the normal load applied to the system. The computer programs which were developed to carry out the calculations are provided in Appendices C and F for the two- and three-dimensional cases, respectively.

One of the primary advantages of using these methods to calculate the pressure distribution lies in the fact that no assumption need be made concerning the state of the fluid in the EHD zone. The technique determines that pressure distribution necessary to obtain the surface deformation resulting in the film thickness profile which is known from experimental measurements. The calculated pressure which results in the measured film thickness is thus obtained independently of the manner in which the fluid is behaving. In addition, it should be noted that the determination of the pressure does not involve the relative velocities of the solid components of the EHD system either.

It may be concluded that the most important factor affecting the accuracy of the calculated pressure distribution is the precision of the measured film thickness profile. As indicated by the discussion of errors in Chapter III, if the film thickness data is accurate to within $\pm$ .025 μm, reasonably accurate values of the pressure as a function of position may be obtained.

One possibly fruitful extension of this work may be to use the pressure distributions obtained by the methods discussed above to study the behavior of the fluid itself in an EHD process. As mentioned in Chapter I, this in fact was one of the primary motivations for the development of these techniques to calculate the pressure. An experimental method exists for measuring the temperature in the EHD zone, and the velocity of a fluid element is known approximately from the kinematics of the solid bodies. With this information, along with the

calculated pressure field, the thermodynamic state of a liquid element and the way in which this state changes with time are known. The result is a relatively complete description of the thermodynamic conditions to which the liquid is subjected during its passage through the EHD region. As a result, the possibility exists to study the behavior of the liquid directly in the EHD zone. With this thermodynamic description, the results of experiments on fluid behavior may be interpreted and correlated more fully with the conditions of the experiment. Such a study has direct application to the field of elastohydrodynamic lubrication. Knowledge of the state of a lubricant which is undergoing an EHD process may prove valuable in lubricant selection and in prediction of certain operating conditions such as film thickness and total frictional force generated.

In addition to its applications to the field of lubrication, the study of fluid behavior in an EHD process may contribute to a more fundamental understanding of the physical properties of liquids subjected to non-equilibrium thermodynamic conditions. As has been noted, thermodynamic conditions in an EHD process are quite severe. The EHD process may therefore provide a convenient experimental means for studying the behavior of liquids subjected to severe non-equilibrium conditions not easily obtained otherwise. With the pressure distribution obtained using the techniques developed herein, and with temperature and velocity fields known, future research may concentrate on the behavior of liquids subjected to these known dynamic states.

One possible means for directly examining liquid behavior

under elastohydrodynamic conditions is the study of the interaction between light waves and the fluid in the EHD zone. The advantage of this approach is that the experimental technique (that is, the incidence and detection of scattering of light waves) will not significantly disturb the EHD process itself. Further research in this area may therefore explore the analytical and experimental possibilities of using light-scattering techniques to study the behavior of liquids in an EHD process.

In addition to helping to set the stage for investigations into liquid behavior under non-equilibrium conditions, the results of this work may be extended to obtain further information about the conditions to which the solid components of the EHD system are subjected. Specifically, once the pressure distribution acting on the surfaces of the solid bodies is known using the techniques described above, values for internal stresses may also be determined. Such results could be obtained by an extension of the elasticity analyses used to arrive at the pressure distribution. With the pressure field known, the potential functions in both the two- and three-dimensional cases could be determined, and subsequently used to find stresses and displacements in the interior of the body. Such information could be of interest in a study of the fatigue of solid components of an EHD system.

APPENDIX A

ON THE NATURE OF THE REACTION FORCE DISTRIBUTION FOR THE CYLINDER AND SPHERE

Since both the cylinder and the sphere are subjected to a pressure loading in the EHD zone, there must be a reaction force which maintains these bodies in equilibrium. It was contended in Chapter II that, since we are primarily concerned with surface displacements in the vicinity of the EHD zone, the exact character of the reaction force is unimportant, as long as it exists far from the EHD region. Consequently, for the purpose of dealing with the problem, the reaction was assumed to be equal and opposite to the EHD pressure, and located on the opposite side of the body. The validity of this assumption will be examined here in more detail by examining the surface displacements on a cylinder subjected to a concentrated load which is equilibrated in two different ways.

Specifically, the cases in Figure 21 will be considered, in which a cylinder is subjected to a concentrated normal load p. In the first case, this load is equilibrated by an equal and opposite load as shown; this reaction configuration is similar to that assumed in solving the two-dimensional problem in Chapter III. In the second case, the load is equilibrated by two loads of magnitude p/2 acting as shown. An expression for the surface displacement will be obtained for each of these two cases, and the results in the vicinity of the applied load p will be compared.

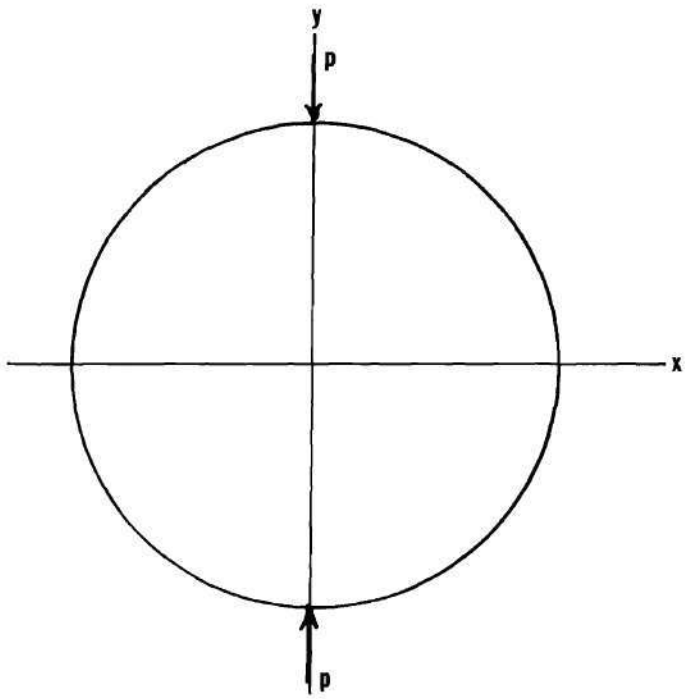

a. Loading Case 1

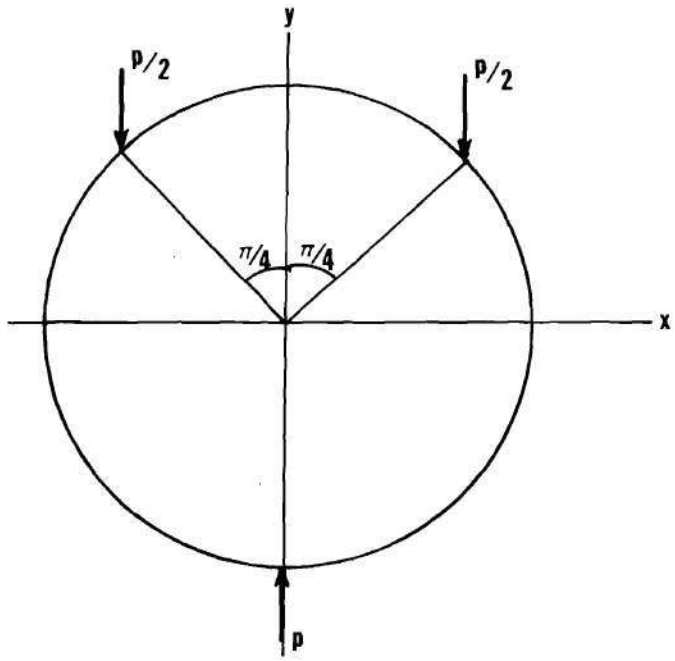

b. Loading Case 2

Figure 21. Concentrated Load Equilibrated in Two Ways

Consider the cylinder in Figure 22 loaded by three concentrated forces (0,p), (0,-p/2), and (0,-p/2) acting at boundary points $z_1 = r_o e^{-i\pi/2}$, $z_2 = r_o e^{+i\alpha}$, and $z_3 = -r_o e^{-i\alpha}$ respectively. Note that $\alpha = \pi/2$ corresponds to loading case 1 in Figure 21, and $\alpha = \pi/4$ corresponds to case 2. The potential functions ϕ and ψ (using the notation of Chapter III) for the loading of Figure 22 are, from equations (21) and (22),

$$\phi(z) = \frac{ip}{2\pi}\left\{ - \ell n[(z_1 - z)/(z_2 - z)^{1/2}(z_3 - z)^{1/2}] + \frac{z}{4r_o^2}[-2\bar{z}_1 + \bar{z}_2 + \bar{z}_3]\right\}$$

$$\psi(z) = \frac{ip}{2\pi}\left\{ - \ell n \frac{(z_1 - z)}{(z_2 - z)^{1/2}(z_3 - z)^{1/2}} - \frac{\bar{z}_1}{z_1 - z} + \frac{1}{2}\frac{\bar{z}_2}{z_2 - z} + \frac{1}{2}\frac{\bar{z}_3}{z_3 - z}\right\} .$$

The resulting displacements, obtained from equation (12), are

$$2\mu(u + iv) = \frac{ip}{2\pi}\left\{ - \frac{\lambda + 3\mu}{\lambda + \mu} \ell n \frac{(z_1 - z)}{(z_2 - z)^{1/2}(z_3 - z)^{1/2}} - \ell n \frac{(\bar{z}_1 - \bar{z})}{(\bar{z}_2 - \bar{z})^{1/2}(\bar{z}_3 - \bar{z})^{1/2}}\right.$$

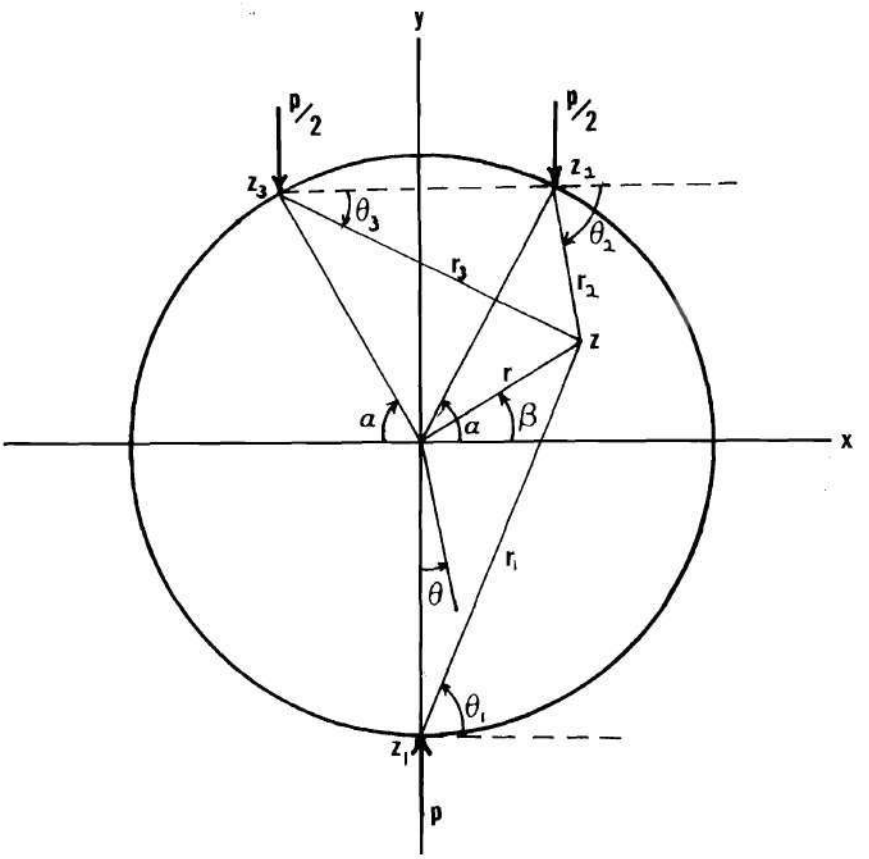

Figure 22. Cylinder Subjected to Three Concentrated Loads

$$- \frac{z_1 - z}{\bar{z}_1 - \bar{z}} + \frac{z_2 - z}{2(\bar{z}_2 - \bar{z})} + \frac{z_3 - z}{2(\bar{z}_3 - \bar{z})}$$

$$- \frac{\mu}{\lambda + \mu} (1 + \sin\beta) \frac{iz}{r_o} \Bigg\}$$

Separating real and imaginary parts, and observing from Figure 22 that

$$z_1 - z = - r_1 e^{i\theta_1}$$

$$z_2 - z = - r_2 e^{-i\theta_2}$$

$$z_3 - z = - r_3 e^{-i\theta_3}$$

results in the individual displacement components

$$u = \frac{P}{4\mu\pi} \left[\frac{2\mu}{\lambda + \mu} \left(\pi + \theta_1 + \frac{\theta_2 + \theta_3}{2} \right) + \sin 2\theta_1 + \frac{1}{2} \sin 2\theta_2 + \frac{1}{2} \sin 2\theta_3 \right.$$

$$\left. + \frac{\mu}{\lambda + \mu} \frac{x}{r_o} (1 + \sin \alpha) \right]$$

$$v = \frac{p}{4\mu\pi} \left[- \frac{2(\lambda + 2\mu)}{\lambda + \mu} \ell n \frac{r_1}{r_2^{1/2} r_3^{1/2}} - \cos 2\theta_1 + \frac{1}{2} \cos 2\theta_2 + \frac{1}{2} \cos 2\theta_3 \right.$$

$$\left. + \frac{\mu}{\lambda + \mu} \frac{y}{r_o} (1 + \sin\alpha) \right] \qquad (84)$$

The vertical component of surface displacement is given by evaluating equation (84) at the surface of the cylinder

$$v(\beta;\alpha) = \frac{\lambda + 2\mu}{4\mu\pi(\lambda + \mu)} \left\{ - \ell n \left| \frac{1 + \sin\beta}{\sin\alpha - \sin\beta} \right| + \sin\beta \, (1 + \sin\alpha) \right\}$$

Since we are interested in displacements in the vicinity of the single concentrated load, the angle β may be replaced by θ, where $\theta = \beta + \pi/2$ as shown in Figure 22. In case 1 of Figure 21, $\alpha = \pi/2$, and the corresponding surface displacement, in terms of θ, is

$$v(\theta;\ \pi/2) = \frac{\lambda + 2\mu}{4\mu\pi(\lambda + \mu)} \left[- \ell n \left| \frac{1 - \cos\theta}{1 + \cos\theta} \right| \ - 2 \cos\theta \right] \tag{85}$$

For case 2, $\alpha = \pi/4$, and the surface displacement is

$$v(\theta;\ \pi/4) = \frac{\lambda + 2\mu}{4\mu\pi(\lambda + \mu)} \left[- \ell n \left| \frac{1 - \cos\theta}{\frac{\sqrt{2}}{2} + \cos\theta} \right| - \left(1 + \frac{\sqrt{2}}{2} \right) \cos\theta \right] \tag{86}$$

In the neighborhood of the concentrated load (i.e. in a region of similar extent to that of the EHD zone), θ is a very small quantity, so that $\cos\theta$ may be replaced by $1 - \frac{1}{2}\theta^2$. Additionally noting that $\ell n(a + x) = \ell n(a) + \frac{x}{a} + \frac{x^2}{2a} + \cdots$, one may express equations (85) and (86), valid for small θ, as

$$v(\theta;\ \pi/2) = \frac{\lambda + 2\mu}{4\mu\pi(\lambda + \mu)} [-2 \ \ell n \ \theta + .75\theta^2 - 2.0] \tag{87}$$

$$v(\theta;\ \pi/4) = \frac{\lambda + 2\mu}{4\mu\pi(\lambda + \mu)} [-2 \ \ell n \ \theta + .561\theta^2 - 1.865] \tag{88}$$

The displacements given by equations (87) and (88) may be compared to one another. The constant term in each expression may be disregarded, as they correspond to rigid-body displacements. Furthermore, for small θ, the θ^2 term is negligible in comparison with the logarithmic term. Hence, there is negligible difference in the surface displacements in the vicinity of the applied load between the two systems shown in Figure 21.

The foregoing analysis is intended to verify that the precise details of the way in which the reaction force is manifested have little bearing on the displacement calculated in the vicinity of the EHD zone. Consequently, the reaction may be assumed to be distributed equal and opposite to the EHD pressure distribution without seriously compromising the generality of the displacements calculated in the EHD region.

APPENDIX B

LEAST-SQUARES SOLUTION OF AN OVERDETERMINED SYSTEM

Equation (46) in Chapter III represents a system of linear algebraic equations for which there are more equations than unknowns. As noted, there will in general be no exact solution to such a system. In the absence of an exact solution, one seeks rather to find an approximate solution which represents a "best possible" solution to the system. Accordingly, given the system of linear equations

$$a_{ij}b_j = c_i \quad , \qquad i = 1, 2, \ldots, n \ ,$$

$$j = 1, 2, \ldots, m \ , \quad n > m$$

the residuals are defined as

$$r_i = a_{ij}b_j - c_i \quad .$$

If a solution could be obtained for which the residuals are all zero, this solution would be exact. Since this is not possible, the solution for which the sum of the squares of the residuals is a minimum is sought. In this way, the solution obtained comes as close as possible to zero residuals, and is therefore in some sense a "best" approximate solution.

The sum of the squares of the residuals is

$$r_i r_i = (a_{ij} b_j - c_i)(a_{ik} b_k - c_i) \ ,$$

or, expanding the product,

$$r_i r_i = a_{ij} a_{ik} b_j b_k - 2 a_{ik} c_i b_k + c_i c_i \quad . \tag{89}$$

In order to find the set of unknowns b_p, $p = 1, 2, \ldots, m$, such that $r_i r_i$ is a minimum, we differentiate equation (89) with respect to each of the b_p, and set the result equal to zero.

$$\frac{d}{db_p} (r_i r_i) = a_{ip} a_{ik} b_k + a_{ij} a_{ip} b_j - 2 a_{ip} c_i = 0 \ , \ p = 1, 2, \ldots, m$$

Recognizing that the first two terms are identical yields the result

$$a_{ip} a_{ik} b_k = a_{ip} c_i ; \ i, k, p = 1, 2, \ldots, m \quad . \tag{90}$$

Hence, the solution to this system of equations, which is given as equation (48) in the text, will be that solution for which the sum of the squares of the residuals will be minimum.

APPENDIX C

LISTING OF COMPUTER PROGRAM FOR TWO-DIMENSIONAL CASE

On the following pages is a documented listing of the computer program developed for calculating the EHD pressure distribution in the two-dimensional case. The program requires as input data the elastic constants for the bodies; the radius of the cylinder; the total load on the system; the film thickness at a specified number of points and the locations of these points, measured from the point of contact in the undeformed configuration; the number of terms to be used in the series for the pressure; and the location of the inlet and outlet points.

The program prints out the calculated coefficients of the expansion for the pressure; the residuals computed at each data point location, as a test of accuracy of the result; and the pressure calculated at specified intervals throughout the EHD zone.

```
      PROGRAM EHDP(DAT,INPUT,OUTPUT,TAPE5=DAT,TAPE4=INPUT,
     1TAPE6=OUTPUT)
C     PROGRAM TO COMPUTE PRESSURE DISTRIBUTION IN A TWO-
C     DIMENSIONAL EHD ZONE FROM FILM THICKNESS DATA
      DIMENSION H(30),BETA1(30),BETA2(30),R(30),A1(30,30)
      DIMENSION A2(30,30),AS(30,30),X(30),U(30),P(51),X1N(51)
      DIMENSION IPIVOT(30),D(30),SL(30,30),UIN(30)
      DIMENSION UC(30),HC(30),RES(30),XT(30),XTIN(51)
      REAL K1,K2
C     PRELIMINARY DATA:
C       SET IFLAG=0 FOR TWO CYLINDERS,=1 FOR CYLINDER+PLATE
C       GAM: INITIAL GUESS FOR NORMAL APPROACH OF BODIES (M)
C       F: TOTAL LOAD (N)
C       M: NO. OF COS TERMS IN SERIES FOR PRESSURE
C       N: NO. OF SIN TERMS IN SERIES FOR PRESSURE
C       L1: NO. OF FILM THICKNESS DATA POINTS TO BE INPUT
C       SP: DESIRED SPACING BETWEEN POINTS AT WHICH PRESSURE
C           IS TO BE PRINTED OUT (M)
C       X1,X2: INLET, OUTLET POINTS, MEASURED FROM POINT OF
C              CONTACT IN UNDEFORMED STATE (M)
      READ(5,*)IFLAG,GAM,F
      READ(5,*)M,N,L1,SP
      READ(5,*)X1,X2
      PI=4.*ATAN(1.)
      A=ABS((X1-X2)/2.)
      OFST=-(X1+X2)/2.
      NN=0
      MM=M-1
      L11=L1+1
      LL=M+N
C     FILM THICKNESS DATA:
C       X(I): DISTANCE OF I-TH DATA POINT FROM POINT OF CON-
C             TACT IN UNDEFORMED STATE (M)
C       H(I): FILM THICKNESS AT X(I) (M)
      READ(5,*)(X(I),H(I),I=1,L1)
      DO 13 I=1,L1
      XT(I)=X(I)+OFST
   13 CONTINUE
C     DATA ON BODY 1 - CYLINDER:
C       YM1: MODULUS OF ELASTICITY (N/M**2)
C       PR1: POISSON'S RATIO
C       R1: RADIUS (M)
      READ(5,*)YM1,PR1,R1
      K1=2.*(1.-PR1*PR1)/(PI*YM1)
      ALP1=A/R1
      DO 5 I=1,L1
      BETA1(I)=XT(I)/R1
    5 CONTINUE
      CALL CYL(ALP1,BETA1,N,M,L1,A1)
      IF(IFLAG.EQ.0)GO TO 10
```

```
C       DATA ON BODY 2; USE IF IFLAG=1
        READ(5,*)YM2,PR2
        K2=2.*(1.-PR2*PR2)/(PI*YM2)
        CALL PLATE(A,XT,N,M,L1,A2)
        RIN=0.0
        GO TO 17
C       DATA ON BODY 2; USE IF IFLAG=0
   10   READ(5,*)YM2,PR2,R2
        K2=2.*(1.-PR2*PR2)/(PI*YM2)
        ALP2=A/R2
        DO 20 I=1,L1
        BETA2(I)=XT(I)/R2
   20   CONTINUE
        CALL CYL(ALP2,BETA2,N,M,L1,A2)
        RIN=1./R2
C       COMBINE MATRICES FOR BODIES 1 AND 2. SL(I,J) IS THE
C         MATRIX OF COEFFICIENTS OF THE UNKNOWN FOURIER
C         COEFFICIENTS OF PRESSURE.
   17   DO 25 I=1,L1
        DO 25 J=1,LL
        SL(I,J)=(A1(I,J)*K1+A2(I,J)*K2)*A/PI
   25   CONTINUE
C       INCLUDE CONDITION THAT PRESSURE GRADIENT VANISH AT INLET
        DO 70 I=1,N
        SL(L11,I)=((-1.)**I*I)*(1.E-10)
   70   CONTINUE
        DO 71 I=1,M
        SL(L11,N+I)=((-1.)**(I-1)*(2.*I-1.)/2.)*1.E-10
   71   CONTINUE
C       FROM SL, FORM MATRIX CORRESPONDING TO MINIMIZATION OF
C         THE NORM OF THE RESIDUAL.
        DO 55 I=1,LL
        DO 55 J=1,LL
        AS(I,J)=0.0
        DO 55 K=1,L11
        AS(I,J)=AS(I,J)+SL(K,I)*SL(K,J)
   55   CONTINUE
C       BEGIN PROCEDURE FOR SOLVING THE SET OF LINEAR EQUATIONS
C         FOR THE UNKNOWN FOURIER COEFF.
        DO 1 I=1,LL
        IPIVOT(I)=I
        ROWMAX=0.0
        DO 2 J=1,LL
    2   ROWMAX=AMAX1(ROWMAX,ABS(AS(I,J)))
    1   D(I)=ROWMAX
        NM1=LL-1
        DO 3 K=1,NM1
        J=K
        KP1=K+1
        IP=IPIVOT(K)
        COLMAX=ABS(AS(IP,K))/D(IP)
```

```
      DO 4 I=KP1,LL
      IP=IPIVOT(I)
      AWIKOV=ABS(AS(IP,K))/D(IP)
      IF(AWIKOV.LE.COLMAX)GO TO 4
      COLMAX=AWIKOV
      J=I
    4 CONTINUE
      IPK=IPIVOT(J)
      IPIVOT(J)=IPIVOT(K)
      IPIVOT(K)=IPK
      DO 3 I=KP1,LL
      IP=IPIVOT(I)
      AS(IP,K)=AS(IP,K)/AS(IPK,K)
      RATIO=-AS(IP,K)
      DO 3 J=KP1,LL
    3 AS(IP,J)=RATIO*AS(IPK,J)+AS(IP,J)
C     FORM RIGHT-HAND SIDE OF THE EQNS.
   90 DO 45 I=1,L1
      UIN(I)=.5*X(I)*X(I)*(1./R1+RIN)-H(I)-GAM
   45 CONTINUE
C     FROM UIN AND SL, FORM RHS OF EQNS. CORRESPONDING TO
C       MINIMIZATION OF THE NORM OF THE RESIDUAL. CONTINUE
C       SOLN. OF LINEAR EQNS. WITH THIS AS RHS.
      UIN(L11)=0.0
      DO 36 I=1,LL
      U(I)=0.0
      DO 36 J=1,L11
      U(I)=U(I)+UIN(J)*SL(J,I)
   36 CONTINUE
      IP=IPIVOT(1)
      Q(1)=U(IP)
      DO 9 K=2,LL
      IP=IPIVOT(K)
      KM1=K-1
      SUM=0.0
      DO 6 J=1,KM1
    6 SUM=AS(IP,J)*Q(J)+SUM
    9 Q(K)=U(IP)-SUM
      Q(LL)=Q(LL)/AS(IP,LL)
      K=LL
      DO 7 NP1MK=2,LL
      KP1=K
      K=K-1
      IP=IPIVOT(K)
      SUM=0.0
      DO 8 J=KP1,LL
    8 SUM=AS(IP,J)*Q(J)+SUM
C     Q(K): DESIRED FOURIER COEFFICIENTS
    7 Q(K)=(Q(K)-SUM)/AS(IP,K)
C     IF NECESSARY, MODIFY VALUE OF GAM TO SATISFY TOTAL LOAD
C       CONDITION, AND RE-SOLVE THE EQUATIONS WITH NEW RHS.
```

```
      FTRIAL=0.0
      DO 34 I=1,M
      T=4.*A*(-1.)**(I-1)/((2.*I-1.)*PI)
   34 FTRIAL=FTRIAL+T*Q(N+I)
      FO=FTRIAL-F
      NN=NN+1
      IF(NN.EQ.3)GO TO 100
      IF(NN.EQ.2)GO TO 110
      F1=FO
      GAM1=GAM
      GAM=GAM/2.
      GO TO 90
  110 GAM2=GAM1
      GAM1=GAM
      F2=F1
      F1=FO
      GAM=GAM1-((GAM1-GAM2)*F1)/(F1-F2)
      GO TO 90
C     COMPUTE PRESSURE AT LOCATIONS DESIRED FOR OUTPUT.
  100 NP=INT(ABS(X1/SP))+INT(ABS(X2/SP))+3
      XTIN(1)=AMIN1(X1,X2)
      XTIN(2)=INT(XTIN(1)/SP)*SP
      NP1=NP-1
      DO 40 I=3,NP1
      XTIN(I)=XTIN(I-1)+SP
   40 CONTINUE
      XTIN(NP)=AMAX1(X1,X2)
      DO 42 L=1,NP
      XIN(L)=XTIN(L)+OFST
      P(L)=0.0
      DO 32 I=1,N
      P(L)=P(L)+Q(I)*SIN(I*PI*XIN(L)/A)
   32 CONTINUE
      DO 35 JJ=1,M
      I=JJ-1
      P(L)=P(L)+Q(N+JJ)*COS((2.*I+1.)*PI*XIN(L)/(2.*A))
   35 CONTINUE
   42 CONTINUE
C     COMPUTE RESIDUALS AT EACH DATA POINT LOCATION.
      TR=0.0
      DO 91 I=1,L1
      UC(I)=0.0
      DO 92 J=1,LL
      UC(I)=UC(I)+SL(I,J)*Q(J)
   92 CONTINUE
      HC(I)=.5*X(I)*X(I)*(1./R1+RIN)-UC(I)-GAM
      RES(I)=H(I)-HC(I)
      TR=TR+RES(I)*RES(I)
   91 CONTINUE
C     OUTPUT:
C       FTRIAL: CALCULATED TOTAL LOAD (N) - USE FOR COMPARI-
C               SON AS A TEST OF ACCURACY OF THE CALCULATIONS.
```

```
C       GAM: NORMAL APPROACH VALUE ARRIVED AT (M)
C       FOURIER COEFF.: COEFFICIENTS OF SIN TERMS LISTED FIRST
C       RESIDUALS: LISTED IN SAME ORDER AS INPUT POINTS (M).
C                  LAST VALUE PRINTED IS SUM OF THEIR SQUARES.
C         X: DISTANCE FROM CONTACT POINT IN UNDEFORMED STATE
        WRITE(6,*)FTRIAL,GAM
        WRITE(6,150)
  150   FORMAT(5X,"FOURIER COEFFICIENTS:")
        WRITE(6,*)(Q(I),I=1,LL)
        WRITE(6,250)
  250   FORMAT(5X,"RESIDUALS:")
        WRITE(6,*)(RES(I),I=1,L1)
        WRITE(6,*)TR
        WRITE(6,550)
        WRITE(6,450)(XTIN(I),P'I),I=1,NP)
  550   FORMAT(10X,"X (M)",10X,"PRESSURE (N/M**2)"/)
  450   FORMAT(9X,F10.5,10X,E11.4)
        WRITE(6,650)
C       IF USER WANTS CALCULATED FILM THICKNESS AT EACH INPUT
C         POINT ENTER 1.  OTHERWISE ENTER 0.
  650   FORMAT(5X,"ENTER 1 FOR FILM THICKNESS")
        READ(4,*)NP
        IF(NP.NE.1)GO TO 93
        WRITE(6,750)
  750   FORMAT(12X,"X (M) ",9X,"FILM THICKNESS (M)"/)
        WRITE(6,450)(X(I),HC(I),I=1,L1)
   93   WRITE(6,850)
C       IF USER WANTS CALCULATED FILM THICKNESS AT OTHER POINTS
C         IN OR NEAR CONTACT, ENTER 1.  OTHERWISE, ENTER 0.
  850   FORMAT(5X,"ENTER 1 FOR ADD'L FILM THICKNESS")
        READ(4,*)NP
        IF(NP.NE.1)STOP
C       ENTER LOCATION OF DESIRED FILM THICKNESS CALCULATION.
C         TO STOP PROGRAM ENTER VALUE > 20.
   94   READ(4,*)XX
        IF(XX.GT.20.)STOP
        XT(1)=XX+OFST
        BETA1(1)=XT(1)/R1
        CALL CYL(ALP1,BETA1,N,M,1,A1)
        IF(IFLAG.EQ.0)GO TO 95
        CALL PLATE(A,XT,N,M,1,A2)
        GO TO 96
   95   BETA2(1)=XT(1)/R2
        CALL CYL(ALP2,BETA2,N,M,1,A2)
   96   DO 97 I=1,LL
        SL(1,I)=(A1(1,I)*K1+A2(1,I)*K2)*A/PI
   97   CONTINUE
        UA=0.0
        DO 98 I=1,LL
        UA=UA+SL(1,I)*Q(I)
   98   CONTINUE
```

```
      HH=.5*XX*XX*(1./R1+RIN)-UA-GAM
      WRITE(6,450)XX,HH
      GO TO 94
      STOP
      END
      SUBROUTINE CYL(ALP,BETA,N,MT,L1,A)
C     SUBROUTINE TO FILL MATRIX CORRESPONDING TO CYLINDER
C     DISPLACEMENTS.
      DIMENSION A(30,30),BETA(30)
      REAL M
      PI=4.*ATAN(1.)
      MM=MT-1
      LL=MT+N
      DO 10 L=1,L1
      NN=0
      IF(ABS(1.-ABS(BETA(L)/ALP)).LT.1.E-10)NN=1
C     CALCULATE ELEMENTS CORRESPONDING TO ANTISYMMETRIC
C     COMPONENTS
      DO 12 I=1,N
      COEF1=I*PI/ALP
      XL=COEF1*(BETA(L)+ALP)
      CALL SICO(XL,S1,C01)
      XL=COEF1*(BETA(L)-ALP)
      CALL SICO(XL,S2,C02)
      IF(NN.NE.1)GO TO 16
      A1=0.0
      GO TO 15
   16 A1=((-1.)**I-COS(COEF1*BETA(L)))*ALOG(ABS((BETA(L)
     1+ALP)/(BETA(L)-ALP)))
   15 B1=SIN(COEF1*BETA(L))*(S2-S1)
      C1=COS(COEF1*BETA(L))*(C01-C02)
      A(L,I)=(1./I)*(A1+B1+C1)
   12 CONTINUE
C     CALCULATE ELEMENTS CORRESPONDING TO SYMMETRIC COMPONENTS
      DO 14 JJ=1,MT
      I=JJ-1
      M=(2.*I+1.)/2.
      COEF2=M*PI/ALP
      XL=COEF2*(BETA(L)+ALP)
      CALL SICO(XL,S1,C01)
      XL=COEF2*(ALP-BETA(L))
      CALL SICO(XL,S2,C02)
      A2=(2.*M*(PI)**2/(M**2*PI**2+ALP**2))*
     1SIN(M*PI)*COS(ALP)*COS(BETA(L))
      IF(NN.NE.1)GO TO 20
      B2=SIN(M*PI)*(2.*ALOG(2.*ALP)-ALOG(4.))
      C2=0.0
      GO TO 25
   20 B2=SIN(M*PI)*(ALOG(ABS((ALP+BETA(L))*(ALP-
     1BETA(L))))-ALOG(4.))
```

```
      C2=SIN(COEF2*BETA(L))*(ALOG(ABS((ALP+BETA(L))/
     1(ALP-BETA(L)))))
   25 D2=SIN(COEF2*BETA(L))*(CO2-CO1)
      E2=(-1.)*COS(COEF2*BETA(L))*(S2+S1)
      A(L,N+JJ)=A2+1./M*(B2+C2+D2+E2)
   14 CONTINUE
   10 CONTINUE
      RETURN
      END
      SUBROUTINE PLATE(A,X,N,MT,L1,AN)
C     SUBROUTINE TO FILL MATRIX CORRESPONDING TO PLATE
C     DISPLACEMENTS
      DIMENSION AN(30,30),X(30)
      REAL M
      PI=4.*ATAN(1.)
      MM=MT-1
      LL=MT+N
      DO 10 L=1,L1
      NN=0
      IF(ABS(1.-ABS(X(L)/A)).LT.1.E-10)NN=1
C     CALCULATE ELEMENTS CORRESPONDING TO ANTISYMMETRIC
C     COMPONENTS.
      DO 12 I=1,N
      COEF1=I*PI/A
      XL=COEF1*(A+X(L))
      CALL SICO(XL,S1,CO1)
      XL=COEF1*(A-X(L))
      CALL SICO(XL,S2,CO2)
      IF(NN.NE.1)GO TO 16
      A1=0.0
      GO TO 15
   16 A1=((-1.)**I-COS(COEF1*X(L)))*ALOG(ABS((A+X(L))/
     1(A-X(L))))
   15 B1=(-1.)*SIN(COEF1*X(L))*(S1+S2)
      C1=COS(COEF1*X(L))*(CO1-CO2)
      AN(L,I)=(1./I)*(A1+B1+C1)
   12 CONTINUE
C     CALCULATE ELEMENTS CORRESPONDING TO SYMMETRIC COMPONENTS.
      DO 14 JJ=1,MT
      I=JJ-1
      M=(2.*I+1.)/2.
      COEF2=M*PI/A
      S=SIN(COEF2*X(L))
      XL=COEF2*(A+X(L))
      CALL SICO(XL,S1,CO1)
      XL=COEF2*(A-X(L))
      CALL SICO(XL,S2,CO2)
      IF(NN.NE.1)GO TO 20
      A2=ALOG(2.)*(2.*SIN(M*PI))
      B2=0.0
      GO TO 25
   20 A2=ALOG(ABS((A-X(L))/A))*(SIN(M*PI)-S)
```

```
      B2=ALOG(ABS((A+X(L))/A))*(SIN(M*PI)+S)
   25 C2=(-1.)*S*(CO1-CO2)
      D2=(-1.)*COS(COEF2*X(L))*(S1+S2)
      AN(L,N+JJ)=(1./M)*(A2+B2+C2+D2)
   14 CONTINUE
   10 CONTINUE
      RETURN
      END
      SUBROUTINE SICO(X,S,C)
C     SUBROUTINE TO EVALUATE SIN AND COS INTEGRALS
      IF(ABS(X).GT.1.E-12)GO TO 25
      S=0.0
      C=0.0
      RETURN
   25 IF(ABS(X).LT.0.1)GO TO 26
C     SICI IS A SUBROUTINE IN CDC MATH-SCIENCE LIBRARY.
      CALL SICI(S,C,X)
      S=S+1.570796
      C=.5772157+ALOG(ABS(X))-C
      RETURN
   26 S=X
      C=0.0
      N=1
      NC=1
      NS=-1
      NTC=0
      NTS=0
      FACT=1.
      COUNT=1.
      PROD=X
      DO 10 I=2,10
      COUNT=COUNT+1.
      FACT=FACT*COUNT
      PROD=PROD*X
      TERM=PROD/(COUNT*FACT)
      IF(N.EQ.1)GO TO 15
      N=1
      IF(NS.EQ.-1)TERM=-TERM
      NS=-NS
      S=S+TERM
      IF(ABS(TERM/S).LT.1.E-5)NTS=1
      GO TO 112
   15 N=0
      IF(NC.EQ.-1)TERM=-TERM
      NC=-NC
      C=C+TERM
      IF(ABS(TERM/C).LT.1.E-5)NTC=1
  112 IF(NTS.EQ.0)GO TO 10
      IF(NTC.EQ.1)RETURN
   10 CONTINUE
      RETURN
      END
```

APPENDIX D

SOLUTION OF NAVIER'S EQUATION IN TERMS OF BOUSSINESQ-PAPKOVICH POTENTIALS

Navier's equation for the equilibrium of a linearly elastic, isotropic, homogeneous body with zero body forces is

$$\nabla^2\bar{u} + \frac{1}{1-2\nu}\nabla\nabla\cdot\bar{u} = 0 \tag{91}$$

where $\bar{u}$ is the displacement vector. A general solution to equation (91) may be obtained in terms of the so-called Boussinesq-Papkovich potentials. The following derivation is similar to that found in Sokolnikoff [43].

According to Helmholtz' Theorem (see [44]), any vector field, such as $\bar{u}$, may be decomposed into the gradient of a scalar function and the curl of a vector function; i.e., we may write

$$\bar{u} = \nabla A + \nabla \times \bar{B} \quad . \tag{92}$$

Since the decomposition defined in equation (92) is not unique, we may, for convenience, arbitrarily set

$$\nabla \cdot \bar{B} = 0 \quad .$$

Taking the divergence of both sides of equation (92) gives

$$\nabla \cdot \bar{u} = \nabla^2 A \tag{93}$$

since the divergence of the curl is zero. Using this result in Navier's equation (91) yields

$$\nabla^2\bar{u} + \frac{1}{1-2\nu}\nabla(\nabla^2 A) = 0 \quad .$$

This may be rewritten as

$$\nabla^2\left(\bar{u} + \frac{1}{1-2\nu}\nabla A\right) = 0 \tag{94}$$

Equation (94) may be used to define the function $\bar{\psi}$; i.e.,

$$\bar{\psi} = -\frac{G}{2(1-\nu)}\left[\bar{u} + \frac{1}{1-2\nu}\nabla A\right] \tag{95}$$

where $\bar{\psi}$ is an arbitrary harmonic vector function,

$$\nabla^2\bar{\psi} = 0 \tag{96}$$

Taking the divergence of equation (95) gives

$$\nabla\cdot\bar{\psi} = -\frac{G}{2(1-\nu)}\left[\nabla\cdot\bar{u} + \frac{1}{1-2\nu}\nabla^2 A\right] \quad .$$

If we substitute for $\nabla\cdot\bar{u}$ from (93), we get

$$\nabla\cdot\bar{\psi} = -\frac{G}{2(1-\nu)}\left[\nabla^2 A + \frac{1}{1-2\nu}\nabla^2 A\right] = -\frac{G}{1-2\nu}\nabla^2 A$$

i.e.,

$$\nabla^2 A = - \frac{1-2\nu}{G} \nabla\cdot\bar{\psi} \tag{97}$$

which is Poisson's equation for A. It may easily be shown that the particular solution to equation (97) is $- \frac{1-2\nu}{2G} \bar{r}\cdot\bar{\psi}$ where $\bar{r}$ is the position vector. Therefore, the general solution to equation (97) may be written as

$$A = - \frac{1-2\nu}{2G} (\bar{r}\cdot\bar{\psi} + \phi) \tag{98}$$

where ϕ is an arbitrary harmonic function,

$$\nabla^2 \phi = 0 \quad . \tag{99}$$

Equation (98) may be used in equation (95) in order to express $\bar{u}$ in terms of the four harmonic functions-ϕ and the three cartesian components of $\bar{\psi}$

$$2G\bar{u} = \nabla(\phi + \bar{r}\cdot\bar{\psi}) - 4(1-\nu)\bar{\psi} \tag{100}$$

Hence, equation (100) provides a general solution to Navier's equation (91) provided the functions ϕ and $\bar{\psi}$ are harmonic. Under most circumstances, ϕ or any one of the components of $\bar{\psi}$ may be arbitrarily set to zero without loss anf completeness [39]. Since the mathematical study of harmonic functions is well developed, this formulation provides a convenient means for solving three-dimensional elasticity problems.

APPENDIX E

SPHERICAL BIPOLAR AND SPHERICAL POLAR COORDINATE SYSTEMS

Spherical bipolar coordinates were used in some of the calculations involved in Chapter IV. Specifically, the singular portion of the radial surface displacement was obtained by expressing ϕ_1 and ψ_1 in equation (58) in terms of their bipolar coordinates, and evaluating the vector equation (52) for the bipolar components of the displacement. The advantage of this particular choice of coordinates, as will be shown presently, lies in the fact that the two poles of the coordinate system may be made to coincide with the points of application of the concentrated loads.

Bipolar coordinates (x_1, x_2, x_3) may be defined by their transformation equations from cartesian coordinates (X,Y,Z) as follows

$$X = \frac{r_o \sin x_2}{\cosh x_1 - \cos x_2} \cos x_3$$

$$Y = \frac{r_o \sin x_2}{\cosh x_1 - \cos x_2} \sin x_3$$

$$Z = -\frac{r_o \sinh x_1}{\cosh x_1 - \cos x_2} \qquad (101)$$

where $-\infty < x_1 < \infty$, $0 \leq x_2 \leq \pi$, $0 \leq x_3 < 2\pi$, and r_o is a positive constant. As expressed in this form, the bipolar coordinates form a system axisymmetric about the Z-axis. Some surfaces x_1 = constant, and x_2 = constant on a half-plane x_3 = constant are shown in Figure 23. It is noted that the coordinate surface $x_2 = \pi/2$ is a sphere of radius r_o. Hence, the radial component of displacement on the surface of the sphere is the x_2-component of the displacement vector evaluated at $x_2 = \pi/2$. This displacement component is obtained by first expressing ϕ_1 and ψ_1 in equation (58) in terms of (x_1, x_2, x_3) by using the relations that

$$\rho_1 = \frac{\sqrt{2}\, r_o e^{-x_1/2}}{[\cosh x_1 - \cos x_2]^{1/2}} \qquad c_1 = \frac{(\cosh x_1 - \cos x_2 - \sinh x_1) e^{x_1/2}}{\sqrt{2}\, [\cosh x_1 - \cos x_2]^{1/2}}$$

$$\rho_2 = \frac{\sqrt{2}\, r_o e^{x_1/2}}{[\cosh x_1 - \cos x_2]^{1/2}} \qquad c_2 = \frac{(\cos x_2 - \cosh x_1 - \sinh x_1) e^{-x_1/2}}{\sqrt{2}\, [\cosh x_1 - \cos x_2]^{1/2}}$$

where ρ_1, ρ_2, c_1 and c_2 are those quantities which are defined in Figure 15, and which appear in equations (58). The vector equation (52) was then used to obtain the x_2-component of displacement in terms of ϕ_1, ψ_1, and their derivatives with respect to x_1, x_2 and x_3. In so doing, it was necessary to obtain the appropriate expression for the gradient in bipolar coordinates, which required determination of the metric coefficients from the transformation

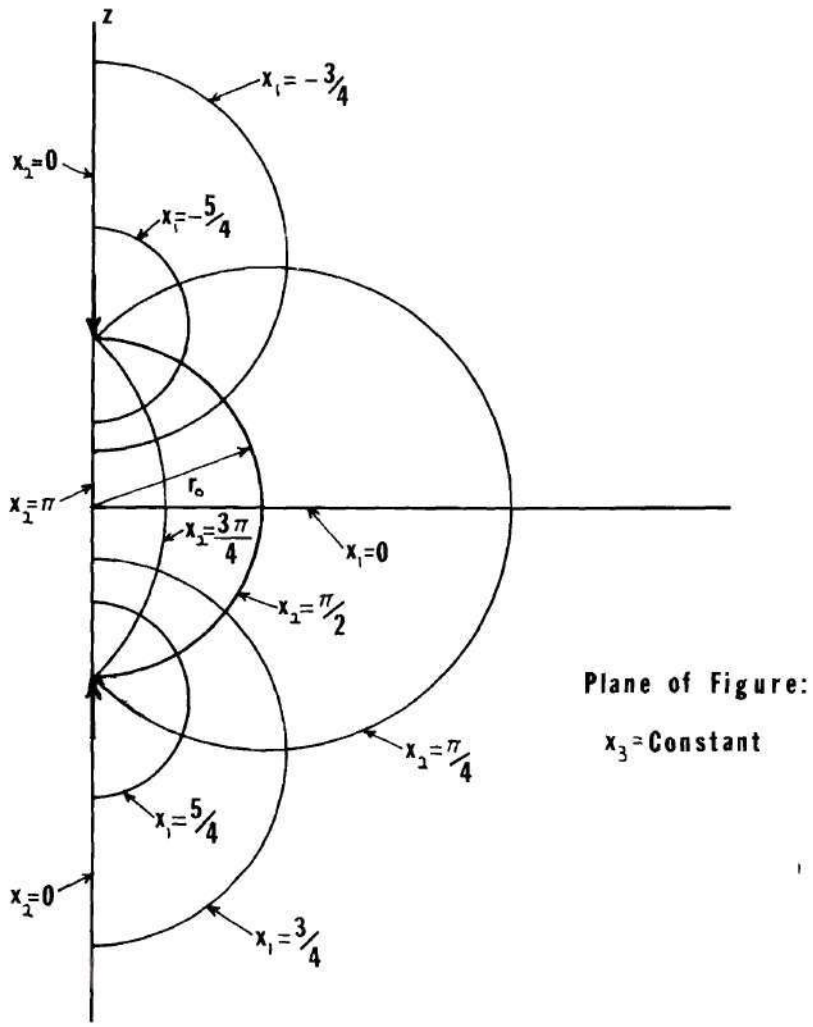

Figure 23. Spherical Bipolar Coordinates

equations (101). The x_2-component of displacement so obtained was then evaluated for $x_2 = \pi/2$ to yield the radial surface displacement given in equation (62) in the text. Hence, the determination of the singular portion of the radial surface displacement is a straightforward operation using spherical bipolar coordinates; the algebra necessary to obtain this expression was, however, quite cumbersome. The advantage of using this particular coordinate system derives from the fact that the singular points of the coordinate system coincide with the singular loading points.

The residual portion of the radial surface displacement was obtained with the use of spherical polar coordinates (y_1, y_2, y_3). The coordinate system is defined in terms of its transformation equations with the cartesian (X,Y,Z) system by

$$X = y_1 \sin y_2 \cos y_3$$

$$Y = y_1 \sin y_2 \sin y_3$$

$$Z = y_1 \cos y_2$$

where $0 \leq y_1 < \infty$, $0 \leq y_2 \geq \pi$ $0 \leq y_3 < \pi$. The coordinate surface $y_1 = r_o$ represents a sphere of radius r_o. The radial component of surface displacement is therefore obtained by evaluating the y_1-component of the displacement vector at $y_1 = r_o$. Potential functions ϕ_2 and ψ_2 given by equations (59) are expressed in terms of spherical coordinates (y_1, y_2, y_3) by noting from Figure 16 that

$$\rho_o = y_1 \quad ; \qquad c = \cos y_2 \quad .$$

Equation (52) was then used to obtain the y_1-component of displacement by expressing the displacement in terms of ϕ_2, ψ_2, and their derivatives with respect to y_1, y_2, and y_3. As before, this involved obtaining the expression for the gradient in spherical polar coordinates, for which it was necessary to evaluate the metric coefficients from transformation equations (102). The radial component of displacement was then evaluated at the surface of the sphere, $y_1 = r_o$, to obtain equation (63).

APPENDIX F

LISTING OF COMPUTER PROGRAM FOR THREE-DIMENSIONAL CASE

A documented listing of the computer program developed for calculating the EHD pressure distribution in the three-dimensional case appears on the following pages. The input data required by the program include the elastic constants for the sphere and the half-space; the radius of the sphere; the total normal load on the system; the film thickness at a specified number of points and the locations of these points, measured from the point of contact in the undeformed state; the number of terms to be used in the pressure expansion; and the location of assumed inlet and outlet points.

The program returns the computed coefficients of the pressure series; the residuals computed at each input point; and the pressure calculated at specified intervals throughout the EHD region.

```
      PROGRAM PDIST(F,DAT,INPUT,OUTPUT,TAPE3=F,TAPE4=DAT,
     1TAPE5=INPUT,TAPE6=OUTPUT)
C     PROGRAM TO COMPUTE PRESSURE DISTRIBUTION IN A THREE-
C     DIMENSIONAL EHD ZONE FROM FILM THICKNESS DATA.
      DIMENSION R1(60),TH1(60),H(60),A1(60,50),A(60,50),
     1B1(60),D(50),SA(50),IPR(50),B(60),RES(60),
     2XC(20),YC(20),N1(10)
      COMMON/B/R0,R,A/C/C1,C2
C     INPUT DATA
C        N  NO. OF DATA POINTS
C          M  NO. OF TERMS IN SERIES FOR PRESSURE
C        N2  HIGHEST EXPONENT OF COS IN PRESSURE SERIES
C        F  TOTAL LOAD
C        XIN,XOUT  INLET, OUTLET POINTS, MEASURED FROM POINT
C          OF CONTACT IN UNDEFORMED STATE
C        N1(I)  HIGHEST EXPONENT OF R CORRESPONDING TO
C          COS**(I-1) TERMS
C        DATA FOR SPHERE
C          E1  MODULUS OF ELASTICITY
C          PR1  POISSON'S RATIO
C          R  RADIUS
C        DATA FOR PLATE
C          E2  MODULUS OF ELASTICITY
C          PR2  POISSON'S RATIO
C        FILM THICKNESS DATA
C          X,Y  LOCATION OF ITH DATA POINT, MEASURED FROM
C            POINT OF CONTACT IN UNDEFORMED STATE
C          H(I)  FILM THICKNESS AT THAT LOCATION
      READ(4,*)N,M,N2,F,XIN,XOUT
      N21=N2+1
      READ(4,*)(N1(I),I=1,N21)
      READ(4,*)E1,PR1,R
      READ(4,*)E2,PR2
      OFST=-.5*(XIN+XOUT)
      R0=.5*(XOUT-XIN)
      DO 19 I=1,N
      READ(4,*)X,Y,H(I)
      XT=X+OFST
      R1(I)=SQRT(XT*XT+Y*Y)
      IF(R1(I).LT.1.E-10)GO TO 18
      TH1(I)=ATAN2(Y,XT)
      GO TO 19
   18 TH1(I)=0.0
   19 CONTINUE
      NR=60
      G1=E1/(2.*(1.+PR1))
      G2=E2/(2.*(1.+PR2))
      C1=((1.-PR1)/G1+(1.-PR2)/G2)/6.28319
      C2=(((16.*PR1-4.)*PR1-2.)*PR1+2.)/(G1*25.13274*R)
      NP1=N+2
      MP1=M+1
C     CALL SUBROUTINE TO FILL MATRIX OF COEFFICIENTS
```

```
      CALL ARRAY(NP1,MP1,N1,N21,R1,TH1)
C     RIGHT HAND SIDE OF EQUATIONS IS B(I)
      DO 10 I=1,N
      B(I)=H(I)-.5*R1(I)*R1(I)/R
   10 CONTINUE
      B(NP1)=F
      DO 15 I=1,NP1
      B1(I)=B(I)
      DO 15 J=1,MP1
      A1(I,J)=A(I,J)
   15 CONTINUE
C     CALL SUBROUTINE FOR SOLUTION OF LINEAR EQUATIONS
C     CORRESPONDING TO MINIMIZATION OF RESIDUALS. LSQHTS
C     CONTAINED IN CDC MATH-SCIENCE LIBRARY. PRESSURE
C     COEFFICIENTS RETURNED IN B(I).
      CALL LSQHTS(A,NR,NP1,MP1,D,SA,IPR,B,IER)
      WRITE(6,150)
      WRITE(3,150)
C     PRINT COEFFICIENTS, TOTAL LOAD, RESIDUALS
  150 FORMAT(5X,"PRESSURE COEFFICIENTS")
      WRITE(6,*)(B(I),I=1,MP1)
      WRITE(3,*)(B(I),I=1,MP1)
C     COMPUTE TOTAL LOAD
      FC=0.0
      DO 17 I=1,M
      FC=FC+A1(NP1,I)*B(I)
   17 CONTINUE
      WRITE(6,250)
      WRITE(3,250)
  250 FORMAT(5X,"TOTAL LOAD")
      WRITE(6,*)FC
      WRITE(6,275)
      WRITE(3,*)FC
      WRITE(3,275)
  275 FORMAT(5X,"RESIDUALS")
C     COMPUTE RESIDUALS
      DO 55 I=1,NP1
      RES(I)=B1(I)
      DO 55 J=1,MP1
      RES(I)=RES(I)-A1(I,J)*B(J)
   55 CONTINUE
      WRITE(6,*)(RES(I),I=1,NP1)
      WRITE(3,*)(RES(I),I=1,NP1)
      WRITE(6,350)
C     SPX,SPY  SPACING BETWEEN POINTS AT WHICH THE PRESSURE
C       IS TO BE COMPUTED
  350 FORMAT(5X,"ENTER SPX,SPY. FOR NO CALC., ENTER 200.,
     1200.")
```

```
      READ(5,*)SPX,SPY
      IF(SPX.GT.RO)GO TO 90
      WRITE(6,450)
      WRITE(3,450)
  450 FORMAT(//10X,"X",8X,"Y",10X,"P"/)
C     COMPUTE PRESSURE AT SPECIFIED LOCATIONS
      NX=INT(-XIN/SPX)+INT(XOUT/SPX)+3
      NY=INT(RO/SPY)+2
      XC(1)=XIN
      XC(2)=-INT(-XC(1)/SPX)*SPX
      NX1=NX-1
      DO 91 I=3,NX1
      XC(I)=XC(I-1)+SPX
   91 CONTINUE
      XC(NX)=XOUT
      YC(1)=0.0
      NY1=NY-1
      DO 92 I=2,NY1
      YC(I)=YC(I-1)+SPY
   92 CONTINUE
      YC(NY)=RO
      IF(ABS(XC(NX)-XC(NX1)).LT.1.E-10)NX=NX1
      IF(ABS(YC(NY)-YC(NY1)).LT.1.E-10)NY=NY1
      NS=1
      IF(ABS(XC(1)-XC(2)).LT.1.E-10)NS=2
      DO 93 J=1,NY
      DO 93 I=NS,NX
      XT=XC(I)+OFST
      RC=SQRT(XT*XT+YC(J)*YC(J))
      IF(RC.GT.RO)GO TO 93
      IF(RC.GT.1.E-10)GO TO 94
      PHC=0.0
      GO TO 95
   94 PHC=ATAN2(YC(J),XT)
C     CALL SUBPROGRAM TO COMPUTE PRESSURE, GIVEN THE
C       COEFFICIENTS
   95 PC=PRESS(M,N1,N21,B,RC,PHC)
C     PRINT PRESSURE AT SPECIFIED LOCATIONS
      WRITE(6,550)XC(I),YC(J),PC
      WRITE(3,550)XC(I),YC(J),PC
  550 FORMAT(5X,F7.4,2X,F7.4,5X,F8.0)
   93 CONTINUE
   90 WRITE(6,650)
C     FILM THICKNESS AT ANY LOCATION (X,Y) MAY BE CALCULATED
C     FROM COMPUTED PRESSURE DISTRIBUTION BY ENTERING (X,Y)
  650 FORMAT(5X,"FOR FILM THICKNESS, ENTER X,Y,"/
     15X,"ELSE ENTER 200.,200.")
      DO 75 I=1,20
      READ(5,*)X,Y
      IF(X.GT.100.)GO TO 79
      XT=X+OFST
```

```
      HO=0.0
      RHO=SQRT(XT*XT+Y*Y)
      IF(RHO.LT.1.E-10)GO TO 71
      PHI=ATAN2(Y,XT)
      GO TO 73
   71 PHI=0.0
   73 NH=3
      R1(1)=RHO
      TH1(1)=PHI
      CALL ARRAY(NH,MP1,N1,N21,R1,TH1)
      HO=.5*RHO*RHO/R+B(MP1)
      DO 77 J=1,M
      HO=HO+A(I,J)*B(J)
   77 CONTINUE
      WRITE(6,750)X,Y,HO
      WRITE(3,750)X,Y,HO
  750 FORMAT(5X,F7.4,2X,F7.4,5X,2PE10.2)
   75 CONTINUE
   79 WRITE(6,850)
C     PRESSURE AT ADDITIONAL LOCATIONS MAY BE OBTAINED
C     BY ENTERING (X,Y)
  850 FORMAT(5X,"FOR ADD'L PRESSURE, ENTER X,Y,"/
     15X,"ELSE ENTER 200.,200.")
      DO 23 I=1,20
      READ(5,*)X,Y
      XT=X+OFST
      RHO=SQRT(XT*XT+Y*Y)
      IF(RHO.GT.100.)GO TO 41
      IF(RHO.LT.1.E-10)GO TO 25
      PHI=ATAN2(Y,XT)
      GO TO 27
   25 PHI=0.0
   27 PR=PRESS(M,N1,N21,B,RHO,PHI)
      WRITE(6,950)X,Y,PR
      WRITE(3,950)X,Y,PR
  950 FORMAT(5X,F7.4,2X,F7.4,5X,F8.0)
   23 CONTINUE
   41 STOP
      END
      SUBROUTINE ARRAY(NP1,MP1,N1,N21,R1,TH1)
C     SUBROUTINE TO FILL MATRIX OF COEFFICIENTS
      DIMENSION S(2),A(60,50),R1(NP1),TH1(NP1),N1(N21)
      COMMON/A/L1,L2,RH,PH
      COMMON/B/RO,R,A/C/C1,C2
      EXTERNAL FUNC,FLOW,UF
      N=NP1-2
      M=MP1-1
      S(1)=2.
      S(2)=2.
      M1=2
      I1=0
C     DETERMINE L1,L2-EXPONENTS OF R, COS FOR A PARTICULAR
C     TERM IN THE SERIES
```

```
      DO 15 I=1,N21
      J1=N1(I)/2+1
      L2=I-1
      L2T=2*(L2/2)
      IF(L2.EQ.0)GO TO 21
      IF(L2T.EQ.L2)GO TO 22
      AL2=0.0
      GO TO 25
   21 AL2=6.28319
      AL3=AL2
      GO TO 25
   22 AL2=AL3*(L2-1.)/L2
      AL3=AL2
   25 N1I=N1(I)
      DO 15 J=1,N1I
      L1=L2+2*(J-1)
      I1=I1+1
      IF(I1.GT.M)GO TO 16
      AL1=(1./(L1+2.)-1./(L1+4.))*RO*RO
C     ROW (NP1) CORRESPONDS TO TOTAL LOAD CONDITION
      A(NP1,I1)=AL1*AL2
C     ROW (N+1) CORRESPONDS TO SETTING GRADIENT TO ZERO
C     AT INLET
      A(N+1,I1)=(-1)**L2
      DO 20 K=1,N
      RH=R1(K)
      PH=TH1(K)
C     CALL SUBPROGRAM TO PERFORM NUMERICAL INTEGRATION.
C     GMI CONTAINED IN CDC MATH-SCIENCE LIBRARY
      A(K,I1)=GMI(FUNC,FLOW,UP,S,M1)
   20 CONTINUE
   15 CONTINUE
   16 DO 12 I=1,N
      A(I,MP1)=1.
   12 CONTINUE
      RETURN
      END
      FUNCTION FUNC(J,X)
C     SUBPROGRAM TO EVALUATE INTEGRAND-REQUIRED FOR USE
C     WITH GMI
      COMMON/A/L1,L2,R1,TH/B/RO,R/C/C1,C2
      DIMENSION X(2)
      GO TO (10,20),J
   10 FUNC=1.0
      GO TO 30
   20 CK1=X(2)*SIN(X(1))
      CK2=R1-X(2)*COS(X(1))
      IF((CK1*CK1+CK2*CK2).GT.(1.E-30))GO TO 24
      RH=0.0
      PH=0.0
      GO TO 25
   24 RH=SQRT(X(2)*X(2)+R1*R1-2.*X(2)*R1*COS(X(1)))
```

```
      PH=TH+ATAN2(CK1,CK2)
   25 RHD=RH/RO
      IF(L1.EQ.0)GO TO 92
      FAC1=RHD**L1
      GO TO 93
   92 FAC1=1.
   93 IF(L2.EQ.0)GO TO 94
      FAC2=COS(PH)**L2
      GO TO 95
   94 FAC2=1.0
   95 FIN=(1.-RHD*RHD)*FAC1*FAC2
      IF(X(2).GT.(1.E-20))GO TO 27
      FUNC=C1*FIN
      GO TO 30
   27 FUNC=FIN*(C1+C2*X(2)*ALOG(X(2)/R))
   30 RETURN
      END
      FUNCTION FLOW(J,X)
C     SUBPROGRAM TO EVALUATE LOWER LIMIT OF INTEGRAL-
C     REQUIRED FOR USE WITH GMI
      GO TO (10,20),J
   10 FLOW=-3.14159
      GO TO 30
   20 FLOW=0.0
   30 RETURN
      END
      FUNCTION UP(J,X)
C     SUBPRORAM TO EVALUATE UPPER LIMIT OF INTEGRAL-
C     REQUIRED FOR USE WITH GMI
      COMMON/A/L1,L2,R1/B/RO
      DIMENSION X(2)
      GO TO (10,20),J
   10 UP=3.14159
      GO TO 30
   20 UP=R1*COS(X(1))+RO*SQRT(1.-(R1*SIN(X(1))/RO)**2)
   30 RETURN
      END
      FUNCTION PRESS(M,N1,N21,P,RH,TH)
C     SUBPROGRAM TO COMPUTE PRESSURE AT ANY LOCATION,
C     GIVEN PRESSURE COEFFICIENTS
      DIMENSION P(M),N1(N21)
      COMMON/B/RO
      RHD=RH/RO
      FAC=(1.-RHD*RHD)
      C=COS(TH)
      PRESS=0.0
      I1=0
      DO 15 I=1,N21
      J1=N1(I)/2+1
      L2=I-1
      N1I=N1(I)
      DO 15 J=1,N1I
      L1=L2+2*(J-1)
```

```
      I1=I1+1
      IF(I1.GT.M)GO TO 16
   19 IF(L1.EQ.0)GO TO 91
      FAC1=RHO**L1
      GO TO 92
   91 FAC1=1.0
   92 IF(L2.EQ.0)GO TO 93
      FAC2=C**L2
      GO TO 94
   93 FAC2=1.0
   94 PRESS=PRESS+P(I1)*FAC*FAC1*FAC2
   15 CONTINUE
   16 RETURN
      END
```

APPENDIX G

DETAILS OF THE EHD SIMULATOR

The film thickness data used for the pressure calculation in Chapter IV was generated by H. S. Nagaraj [36] using the experimental EHD apparatus in the Tribology and Rheology Laboratory at Georgia Institute of Technology. Some details of this experimental rig are provided below.

Sphere

- Material - AISI 52100 (chromium steel)
- Young's modulus - 207 GPa
- Poisson's ratio - 0.3
- Diameter - 31.8 mm

Plate

- Material - synthetic sapphire
- Young's modulus - 365 GPa
- Poisson's ratio - 0.25

Fluid

- Material - naphthenic base oil N1
- Viscosity at $38^{o}C$ - 2.2×10^{-2} Ns/m^2
- Viscosity at $99^{o}C$ - 3.2×10^{-3} Ns/m^2

Additional detailed information about the EHD Simulator are available in [36].

BIBLIOGRAPHY

1. McKinney, J. E., Goldstein, M., "PVT Relationships for Liquid and Glassy Poly (vinyl acetate)", J. of Res. of NBS, A78, p. 331, 1974.

2. Gee, G., "The Glassy State in Polymers", Contemp. Phys., 11, p. 313, 1970.

3. Greet, R. J., Turnbull, D., "Glass Transition in o-Terphenyl", J. Chem. Phys., 46, p. 1243, 1967.

4. Yano, O., Wada, Y., "Dynamic Mechanical and Dielectric Relaxations of Polystyrene Below the Glass Temperature", J. Polym. Sci., 9, Part A2, p. 669, 1971.

5. Cummins, H. Z., Gammon, R. W., "Rayleigh and Brillouin Scattering in Liquids: the Landau-Placzek Ratio", J. Chem. Phys., 44, p. 2785, 1966.

6. Turchina, V., Sanborn, D. M., Winer, W. O., "Temperature Measurements in Sliding Elastohydrodynamic Point Contacts", Trans. ASME, J. Lub. Tech., 96, Series F, No. 3, 1974.

7. Ausherman, V. K., Nagaraj, H. S., Sanborn, D. M., Winer, W. O., "Infrared Temperature Mapping in Elastohydrodynamic Lubrication", Trans. ASME, J. Lub. Tech., 98, Series F, No. 2, 1966.

8. Dowson, D., Higginson, G. R., Elastohydrodynamic Lubrication, Pergamon Press, N.Y., 1965.

9. Love, A. E. H., A Treatise on the Mathematical Theory of Elasticity, Dover, N. Y., 1944.

10. Archard, J. F., Baglin, K. P., "Non-dimensional Presentation of Frictional Tractions in Elastohydrodynamic Lubrication", Part I, Fully-Flooded Results", Trans ASME, J. Lub. Tech., Series F, 97, p. 388, 1975.

11. Murch, L. E., Wilson, W. R. D., "A Thermal Elastohydrodynamic Inlet Zone Analysis", Trans. ASME, J. Lub. Tech., 97, Series F, p. 212, 1975.

12. Cameron, A., Gohar, R., "Theoretical and Experimental Studies of the Oil Film in Lubricated Point Contact", Proc. Roy. Soc. London, A, 291, p. 520, 1966.

13. Trachman, E. G., Cheng, H. S., "Thermal and Non-Newtonian Effects on Traction in Elastohydrodynamic Contacts", Elasto-hydrodynamic Lubrication: Second Symposium, Inst. Mech. Eng. Paper C37/72, 1972.

14. Kannel, J. W., Walowit, J. A., "Simplified Analysis for Traction Between Rolling-Sliding Elastohydrodynamic Contacts", Trans. ASME, J. Lub. Tech., Series F, 93, p. 39, 1971.

15. Herrebrugh, K., "Solving the Incompressible and Isothermal Problem in Elastohydrodynamic Lubrication through an Integral Equation", Trans. ASME, J. Lub. Tech., Series F, 90, p. 262, 1968.

16. Taylor, C., O'Callaghan, J. R., "A Numerical Solution of the Elastohydrodynamic Lubrication Problem Using Finite Elements", J. Mech. E. Sci., 14, p. 229, 1972.

17. Cheng, H. S., Sternlicht, B., "A Numerical Solution for the Pressure, Temperature, and Film Thickness Between Two Infinitely Long, Lubricated Rolling and Sliding Cylinders, Under Heavy Loads", Trans. ASME, J. Basic Eng., 87, p. 695, 1965.

18. Ranger, A. P., Ettles, C. M. M., Cameron, A., "The Solution of the Point Contact Elastohydrodynamic Problem", Proc. Roy. Soc. London, A, 346, p. 227, 1975.

19. Hamrock, B. J., Dowson, D., "Isothermal Elastohydrodynamic Lubrication of Point Contacts, I - Theoretical Formulation", Trans. ASME, J. Lub. Tech., 98, p. 223, 1976.

20. Chow, T. S., Saibel, E., "The Elastohydrodynamic Problem with a Viscoelastic Fluid", Trans. ASME, J. Lub. Tech., Series F, 93, p. 25, 1971.

21. Jacobsen, B., "On the Lubrication of Heavily-Loaded Spherical Surfaces Considering Surface Deformation and Solidification of the Lubricant", Acta Polytechnica Scandinavica, M. E. Series, ME54, 1970.

22. Jacobsen, B., "On the Lubrication of Heavily-Loaded Cylindrical Surfaces Considering Surface Deformation and Solidification of the Lubricant", Trans. ASME, J. Lub. Tech., Series F, 95 p. 321, 1973.

23. Cope, D. L., Haines, D. J., "Interferometric Determination of Elastohydrodynamic Lubrication Contact Pressures", Proc. Inst. Mech. Eng., 184, Pt. 1, p. 633, 1969-70.

24. Cheng, H. S., Orcutt, F. K., "A Correlation Between the Theoretical and Experimental Results on the Elastohydrodynamic Lubrication of Rolling and Sliding Contacts", Proc. Inst. Mech. Eng., 180, Pt. 3B, p. 156, 1965-66.

25. Hamilton, G. M., Moore, S. L., "Deformation and Pressure in an Elastohydrodynamic Contact", Proc. Roy. Soc. London, A, 322, p. 313, 1971.

26. Bartz, W. J., Ehlert, J., "Influence of Pressure Viscosity of Lubrication Oils on Pressure, Temperature and Film Thickness in Elastohydrodynamic Rolling Contacts", Trans. ASME, J. Lub. Tech., Series F, 98, p. 500, 1976.

27. Foord, C. A., Wedeven, L. D., Westlake, F. J., Cameron, A., "Optical Elastohydrodynamics", Proc. Inst. Mech. Eng., Part I, 184, pp. 487-505, 1969-70.

28. Sanborn, D. M., Winer, W. O., "Fluid Rheological Effects in Sliding Elastohydrodynamic Point Contacts with Transient Loading: 1-Film Thickness", Trans. ASME, J. Lub. Tech., 93, Series F, No. 2, 1973.

29. Kunz, R., Winer, W. O., "Prediction of Traction in Sliding EHD Contacts", Trans. ASME, J. Lub. Tech., Series F, 98, p. 362, 1976.

30. Muskhelishvili, N. I., Some Basic Problems of the Theory of Elasticity, Noordhoff, Groningen, 1953.

31. Jahnke, E., Emde, F., Tables of Functions, Dover, New York, 1945.

32. Control Data Corporation, Math-Science Library, 3.

33. Sheid, F., Theory and Problems of Numerical Analysis, Schaum's Outline Series, McGraw-Hill, New York, 1968.

34. Control Data Corporation, Math-Science Library, 6.

35. Wymer, D. G., Cameron, A., "Elastohydrodynamic Lubrication of a Line Contact", Proc. Inst. Mech. Eng., 188, p. 221, 1974.

36. Nagaraj, H. S., "Investigation of Some Temperature-Related Phenomena in Elastohydrodynamic Contacts Including Surface Roughness Effects", Ph.D. Thesis, School of Mechanical Engineering, Georgia Institute of Technology, Atlanta, 1976.

37. Papkovich, P. F., "Solution Générale des équations différentielles fondomentales d'élasticité, exprimée par trois fonctions harmoniques", Comptes Rendus, 195, p. 513, 1932.

38. Lure, A. I., Three-dimensional Problems of the Theory of Elasticity, Interscience, N.Y., 1964.

39. Eubanks, R. A., Sternberg, "On the Completeness of the Boussinesq-Papkovich Stress Functions", J. Rational Mech. Anal., 5, p. 735, 1956.

40. Sternberg, E., Rosenthal, F., "The Elastic Sphere Under Concentrated Loads", Trans. ASME, J. Appl. Mech., 74, Series E, p. 413, 1952.

41. Kantorovich, L. V., Krylov, V. I., Approximate Methods of Higher Analysis, Interscience, N.Y., 1958

42. Control Data Corporation, Math-Science Library, 5.

43. Sokolnikoff, I. S., Mathematical Theory of Elasticity, McGraw-Hill, N.Y., 1956.

44. Fung, Y. C., Foundations of Solid Mechanics, Prentice-Hall, Englewood Cliffs, N.J., 1965.

VITA

Richard Kerr Kunz was born on December 25, 1951 in Geneva, New York, the son of Clarence E. and Mildred K. Kunz. His older brother, Donald, currently resides in Sunnyvale, California.

Mr. Kunz attended Geneva public schools, and graduated from Geneva High School in 1970 as valedictorian. He subsequently attended Cornell University, from which he received the Bachelor of Science Degree in Mechanical Engineering, with honors, in January 1974. While at Cornell, he became a member of Tau Beta Pi, Phi Kappa Phi, and ASME. Mr. Kunz continued his education at the Georgia Institute of Technology, where he received a Master of Science of Mechanical Engineering in December 1974, under the direction of Dr. Ward O. Winer. His master's thesis was entitled "Thermal and Traction Behavior in Sliding Elasto-hydrodynamic Contacts". While at Georgia Tech, he joined the Society of Sigma Xi. After being awarded a National Science Foundation Graduate Fellowship, Mr. Kunz entered the doctoral program in the School of Engineering Science and Mechanics at Georgia Tech, under the direction of Dr. George M. Rentzepis.

Mr. Kunz is married to the former Stephanie Latta of Glendale, Ohio.